Elongational viscosity of polymer melts and its utilisation for plastics technologies optimisation

Bc. Rostislav Vilém

Master's thesis
2021

Tomas Bata University in Zlín
Faculty of Technology

Univerzita Tomáše Bati ve Zlíně
Fakulta technologická
Ústav inženýrství polymerů

Akademický rok: 2020/2021

ZADÁNÍ DIPLOMOVÉ PRÁCE

(projektu, uměleckého díla, uměleckého výkonu)

Jméno a příjmení:	**Bc. Rostislav Vilém**
Osobní číslo:	**T19395**
Studijní program:	**N0722A130001 Inženýrství polymerů**
Studijní obor:	**Inženýrství polymerů**
Forma studia:	**Prezenční**
Téma práce:	**Elongational viscosity of polymer melts and its utilisation for plastics technologies optimisation**

Zásady pro vypracování

In the frame of diploma works elongational viscosity of polymer melts will be evaluated under specified temperature conditions via various methodologies including Rheotens, Sentmanat, and Cogswell. Defined behavior of elongational viscosity will be consequently combined with specific plastics processes as polymer foaming and spinning.

Forma zpracování diplomové práce: **tištěná/elektronická**
Jazyk zpracování: **Angličtina**

Seznam doporučené literatury:

1. Cheremisinoff, N.P., Cheremisinoff, P.N. Handbook of Applied Polymer Processing Technology. CRC Press, 1996. ISBN 9780824796
2. Tadmor, Z., Gogos, C.G.Principles of Polymer Processing. John Wiley & Sons, 2013. ISBN 9780470355923.
3. Han C. D.Rheology and procesing of polymeric materials: Polymer processing. Oxford, 2007. ISBN 978-0195187830.
4. Albrecht, W., Fuchs, H., Kittelmann, W. Nonwoven Fabrics: Raw materials, manufacture, applications, characteristics, testing processes. Wiley, 2006. ISBN 978-3-527-60531-.
5. Kempner, D., Sendijarevic, V.Polymer foams and foam technology, 2nd edition. Hanser, 2012. ISBN 978-1569903360

Vedoucí diplomové práce: **doc. Ing. Tomáš Sedláček, Ph.D.**
Ústav inženýrství polymerů

Datum zadání diplomové práce: **1. února 2021**
Termín odevzdání diplomové práce: **14. května 2021**

L.S.

prof. Ing. Roman Čermák, Ph.D.
děkan

Ing. Jana Navrátilová, Ph.D.
ředitel ústavu

Ve Zlíně dne 1. dubna 2021

PROHLÁŠENÍ AUTORA
DIPLOMOVÉ PRÁCE

Beru na vědomí, že:

- diplomová práce bude uložena v elektronické podobě v univerzitním informačním systému a dostupná k nahlédnutí;
- na moji diplomovou práci se plně vztahuje zákon č. 121/2000 Sb. o právu autorském, o právech souvisejících s právem autorským a o změně některých zákonů (autorský zákon) ve znění pozdějších právních předpisů, zejm. § 35 odst. 3;
- podle § 60 odst. 1 autorského zákona má Univerzita Tomáše Bati ve Zlíně právo na uzavření licenční smlouvy o užití školního díla v rozsahu § 12 odst. 4 autorského zákona;
- podle § 60 odst. 2 a 3 autorského zákona mohu užít své dílo – diplomovou práci nebo poskytnout licenci k jejímu využití jen s předchozím písemným souhlasem Univerzity Tomáše Bati ve Zlíně, která je oprávněna v takovém případě ode mne požadovat přiměřený příspěvek na úhradu nákladů, které byly Univerzitou Tomáše Bati ve Zlíně na vytvoření díla vynaloženy (až do jejich skutečné výše);
- pokud bylo k vypracování diplomové práce využito softwaru poskytnutého Univerzitou Tomáše Bati ve Zlíně nebo jinými subjekty pouze ke studijním a výzkumným účelům (tj. k nekomerčnímu využití), nelze výsledky diplomové práce využít ke komerčním účelům;
- pokud je výstupem diplomové práce jakýkoliv softwarový produkt, považují se za součást práce rovněž i zdrojové kódy, popř. soubory, ze kterých se projekt skládá. Neodevzdání této součásti může být důvodem k neobhájení práce.

Prohlašuji,

- že jsem diplomové práci pracoval samostatně a použitou literaturu jsem citoval. V případě publikace výsledků budu uveden jako spoluautor.
- že odevzdaná verze diplomové práce a verze elektronická nahraná do IS/STAG jsou obsahově totožné.

Ve Zlíně dne:

Jméno a příjmení studenta:

……..
podpis studenta

ABSTRAKT

Viskozita je základní reologická veličina. Viskozita, a zejména elongační viskozita, je velmi efektivním nástrojem pro optimalizaci technologických podmínek při zpracování polymerních tavenin.

Tato práce si klade za cíl, u vybraných testovaných polymerních materiálů a jejich směsí – vybrány byly dva vstupní materiály, PP TOTAL jako zástupce lineárního typu polypropylenu a PP DAPLOY jako představitel rozvětvených polypropylenů – srovnat výsledky z charakterizace elongační viskozity získané pomocí dostupných experimentálních technik a porovnat tyto získané výsledky s technologickými poznatky z výrobních postupů při zpracování polymerních tavenin do podoby pěn. Tokové vlastnosti použitých materiálů byly navíc charakterizovány i pomocí online, kapilárního a rotačního reometru. U pěn připravených z vybraných polymerních materiálů byly pro účely jejich srovnání dále charakterizovány i jejich užitné vlastnosti, jako velikost pórů, hustota, nebo struktura.

Při porovnání výsledků z pozorování procesu výroby pěn a porovnání jejich finálních vlastností, se jako nejvýhodnější experimentální metodika charakterizace reologických vlastností – elongační viskozity – jeví zařízení Rheotens. Tato metoda se navíc ukázala i s výhodou aplikovatelná pro optimalizaci procesu výroby vláken.

Klíčová slova: reologie, elongační viskozita, polymerní pěna, reometry

ABSTRACT

Viscosity is a fundamental rheological quantity. Viscosity, in particular, elongation viscosity, is a very effective tool for optimising the technological conditions in the processing of polymer melts.

This work aims to compare the results from the elongation viscosity characterisation obtained using the available experimental techniques to compare these results with the technological insights from the manufacturing processes of polymer melts such as foams production. In addition, the flow characteristics of the used materials were also characterised by an online, capillary and rotational rheometer. For foams prepared from selected polymer materials, their performance characteristics, such as pore size, density, or structure, were further characterized for comparison.

When comparing the results from observing the foam production process and comparing their final properties, the Rheotens device appears to be the most advantageous experimental methodology for characterizing the rheological properties - elongation viscosity. In addition, this method has also proved to have the advantage of being applied to optimise the fibre production process.

Keywords: rheology, elongation viscosity, polymer foam, rheometers

ACKNOWLEDGMENTS

I want to express my great gratitude to my supervisor, doc. Ing. Tomáš Sedláček Ph.D. for valuable advice and information throughout the process of writing my work and to Ing. Roman Kolařík Ph.D. for help in the practical part of the work.

I hereby declare that the print version of my Bachelor's/Master's thesis and the electronic version of my thesis deposited in the IS/STAG system are identical.

CONTENTS

INTRODUCTION

As a study of the deformation and flow of matter [1], rheology plays an important role in polymer processing and also in all other production processes where materials flow, such as printing and coating. The flow of polymer melts can be divided into two basic groups: shear and elongational flows. The rheological properties that express the material's resistance to both types of flow are shear and extensional viscosities, respectively [2]. Extensional (elongation) viscosity plays an important role as a material parameter in foam production, fibre spinning, film blowing and other processes.

For this reason, it has been receiving attention in academia for more than a hundred years [3]. Even though many articles have been published on the topic of elongational viscosity, often in the Journal of Non-Newtonian Fluid Mechanics [4], there are still gaps in this field of knowledge, such as the topic of this work, which seeks to link rheological measurements with the processing of polymeric foams.

To measure extensional viscosity and subsequently to describe elongational flow mathematically, several devices were invented and developed, as closely described further in this thesis. There is also literature available on polymeric foams [5]. Today, polymeric foams make up a wide range of products that we are used to using in everyday life. Two common polymeric materials were used for the production of foams. Frequently used materials for preparing foams and the determination of rheological properties have been chosen to approach more realistic processes. For this reason, the first method of rheological characterization in this thesis is an online rheometer and only then laboratory rheometers.

I. THEORY

1 RHEOLOGY

Rheology is the science of deformation and flow of matter. [1]

From a rheological point of view, any material can flow if it is given enough time. Several basic types of flows will be presented below. To the base description of the matters' flow and deformation, simplified models had to be introduced as a model of an ideal elasticity and ideal viscosity. Polymeric melts combine both, and we describe them with viscoelastic models. An ideally elastic material is a type of material where all the energy accumulated in the material sample under its load is re-used to lighten that sample. So there is no dissipation of the embedded mechanical energy in the heat for these materials under harmonic stress. An ideal viscosity material is a material where all the energy embedded in the material sample at its load is dissipated into heat. There is, therefore, no re-use of the embedded mechanical energy under harmonic stress. Spring is used as an approximation of elastic behaviour, and the idea of a piston is used to approximate the viscous behaviour. The piston, the spring and their combinations are then utilized in rheological models. One of the basic models is the Maxwell model. This model is a combination of elastic behaviour (spring) and viscous behaviour (piston). It should be noted that we do not have a comprehensive theory that can describe some polymeric materials' rheological behaviour. Thus we must rely on empirically obtained data and observed rheological behaviour of those materials. [6; 7]

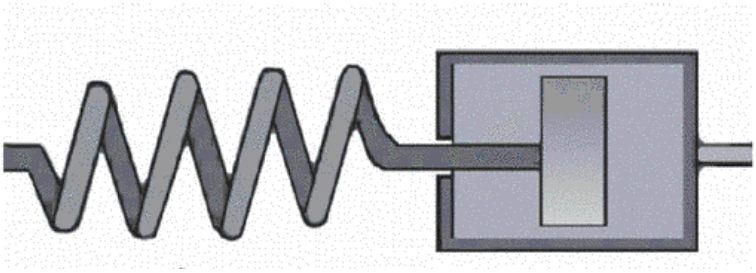

Figure 1: Scheme of the Maxwell model [8]

Figure 1 shows the characteristic scheme of Maxwell model, the mathematical expression of the Maxwell model is presented by Equation 1:

$$\tau_{ij} + \lambda \cdot \dot{\tau}_{ij} = 2 \cdot \eta \cdot D_{ij} \tag{1}$$

where τ_{ij} stands for the stress tensor, which characterises the melt's stress state at flow, thus the force F_j general action on the surface A_i, see Equation 2:

$$\tau_{ij} = \frac{F_j}{A_i} \tag{2}$$

The relaxation time λ is characteristic for each material expressig the ability to rearrange molecules from one state to another. The co-deformation time derivation of the stress tensor $\dot{\tau}_{ij}$ means the change in stress over time. Concurrently this term represents the elastic component of the behaviour. If it is zero, the equation describes only viscous behaviour. The viscosity η express the resistance to flow and D_{ij} represents the strain rate tensor which characterises the way how the melt is stressed. It could be said that express the flow mode, whether it is shear or elongational. The two basic flow types most often used to characterize polymeric liquids are shear and elongational flow. [6; 9]

1.1 Viscosity

As it was already mentioned above, viscosity is the resistance to flow. The higher is the viscosity, the higher is the resistance to flow.

In general, the material viscosity is related to the shear stress and the shear rate deformation. Based on this dependence, liquids can be divided into Newtonian and non-Newtonian. The dependencies for these two types of liquids are shown in Figure 2. For some liquids, the relationship between shear stress and shear rate deformation is not linear. Such liquids are non-Newtonian liquids, and this group includes polymer melts. [10]

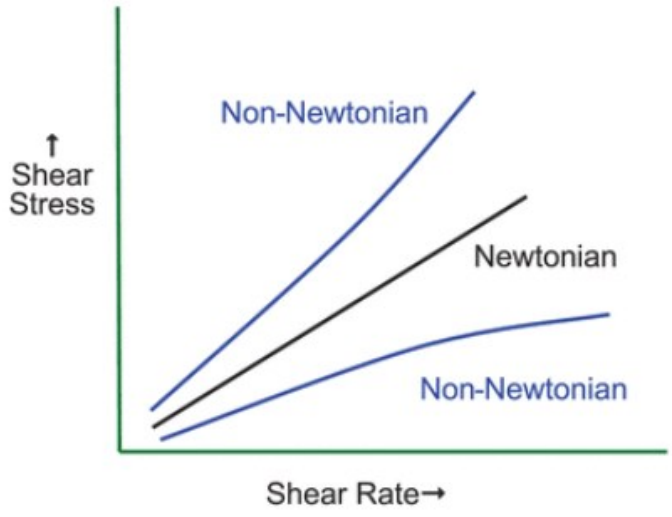

Figure 2: Shear stress versus shear rate for Newtonian and non-Newtonian liquids [10]

Non-Newtonian liquids can be divided by their response to stress into dilatant and shear thinning liquids. For dilatant liquids, viscosity increases with the increasing shear rate deformation. Such liquids include, for example, starch suspensions. The pseudoplastic is characterised by a decrease in viscosity with a decreasing shear rate deformation, see Figure

3. Typical representatives of pseudoplastic liquids are polymer melts. Based on the response to the time of deformation at a constant shear rate, non-Newtonian liquids are classified into rheopectic and thixotropic. In rheopectic fluids with shear duration, viscosity increases, such as ink for the printer. In contrast, for thixotropic fluids, viscosity decreases with the duration of shear, such as paint substances. [10]

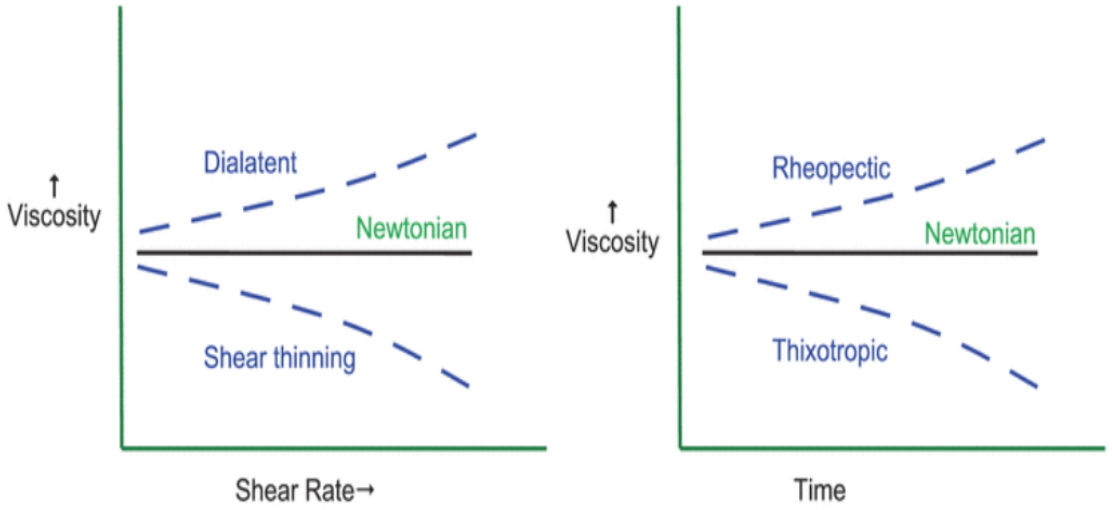

Figure 3: Viscosity dependency on shear rate and time dependency [10]

During processing, the polymer melt is forced to flow, which means it is shear stressed. Polymer viscosity dependence on the shear rate is depicted in Figure 4. In different processes, there are different shear rates, therefore different viscosity response. Generally, polymers could be processed by processes such as injection moulding, compression moulding, spinning and extrusion. All of these processes give the polymer a new shape. If the material more resists the flow, it needs to be forced more to achieve the desired shape. Therefore, viscosity plays an essential role in polymer processing. [9]

The resulting dependence of viscosity on the shear rate is determined by the relative rate of formation and decay of the polymer chain entanglements. The intensity of the decline between Newtonians two plateaus is due to the distribution of the polymer's molecular weight (MWD). Narrow distribution means a long first plateau and a gradual decline, while wide distribution means a short plateau and a sharper decline than in the narrow distribution. [11]

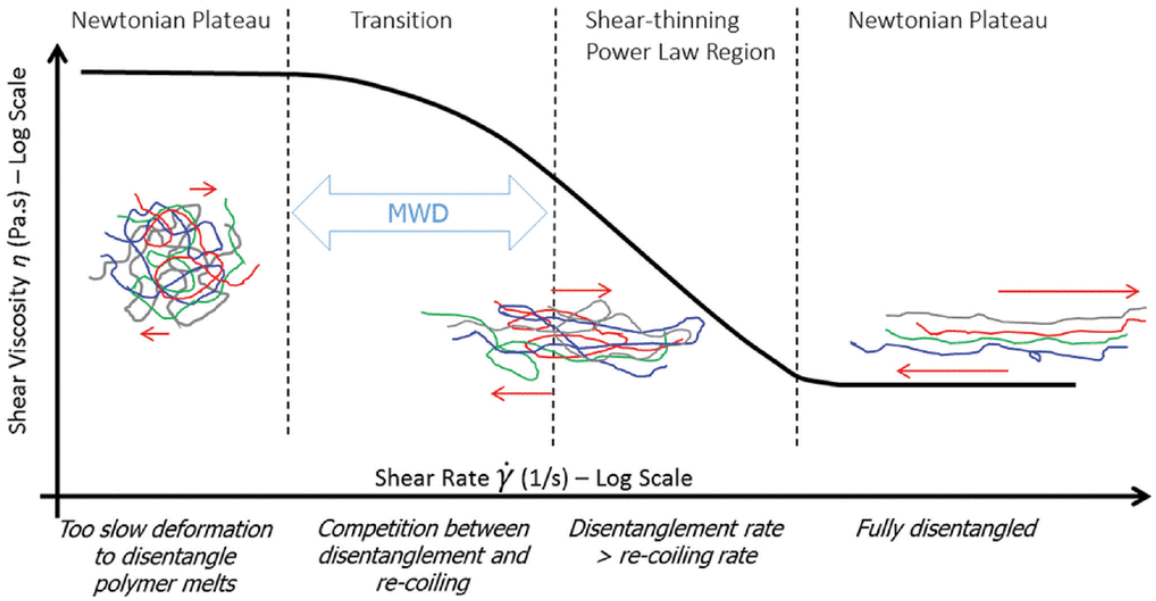

Figure 4: Typical viscosity curve for polymer melt [11]

Not only the distribution of molecular weight but the molecular weight itself affects viscosity. The longer the polymer chains are, the greater the molecular weight is, and the greater is the viscosity, see Figure 5. Thus, with higher molecular weight, the viscosity rises, and thus also the polymer is more difficult to process. On the other hand, higher molecular weight improves some mechanical properties, such as stiffness and strength. [12]

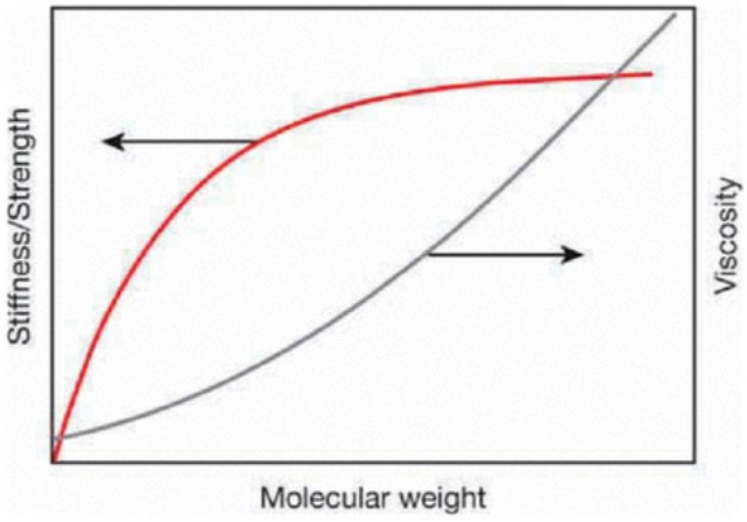

Figure 5: The dependency of rheological and mechanical properties on molecular weight [11]

1.2 The dependence of viscosity on temperature and pressure

In previous chapters, it has been explained that viscosity of polymer melts depends on factors such as shear rate, molecular weight, distribution of molecular weight. These factors are important, but there are two more important processing factors, temperature and pressure. As temperatures rise, chain mobility increases, which leads to decreasing viscosity. Figure *6* also shows that the drop in the viscosity curve is moving towards a higher shear rate. [13]

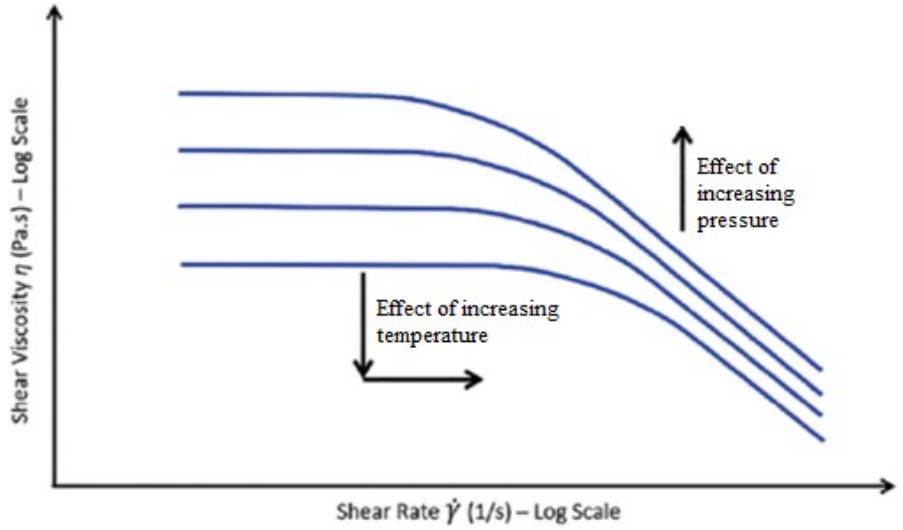

Figure 6: Effect of temperature and pressure on viscosity [13]

Equation 3 illustrates in simplistic terms the viscosity dependency on temperature *T*, where *e* is the Euler number, and α is the constant. Due to exponential dependency, a small change in temperature could lead to a significant decline in viscosity. The simplified mathematical expression of the viscosity dependence on pressure is represented by Equation 4.

$$\eta = e^{\frac{\alpha}{T}} \tag{3}$$

$$\eta = e^{\beta \cdot p} \tag{4}$$

where β is the proportionality constant and p is the pressure. Substantial pressure viscosity effects occur under higher pressures of the order of tens of MPa. Such pressure is however common in injection moulding process, for example. [13]

For the material's practical process, it is useful to know its rheological behaviour. Although, there is no need to measure the entire viscosity curve for a specific material. Depending on the process, it is sufficient to define the relevant part of the viscosity curve. For example, in Figure 7, the extrusion process can be seen to range from 0.1 to 100 reciprocal seconds. So for an extrusion simulation, this is essential part of the curve. Figure 7 also present that

different rheometers are suitable for evaluation of different shear rate regions. Therefore, for extrusion, rheological data from the capillary rheometer is appropriate. [12]

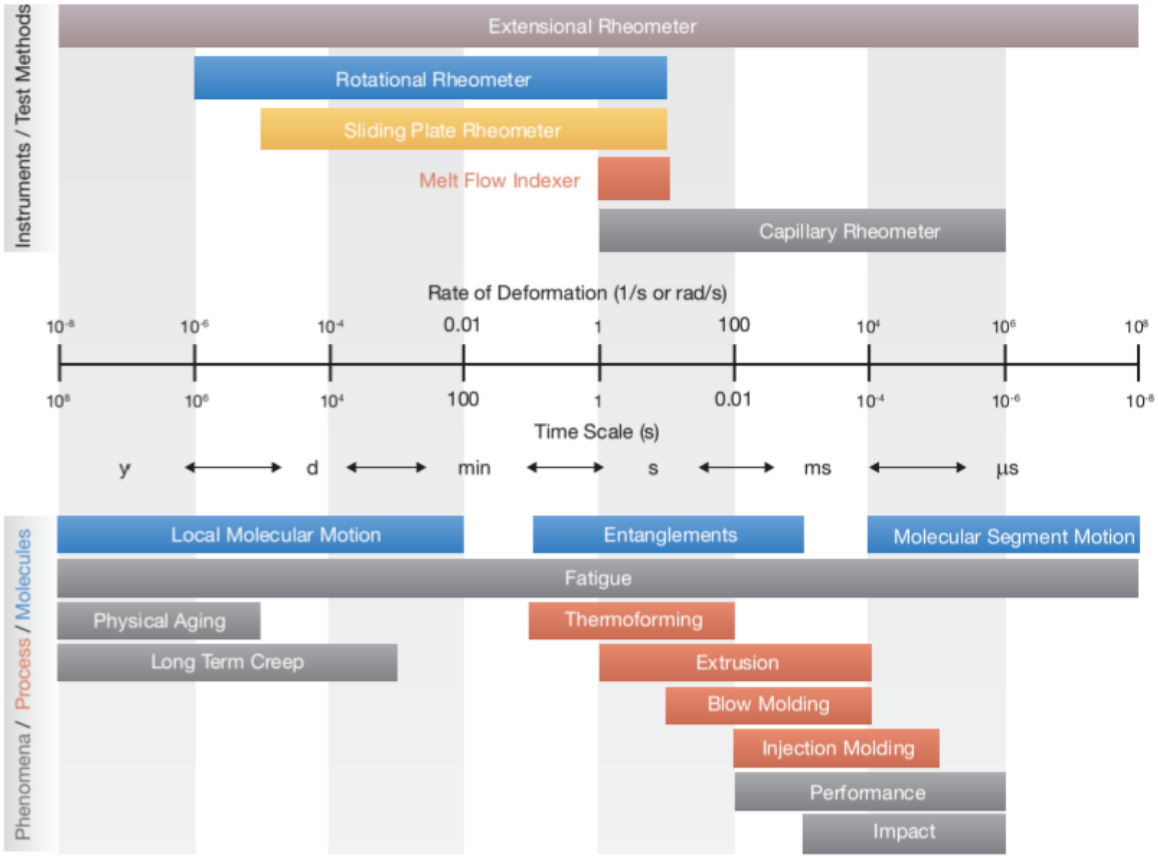

Figure 7: The relation between the rate of deformation, test methods and processing [12]

Nevertheless, it should be highlighted that several types of polymer melt flows are employed for polymer processing modelling. A flow between two parallel plates could be used to describe the material process inside a screw extruder. In contrast, a pressure-driven flow could be used to simulate the melt flow through the channel.

1.3 Parallel plate flow

The melt flow can be approximated by a series of layers (imaginary elements) that can move one after another. In this approximation is introduced the assumption of zero velocity at the both walls. If we set the upper plate in motion with force F_x, the material layers below will start to move, but with decreasing speed v towards the lower fixed plate, as presented in Figure 8 using the orange arrows. The action of force is an action that evokes a reaction, stress. Stress is trying to maintain balance, to restore the original state. [8; 9]

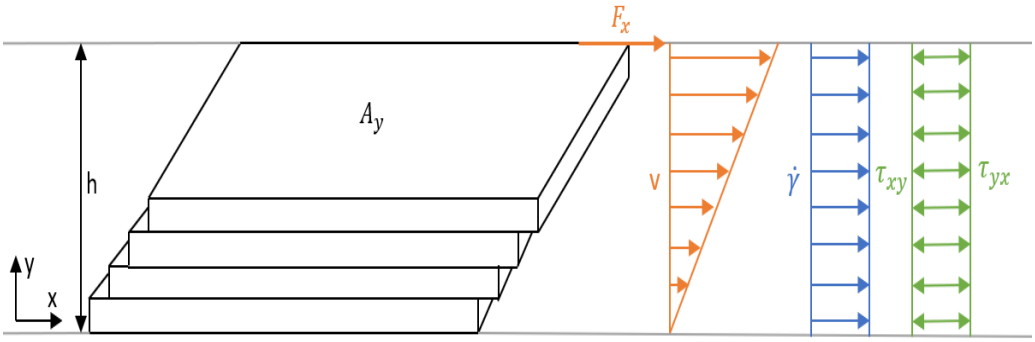

Figure 8: Scheme of simple shear flow [12]

This stress is called shear stress and can be expressed using Equation 5.

$$\tau_{yx} = \frac{F_x}{A_y} \tag{5}$$

where τ_{yx} is the shear stress induced by the force relative to the surface A_y. Shear stress can also be expressed using Equation 6. In the next considerations, we will consider the melt's response purely. The shear stress τ_{yx} to τ_{xy} will be renamed because these stresses are equal, τ_{yx} is stress-induced by action, and τ_{xy} is stress-induced by a reaction.

$$\tau_{xy} = \eta \cdot \dot{\gamma}_{xy} \tag{6}$$

where $\dot{\gamma}_{xy}$ stand for the rate of shear deformation, which characterised the intensity of shear flow. The shear rate in the gap between the surfaces depends on the gap height h and the velocity v of the moving surface, see Equation 7. [9; 12]

$$\dot{\gamma}_{xy} = \frac{v}{h} \tag{7}$$

1.4 Pressure-driven flow

The second case of viscometric flow is the pressure-driven flow in a round channel or between two stationary plates. The driving force is a pressure gradient where a lower pressure is in front of the melt front. The resulting speed profile can be seen in Figure 9. The length of the arrows in the velocity profile represents the velocity of each layer. The velocity at the walls is zero, and therefore the shear rates are very high near the walls. The velocity increases towards the centre of the channel, following a parabolic profile, and it is highest at the centre. The difference in velocity between the two layers at the wall is much more significant than the difference in velocity between the layers at the channel's centre. Therefore, the shear rate is higher near the walls compared to the centre of the channel. The shear rate in pressure-driven flow is defined by the flow channel radius R and the volume flow rate Q, see Equation 8: [10; 14]

$$\dot{\gamma} = \frac{4 \cdot Q}{\pi \cdot R^3} \tag{8}$$

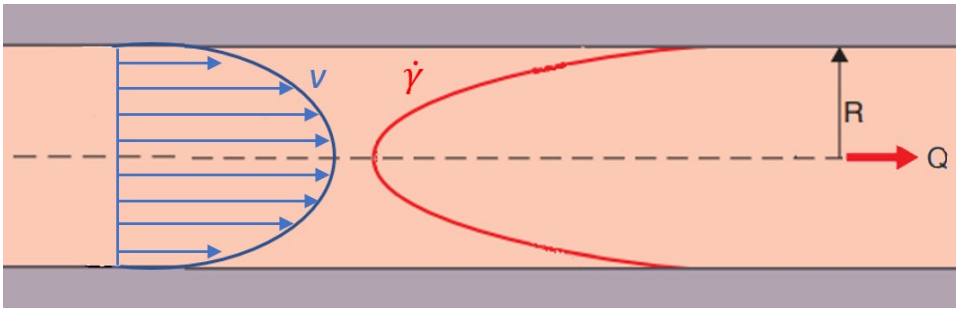

Figure 9: Velocity and shear rate profiles in the channel [15]

2 ELONGATION VISCOSITY

It could be stated that the shear flow previously mentioned are important for processing of polymer melts in general, but elongation flow is another important processing type. Thus there is a need to describe and discuss elongation viscosity and elongation flow. Elongation viscosity is essential in the processes (such as spinning, blow moulding, foaming and casting) where the material is extensively stretched.

The shear flow was characterised as a change in velocity perpendicular to the direction of the flow. On the other hand, elongation flow is characterised by a change in velocity in the flow direction. Generally, elongation viscosity η_E is related to shear η_0 by Trouton's ratio, see Equation 9. Typically, this value ranges from 3 for Newtonian systems to up to 1000 for non-Newtonian systems. However, Trouton's ratio only applies in the low-speed region, so elongation viscosity should be measured as an independent material quantity.

$$Tr = \frac{\eta_E}{\eta_0} \tag{9}$$

There are three basic types of elongation flow, presented in Figure 10. Simple or uniaxial extension flow, which can occur in the process of fibre spinning. Equibiaxial extension occurs when bubbles expands during polymer foams production, and planar extension occur inside a rectangular extrusion dies in the place of abrupt profile contraction. The type of elongation flow will provide different elongational properties specific to their deformation type. [14]

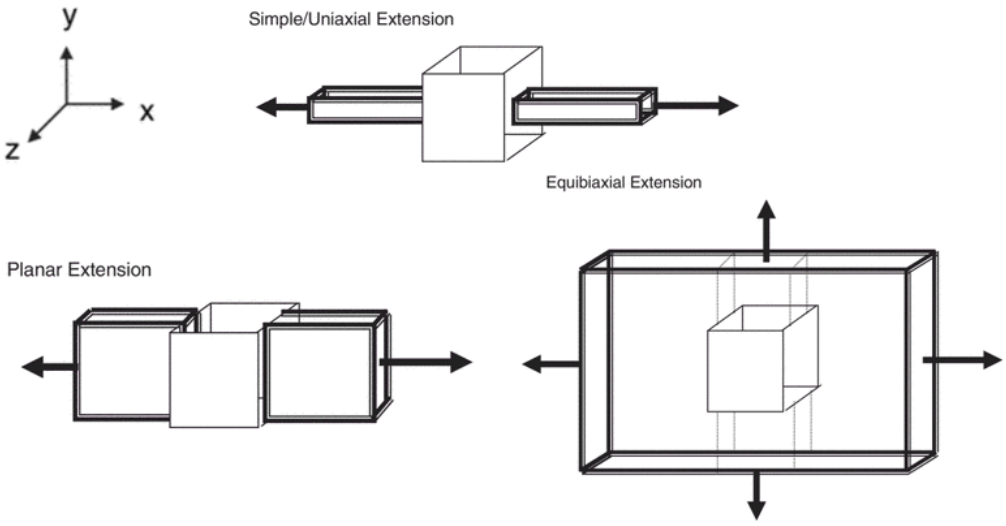

Figure 10: Three types of extensions [16]

As a result of the force's application in the direction of the flow, a specific element of the melt, see Figure 11, will become elongated and accelerate through the force's application. A uniaxial extension is the simplest extensional flow: stretching of the material at a velocity v_1 imposes the strain rate $\dot{\varepsilon}$ in direction *x* and compression $-\frac{1}{2}\dot{\varepsilon}$ in the perpendicular directions *z* and *y*. Equations from 10 to 12 show the velocity distributions in uniaxial extension. [14; 16]

$$v_x = \dot{\varepsilon}(t) \cdot x \tag{10}$$

$$v_y = -\frac{1}{2}\dot{\varepsilon}(t) \cdot y \tag{11}$$

$$v_z = -\frac{1}{2}\dot{\varepsilon}(t) \cdot z \tag{12}$$

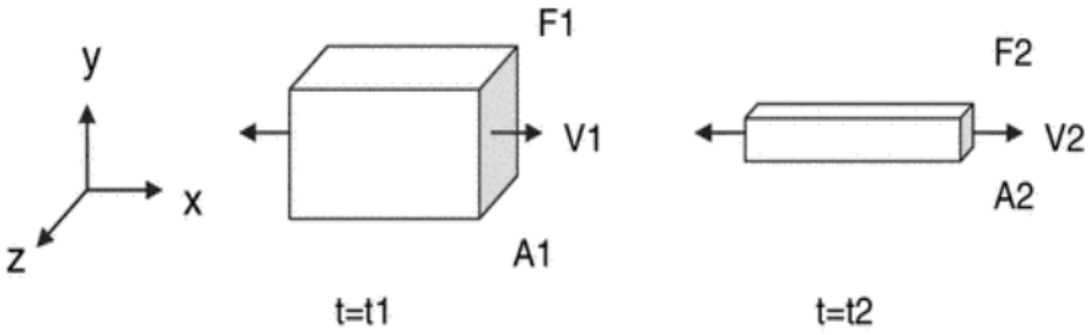

Figure 11: Schema of the melt element under uniaxial extensional flow [16]

The normal stress σ_N may be defined as the force *F(t)* divided by the area *A*(*t*) in the direction of flow, see Equation 13:

$$\sigma_N = \frac{F(t)}{A(t)} \tag{13}$$

Note that both the area and force are a function of time. The elongation viscosity is defined as the normal stress divided by the rate of deformation, see Equation 14:

$$\eta_E = \frac{\sigma_N}{\dot{\varepsilon}} \tag{14}$$

The rate of deformation is characterised by Equation 15:

$$\dot{\varepsilon} = \frac{dv}{dx} \tag{15}$$

In biaxial extension the *x* and *y* velocity profile is the same and positive (as for uniaxial flow), while the extension rates in *z* directions are negative (compression), see Equations 16, 17 and 18:

$$v_x = \frac{1}{2}\dot{\varepsilon}(t) \cdot x \tag{16}$$

$$v_y = \frac{1}{2}\dot{\varepsilon}(t) \cdot y \tag{17}$$

$$v_z = -\dot{\varepsilon}(t) \cdot z \tag{18}$$

In planar extension, one dimension of the material is extended, the second dimension is maintained constant, and the third dimension is compressed. Equations 19–21describe the velocity distributions in planar extension: [14]

$$v_x = \dot{\varepsilon}(t) \cdot x \tag{19}$$

$$v_y = 0 \tag{20}$$

$$v_z = -\dot{\varepsilon}(t) \cdot z \tag{21}$$

2.1 History of elongational viscosity measurement

The first reference to extensional viscosity comes from Trouton. In his paper from 1906 [3], he used the term coefficient of viscous traction when he intended to describe the viscosity of an incompressible Newtonian fluid as pitch and waxes. At that time, scientifically measuring of extensional viscosity was a challenging task. Main problems occurred in clamping the fluid, which needed to be heated and stretched. Another problem was controlling the temperature and achieving sufficient strain and strain rates to be meaningful for processing description. In 1969, Meissner published an article [17] describing the use of one of the first elongation measurement method for polymer that used rotary clips submerged in a hot oil bath, see Figure 12.

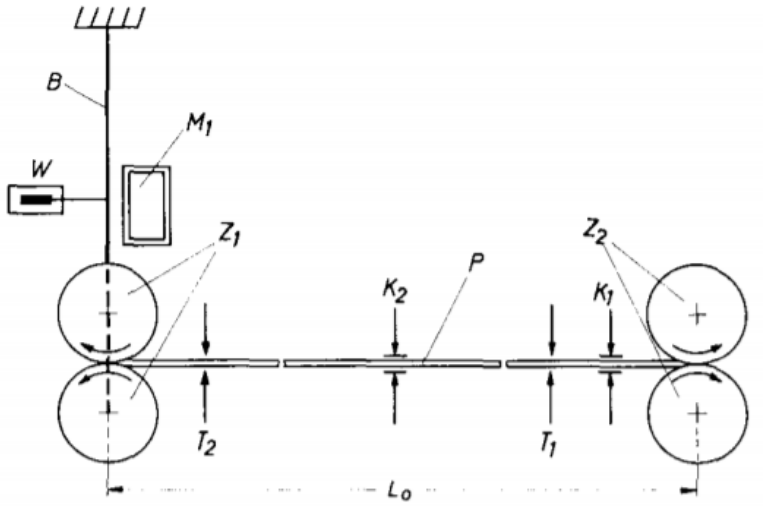

Figure 12: Schema of Meissner's rheometer [17]

In the following years, Münstedt joined Meissner in the field of elongational viscosity characterization, for example, in his article from 1972 [18]. Another successful measurement method was published in 1972 by Cogswell method [19], which is suitable for high deformation rates. For measurement, it uses the recording of the pressure value in the capillary rheometer. Binding [20] and Gibson [21] then followed Cogswell's work. In 2003 Sentmanat introduced a rotary viscosimeter [22] and patented it in 2004, see Figure 13. However, this viscosimeter is only suitable for higher molecular weight polymers. [23; 24]

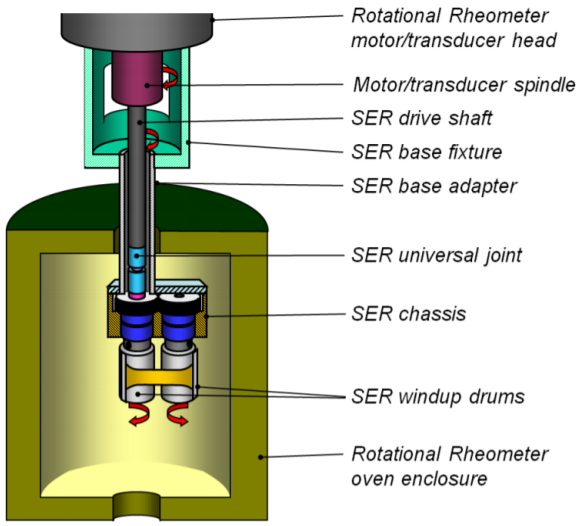

Figure 13: Description of the rheometer from Sentmanat's contribution to ANTEC in 2003 [22]

2.2 Technological processes crucially affected by elongation viscosity

Although elongation viscosity is a vital material parameter for many processing processes, three processes are selected for which elongational viscosity is essential. It is fibre spinning, foam extrusion and blow moulding.

2.2.1 Fibre spinning

Three conventional spinning processes making synthetic fibres are melt spinning, wet spinning, and dry spinning. The spinning process is based on extruding either a polymer in a solvent solution or a molten state through very fine holes with a diameter in the order of micrometers. Fibres are simultaneously extruded through a spinneret, a die comprising from 1 to 40 000 holes. In melt spinning, the bulk polymer is melted and extruded through a spinneret, and the liquid solidifies while passing through a cooling medium, see Figure 14. The molten fibres are stretched by force exerted by the take-up device positioned beneath the spinneret. During stretching, the molten fibres undergo, in the presence of quench air being blown across the fibres, phase transformation into semicrystalline phase and eventually solidifies. In the wet-spinning process, a spin dope is pumped into the spinneret, and the filaments thus produced in the spinning bath are passed through coagulating baths to yield solid filaments, see Figure 14. The originally added solvent is removed in coagulating baths by the mechanism of diffusion. The wet spinning process is less popular than the melt spinning process because it is more expensive to remove the solvent from the filaments spun. In general, more than one coagulating bath is needed to remove the solvent.

The dry spinning process, where a spin dope is pumped into the spinneret, is placed in an enclosed chamber (the drying tower) for solvent recovery, see Figure 14. Dry spinning is usually recommended when the polymer has no finite melting point or is easily degraded when heated. There are other ways of producing fibres such as air-gap spinning, shaped-fibre spinning, electrospinning or processes to produce nonwovens, but these will not be discussed in more detail in this thesis. [25; 26]

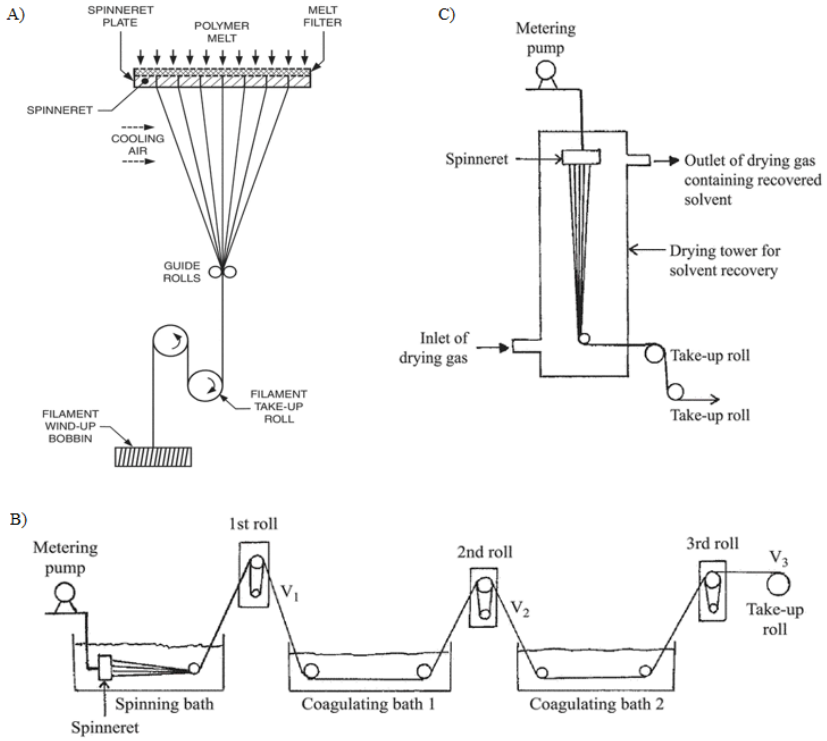

Figure 14: Schematic of the A) melt spinning, B) wet spinning, and C) dry spinning processes [25]

In all the described fibre spinning methods, the fibres are extensively stretched after exiting the die, as presented in Figure 15. Therefore, elongation viscosity is an important material parameter that can determine how well the polymeric material will form the fibres. [15]

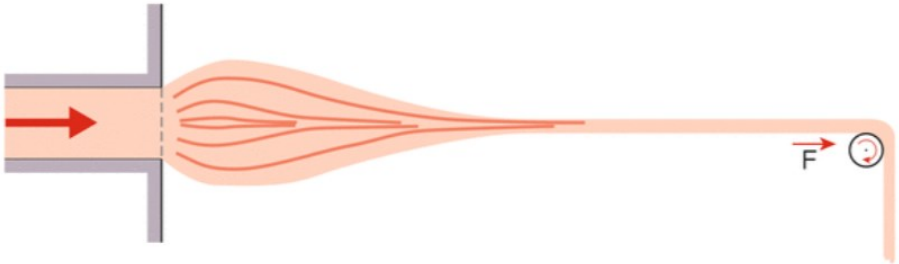

Figure 15: Schematic diagram of fibre elongation [15]

2.2.2 Polymer foams

Polymer foams are mostly made by two processes, namely, foam extrusion and structural foam injection moulding. Polymer foams are two-phase materials consisting of a solid polymer matrix and gaseous pores. In order to create a porous structure, blowing agents need to be used. These agents can be divided into physical and chemical blowing types. There are two methods of incorporating the blowing agents into a polymer melt. A continuous foaming process in which the polymer matrix undergoes gas saturation and foaming in one step. The second one is when the gas is incorporated into solid polymer under high pressure, a two-step process consisting of foaming agent saturation and actual foaming. Chemical blowing agents are mostly low-molecular-weight organic compounds that decompose at a critical temperature and release a gas, such as nitrogen or carbon dioxide. Examples of physical blowing agents include nitrogen, carbon dioxide and fluorocarbons. Depending on the application, foams can be divided into high-density and low-density foams. High-density, which consists of about 75–90 % of the bulk polymer, is generally used in structural applications, for instance, battery cases, doors or air-conditioner housing. Low-density foams, which consists of about 10–20 % of the bulk polymer, is used in many applications such as heat and sound insulation, shock mitigation or construction applications. Figure 16 shows the process of manufacturing thermoplastic foam particles. The particles are brought into the mould cavity with pneumatic conveyor equipment. These particles are fed out of a filling container into the filling injector, which brings the particles into the mould cavity. Air is used as a conveying medium. The conveying air streams through the perforated wall of the mould. The conveying is procured by pressure drop. Further processing of the foam particles is based on their placement in the mould, where they subsequently expanded by the action of heat, fill the cavity of the mould and acquire the shape of the final product. [27; 28]

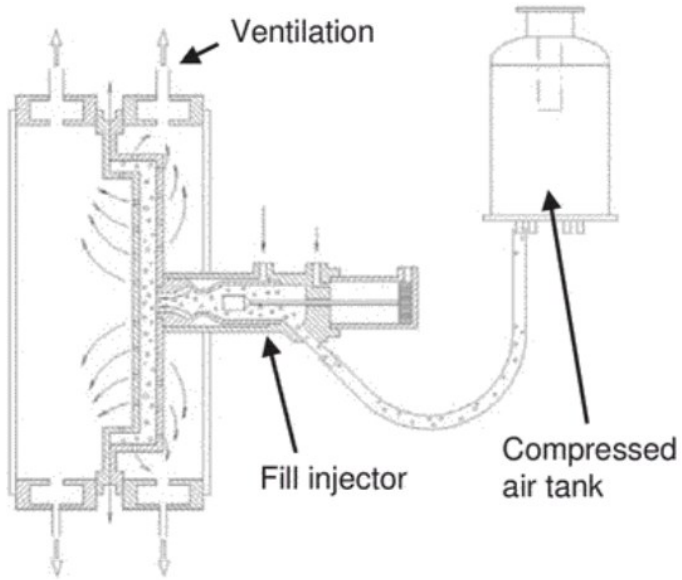

Figure 16: Schema of the mold with filling injector and pressure filling container [28]

In foam production, there is also a large elongation flow, specifically during the expansion of the blowing agent in the polymer matrix. Figure 17 depicts extension of polymer melt element between two bubbles. The elongation viscosity significantly affects the final form of the foam structure. Therefore, knowledge of this material characteristic is important here. [27; 28]

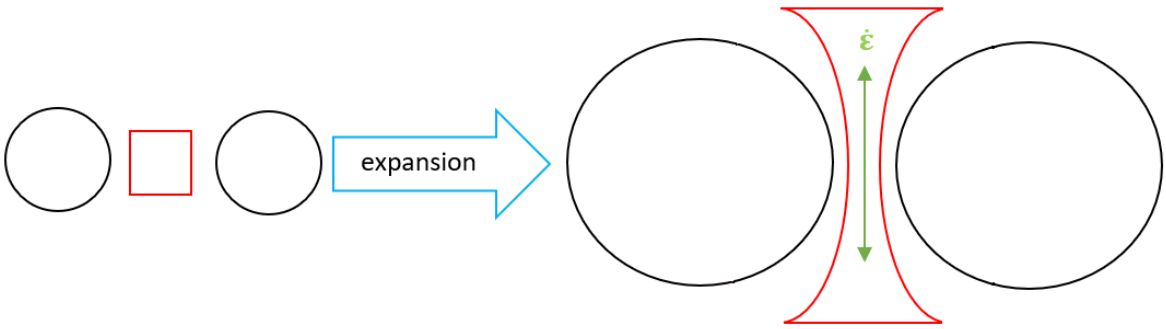

Figure 17: Schema of elongation flow in foaming process

2.2.3 Film blowing

In this process, a thin-walled cylinder is continuously extruded through an annular die and pinched at the top. At the bottom of the die, the air is introduced, inflating the tube to form a bubble, see Figure 18. An air ring is also used to rapidly cool the hot bubble and solidify it at some distance above the die exit. Expansion caused by the air pressure and the vertical pull results in a thinning of the cylinder. Thin films have many uses, for example, in the food industry or packaging. [26]

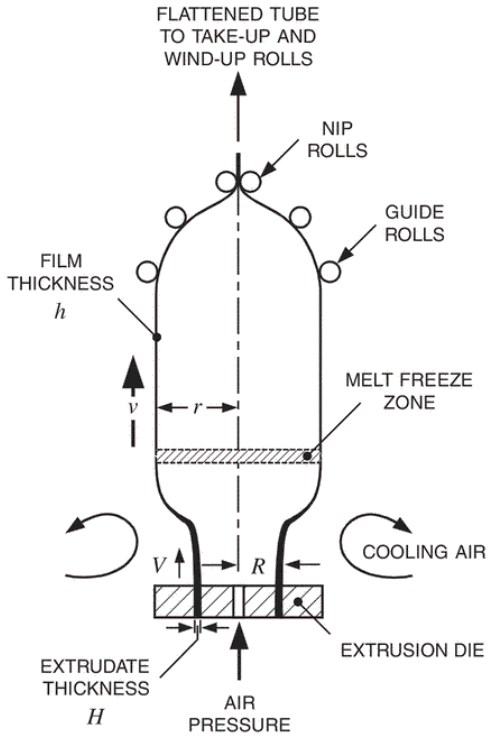

Figure 18: Schematic diagram of film blowing [26]

In this process, there is an intense elongation flow in the output of the material from the die, see Figure 19, where it is extended by blowing into a bubble ($\dot{\varepsilon}_1$) and elongated by a pull ($\dot{\varepsilon}_2$). There is a need to control the material's acceleration so that the material withstand the elongation flow, and there are no negative phenomena such as shark skin effect. [26]

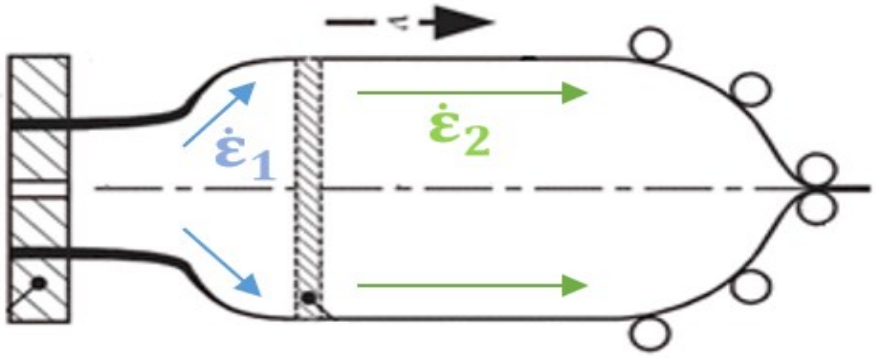

Figure 19: Schema of elongation in the film blowing process [26]

2.3 Process defects affected by elongation viscosity

Elongation viscosity plays an essential role wherever there is a speed redistribution (change of speed). These are places like sudden shrinkage in the extrusion die, joining layers inside the coextrusion die, extrusion of profiles. In these places, negative phenomena like vortex formation, instability and shark skin can occur. For the injection molding process, the great elongation viscosity of the injected melt reduces its leakiness. The product may not then achieve the desired shape at all. Elongation viscosity is also more sensitive to the polymer structure than shear viscosity thus profitable control of the supplied material could be performed with advantage by elongation viscosity evaluation. [9]

2.3.1 Shark skin effect

This defect occurs in extrusion and it is manifested by the wrinkled surface with the ridges running perpendicular to the extruded product's extrusion direction. To tear the free surface is due to too high shear stress on the channel wall. The formation mechanism is to change the velocity in the direction of the flow (elongation flow). The melt velocity profile is standard parabolic in the flow channel, see Figure 20, having a zero velocity on the channel wall. The melt accelerates on the surface by exiting the flow channel and transforms the speed profile into a rectangular one. If this acceleration is too fast, elongation too high, higher than the material can withstand, then it goes to tear the extruded profile's free surface. This effect primarily depends on temperature and extrusion speed. High-viscosity polymers with narrow molecular weight distribution seem to be most susceptible to shark skin instability. A less severe form of shark skin is mates of the surface, where the matte surface alternate with a glossy surface. [9; 29]

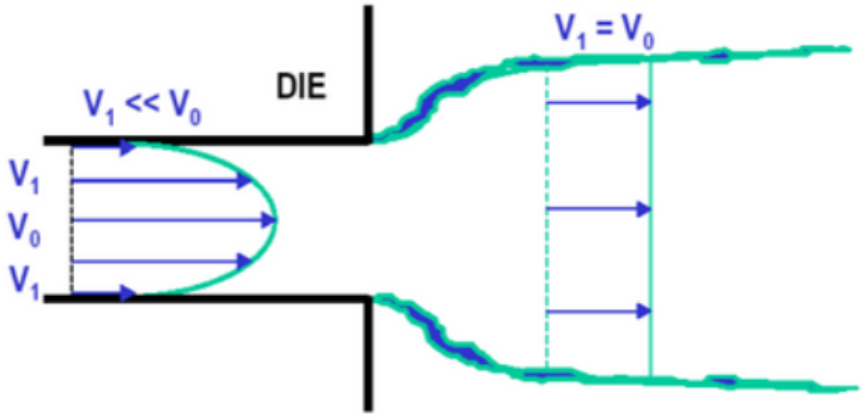

Figure 20: Output speed redistribution scheme from the extrusion die [30]

2.3.2 Wave instability

Wave instability occurs in the process of multiple layer extrusion. They are demonstrated through the undulation at the interface of two layers. The wave is characterized by large amplitude, and the resulting pattern on the product can almost appear as a parabola, see Figure 22. This problem arises at the first contact of two polymer melt layers having different flow speeds. If the flow of the first layer is much faster in comparison with the second one ($\dot{\varepsilon}_1 \gg \dot{\varepsilon}_2$), see Figure 21, causing that the second layer is not able to handle that kind of acceleration, consequently generates cracks, and the first material flows into them.

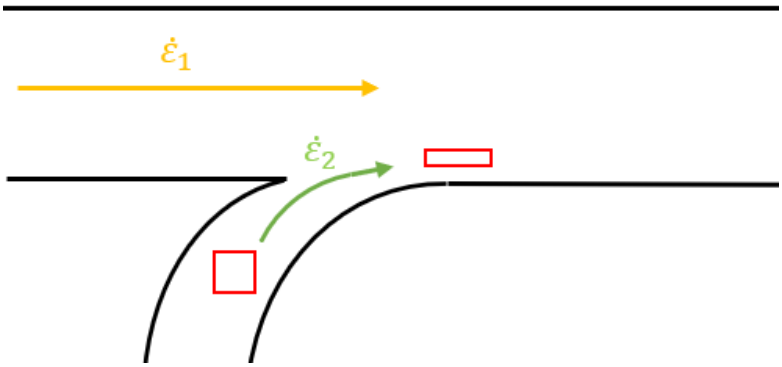

Figure 21: Two-channel junction schema where the melt element is stretched, represented by a red square [31]

Therefore, it is important to ensure a well-controlled channel flows in order to avoid such a large speed redistribution and minimise tensile deformation. The instability can also be corrected by adjusting individual materials' flow speeds or optimising the elongation viscosity of employed materials (the higher the elongation viscosity of the material, the less stable the co-extrusion flow). [32; 33]

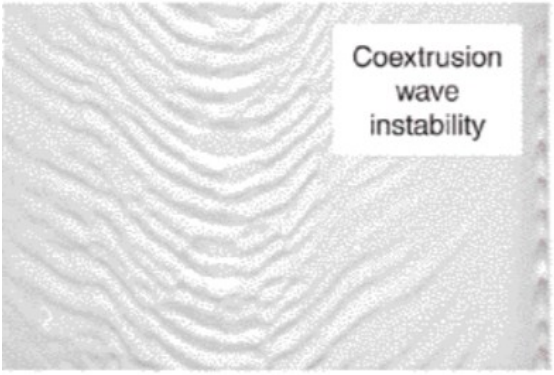

Figure 22: Interlayer instability wave pattern [32]

3 ELONGATION VISCOSITY MEASUREMENTS

The determination of the elongation viscosity can be divided into two groups. The first group includes methods that directly record the elongation of the polymeric material, most often by recording the force required for stretching. The second group consists of methods that calculate the elongation viscosity from other measured quantities, for instance, pressure losses.

3.1 Direct measurement of elongational viscosity

One of the multiple types of elongation flow is uniaxial extensional flow, also called simple extensional flow. It is a standard rheological flow like simple shear and is the most common measured flow type. So the common measurement of elongation viscosity is based on uniaxial flow deformation. Elongation viscosity is important for understanding processes such as fibre spinning, thermoforming, film blowing, film casting, blow moulding and foaming. These processes include a significant amount of extensional flow, which impacts both the final properties of the product and the design of flow channels. Although essential to the processes mentioned above, the knowledge of elongation viscosity can also be applied for injection moulding or profile extrusion optimisation, where it can be useful, for example, in designing moulds or dies. There are several methods for elongation viscosity evaluation, as describe bellow. [34; 35]

3.1.1 Uniaxial extensional rheometers

One of the first elongational rheometers was developed by Meissner. A rectangular strip specimen is extended in the horizontal direction by two rotary clamps in an oil bath. Meissner's rheometer belongs to the extensional rheometers group, where the polymeric samples are stretched in one direction, during which time the elongational stress is measured under a defined elongational rate. Some other examples of these rheometers are the Münstedt extensional rheometer, the Sentmanat extensional rheometer (SER), and vertical buoyancy bath. While a schema of Meissner’s extensional rheometer incorporating rotary clamps is shown in Figure 23, detail description of SER follows. [35]

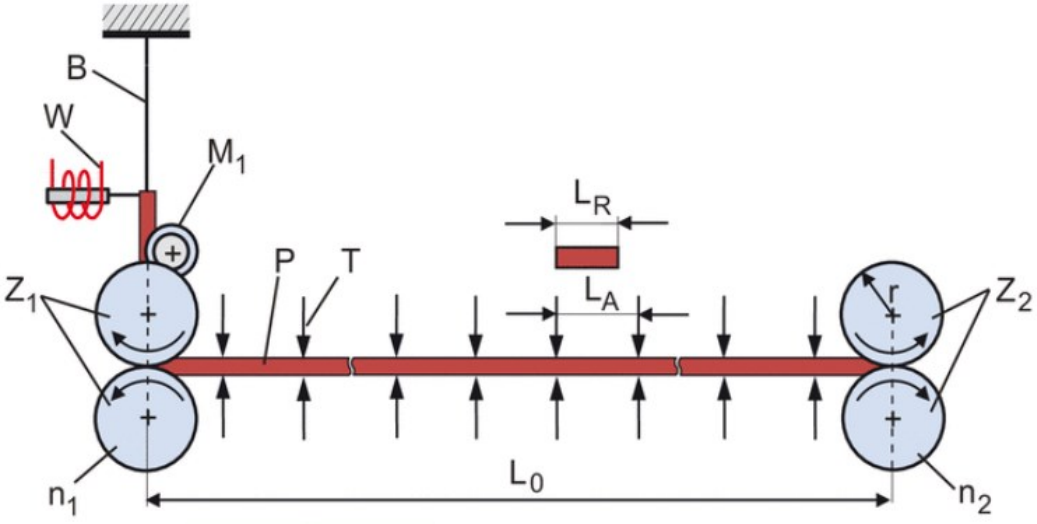

Figure 23: Schematic diagram of an extensional rheometer [36]

Sentmanat developed an extensional rheometer that takes advantage of the high strain and true applied strain rate capabilities of a fibre wind-up technique. This patented rheometer employs a dual wind-up drum technique that allows a sample's ends to be stretched using two counter-rotating drums whose resistance to rotation is hampered by the stretching sample's material response. The rheometer consists of two drums, master drum A and slave drum B, which are stored in bearings C (see Figure 24). Drums are mechanically driven by intermeshing gears D which are inside the chassis E. Driveshaft F rotates the master drum and an equal but opposite rotation of the slave drum. This rotation is caused by connecting with the ends of the samples H. Securing clamps I ensure a good connection between sample and drums. The stretching force acting on the master drum is borne by the driveshaft and subsequently by the drive motor and contributes nothing to the resultant torque T borne by the chassis and torque shaft G. Other symbols in Figure 24 are L_0 unsupported length, drive shaft rotation rate Ω and tangential force F. [37]

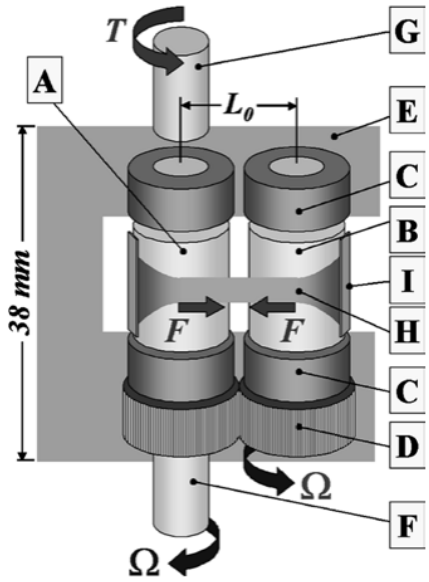

Figure 24: Schema of SER [37]

By a constant drive shaft rotation rate *Ω*, the Hencky strain rate applied to the sample specimen can be calculated using Equation 22.

$$\dot{\varepsilon} = \frac{2 \cdot \Omega \cdot R}{L_0} \tag{22}$$

where R is the radius of the equal dimension wind-up drums, and L_0 is the fixed length, which is equal to the centreline distance between the master and slave drums. The tangential stretching force F on the slave drum is counteracted by the force F', which is acting at the point of contact of the intermeshing gears, see Figure 25. For a 1:1 gear ratio, the gear force F' can be resolved from a sum of moments about the slave drum's axis of rotation, O' from Figure 25, resulting in the following Equation 23, where F_F is any frictional force contribution that may exist from the gears and bearings.

$$F' = \frac{2 \cdot R \cdot (F + F_F)}{L_0} \tag{23}$$

This force on the intermeshing gears is then translated as a radial force on the bearings centred along the slave drum's axis of rotation O'. The torque shaft is fixed to the chassis along the master drum's axis of rotation O. A summation of moments about axis O leads to the Equation 24. [37]

$$T = F' \cdot L_0 \tag{24}$$

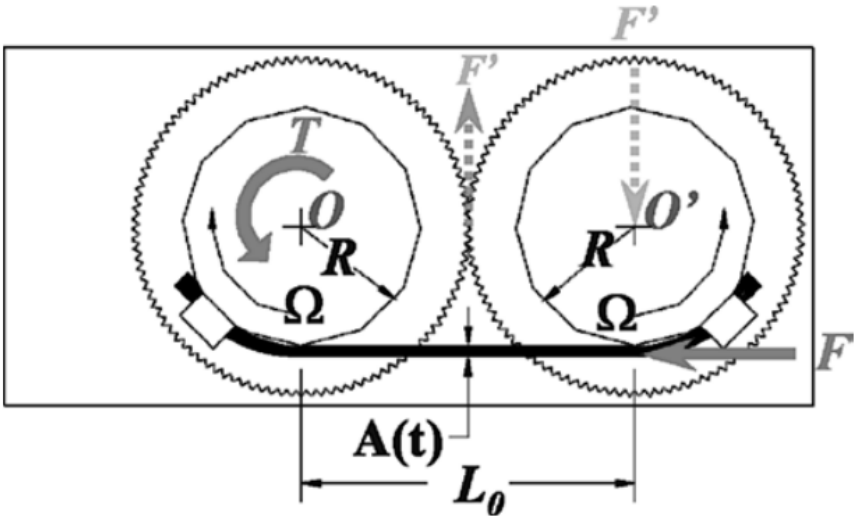

Figure 25: Illustration of force distribution on drums [37]

The addition of Equation 23 to Equation 24 leads to the relation expressed by Equation 25.

$$T = 2 \cdot R \cdot (F + F') \tag{25}$$

Under ideal conditions, the force friction component F' is minimal and can be neglected. So the expression for measured torque in Equation 25 can be simplified to Equation 26.

$$T = 2 \cdot R \cdot F \tag{26}$$

The instantaneous cross-sectional area $A(t)$ of the stretched specimen changes exponentially with time t for a constant Hencky strain rate experiment and can be expressed as Equation 27, where A_0 is the initial cross-sectional area of the unstretched specimen.

$$A(t) = A_0 \cdot e^{(-\dot{\varepsilon} \cdot t)} \tag{27}$$

For a constant Hencky strain rate, the tensile stress growth function $\eta_E^+(t)$ of the stretched sample can be expressed as Equation 28.

$$\eta_E^+(t) = \frac{F(t)}{\dot{\varepsilon}_H \cdot A(t)} \tag{28}$$

Figure 26 illustrates the typical course of the tensile stress growth curves for rib smoked sheet grade natural rubber (NR-RSS2) at room temperature performed at constant Hencky strain rates ranging from 0.00 s^{-1} to 10 s^{-1}. [37]

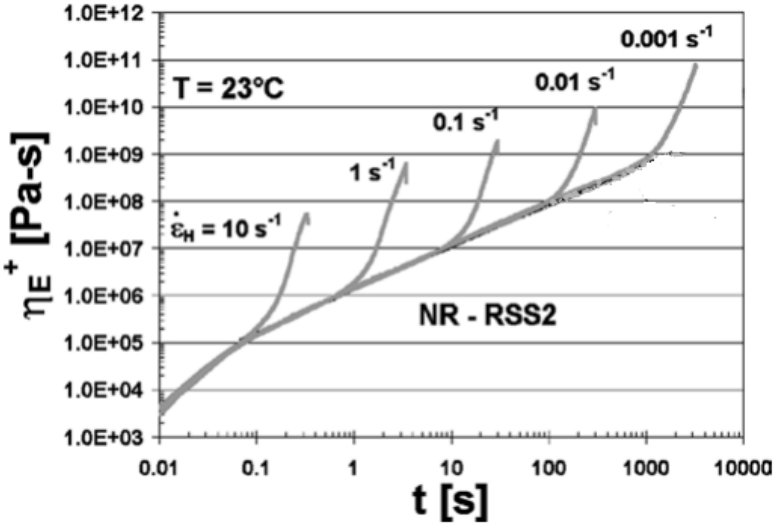

Figure 26: Tensile stress curves for NR-RSS2, where the axes are in logarithmic scale [37]

3.1.2 Biaxial and multiaxial extensional rheometers

Biaxial and multiaxial extensional rheometers are possible to employ for characterisation of high viscosity polymers and rubber. Rheometers have translating clamps that move in the orthogonal axis. They can move the sample in all directions, generating an equibiaxial extension of the sample. A rotating clamp device for high viscosity liquids sheets has been developed by Meissner and co-workers in 1982, see Figure 27. It is analogous to the rotating clamp for a uniaxial extension, see Figure 23. For equibiaxial extension, eight pairs of cylindrical rollers are arranged in an octagonal pattern. Other arrangements can give uniaxial, planar, or any other combination of extensions. Figure 27 shows three types of arrangements of rotating clamps. A is an equibiaxial arrangement, where S is a sample and C_i is one of eight pairs of scissors. Transducers T to L record the forces. B is a planar arrangement, where clamps A to F rotate with constant speed, while G and H remain stationary and recording only force. C is a multiaxial arrangement with ellipse axes, where the sample can be deformed in different directions [34; 38]

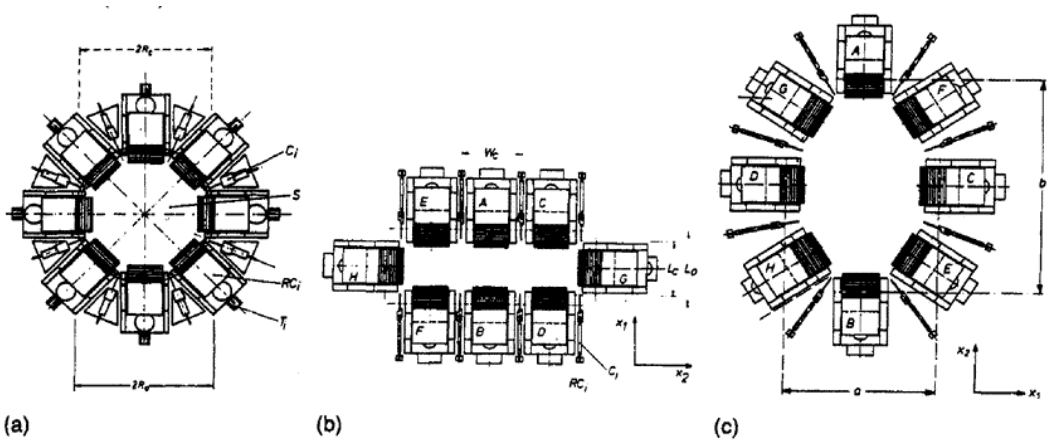

Figure 27: Various arrangements of rotating clamps [38]

3.1.3 Bubble blowing systems

In this method, a sheet is clamped between two plates with circular holes, and a pressure differential is introduced to deform it and blow it into the bubble. The deformation and applied pressure are monitored over time. By the radius of the bubble, the extensional rate and the extensional strain can be measured. The pressure difference and the interfacial tension allow evaluation of the elongational stress. This system is schematically depicted in Figure 28. This method can be used to measure polymer membranes' extensional properties for blow molding and thermoforming applications. [34]

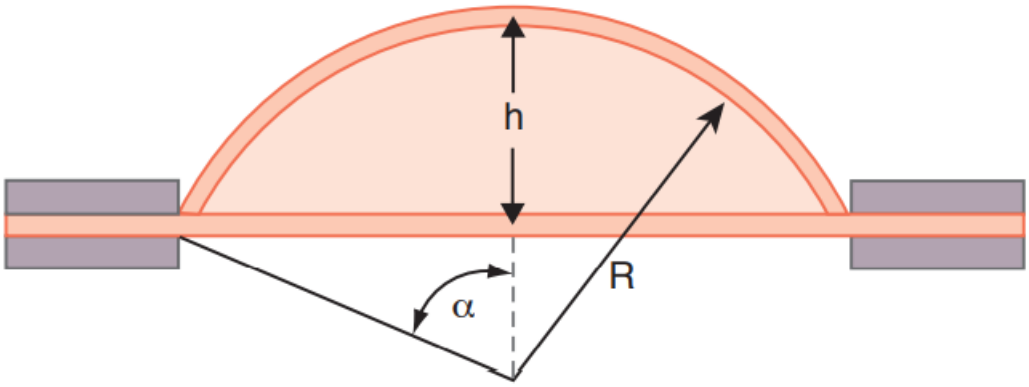

Figure 28: Schema of the bubble blowing system [15]

3.1.4 Fibre spinning systems

Fibre spinning rheometers provides reliable results for low viscosity samples. The polymer is continuously extruded and stretched by rotating wheels, and the wheels measure the force with a load cell, see Figure 29. These methods include the tensile tester, which is called Rheotens. It was developed by Meissner between the years 1969 and 1971. In the Rheotens system, the polymer melt is first subjected to simple shear flow in the extrusion die, followed by uniaxial extension under constant force in the spin line. In the Rheotens test, there is the drawdown force needed for elongation of an extruded strand measured as a function of a slowly increasing draw-down speed. The measured tensile force F at the take-up is a complicated function of the properties of the polymer melt, the die diameter d_0, the length L_0 of the die land and the length L of extruded string, as well as the processing conditions such as extrusion pressure p, die exit velocity v_0, melt temperature T, and drawdown velocity v. [34; 39]

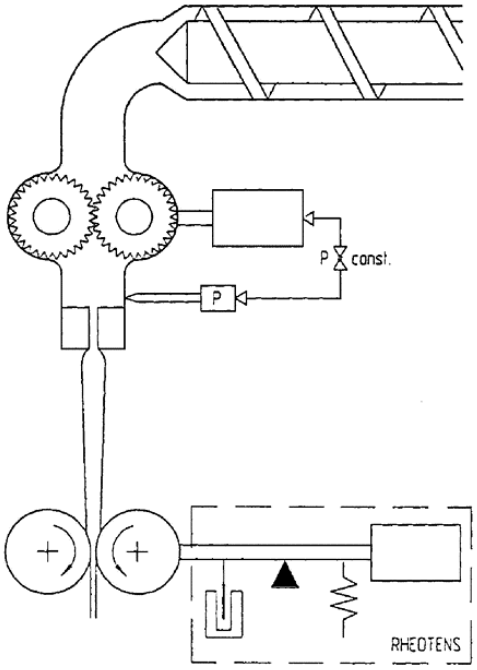

Figure 29: Schema of the Rheotens extensional rheometer [39]

The tension stress σ in the polymer melt at the end of the extruded string, concretely between the wheels of the Rheotens, depends only on the rheological history. It is a function of the Deborah number and is proportion to a modulus G, the plateau modulus of the polymer melt. Deborah's number indicates the ratio between the material's characteristic relaxation time and the observation time. By arguments detailed by Wagner and Bernnat in 1998, it can be

shown that a master curve for melt tension can be obtained by scaling the draw ratio *(V = v/v0)*, by a shift factor *b*, see Equation 29.

$$\sigma = Gf\left(\frac{V}{b}\right) \tag{29}$$

The drawdown force *F* is the result of tension and cross-section of the strand, *[A(L) = A0/V]*, where A_0 is the cross-section of the die. Then the force can be expressed as Equation 30.

$$F = \frac{\sigma \cdot A_0}{V} \tag{30}$$

The invariance of the force-extension diagram is obtained as Equation 31.

$$b \cdot F(V) = \frac{\sigma\left(V/b\right) \cdot A_0}{V/b} = F_r\left(V/b\right) \tag{31}$$

Equations 30 and 31 represent Rheotens grandmaster curves covering also special cases of the Rheotens super-master curves (invariance changes in mass flow rate or extrusion pressure at constant geometry of die), and Rheotens master curves (invariance concerning changes of temperature and constant geometry of die and average molar mass of the polymer melt at constant extrusion pressure). Examples of typically measured curves are shown in Figure 30. [34; 39]

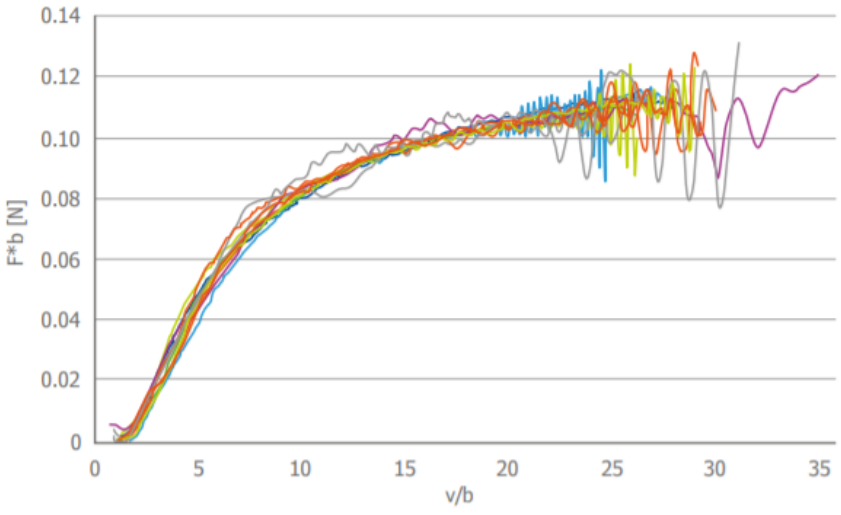

Figure 30: Typical Rheotens grandmaster curves [40]

The model is based on the following experimental evidence. When optical methods measure the filament velocity along the spinline, it is found that below a critical draw ratio *Vp*, the velocity increases in approximation linearly with the spinline length *x*. In contrast, for higher

draw ratios, the velocity increases over-proportionally with *x*. In the linear regime, the extensional rate is constant. It can be expressed by Equation 32, where $\{Vs = {}^{v}/_{v_0}, (x = 0)\}$, is the extrapolated starting point of the drawdown and describes an effective extrudate swell of the filament due to the viscoelastic deformation of the polymer melt in the extrusion die.

$$\dot{\varepsilon} = \frac{v_0}{L} \cdot (V - V_s) \tag{32}$$

The drawdown force *F* can be readily obtained as Equation 33:

$$F = F_p \frac{V - V_s}{V_p - V_s} \tag{33}$$

where F_p is the drawdown force necessary to achieve the critical draw ratio V_p and the critical tension σ_p at the end of the spinline. The melt tension can be expressed as Equation 34:

$$\sigma_p = \frac{F_p \cdot V_p}{A_0} \tag{34}$$

Elongation viscosity can then calculate in Equation 35:

$$\eta = \frac{\sigma_p}{\left({}^{v_0}/_{L}\right) \cdot \left(V_p - V_s\right)} \cdot \left(\frac{V}{V_p}\right) \tag{35}$$

Equations 32–35 are valid in the linear starting part where extensional strain rate is constant, so the elongational viscosity increases with increasing deformation. For excessive-velocity increase along the spinline can be described by a power-law dependence (with power-law index n < 1). Then the expression for melt tension is described in Equation 36:

$$\sigma(x) \approx \left(\frac{\partial v(x)}{\partial x}\right)^n \tag{36}$$

Combining the power-law model with the viscoelastic start-up regime, the drawdown force could be defined in Equation 37:

$$F = F_p \cdot P(V) \tag{37}$$

where factor *P* can be expressed as Equation 38:

$$P(V) = 1 + \frac{n}{(n-1)} \cdot \frac{V_p}{\left(V_p - V_s\right)} \cdot \left[\left(\frac{V}{V_p}\right)^{\frac{n-1}{n}} - 1\right] \tag{38}$$

The extensional rate $\dot{\varepsilon}$ at the end of the spinline, where $(x = L)$, is obtained as Equation 39:

$$\dot{\varepsilon} = \frac{v_0}{L} \cdot (V_p - V_s) \cdot \left(\frac{V}{V_p}\right)^{\frac{1}{n}} \cdot P(V) \tag{39}$$

Then the apparent elongational viscosity at the end of the spinline is given by Equation 40:

$$\eta = \frac{\sigma_p}{\left(\frac{v_0}{L}\right) \cdot (V_p - V_s)} \cdot \left(\frac{V}{V_p}\right)^{\frac{n-1}{n}} \tag{40}$$

Thus the model has four free parameters: the effective extrudate swell described by V_s, the critical draw ratio V_p, the critical tension σ_p, and the power-law index n. A typical example of calculated curves from the equations above shows Figure 31. [39]

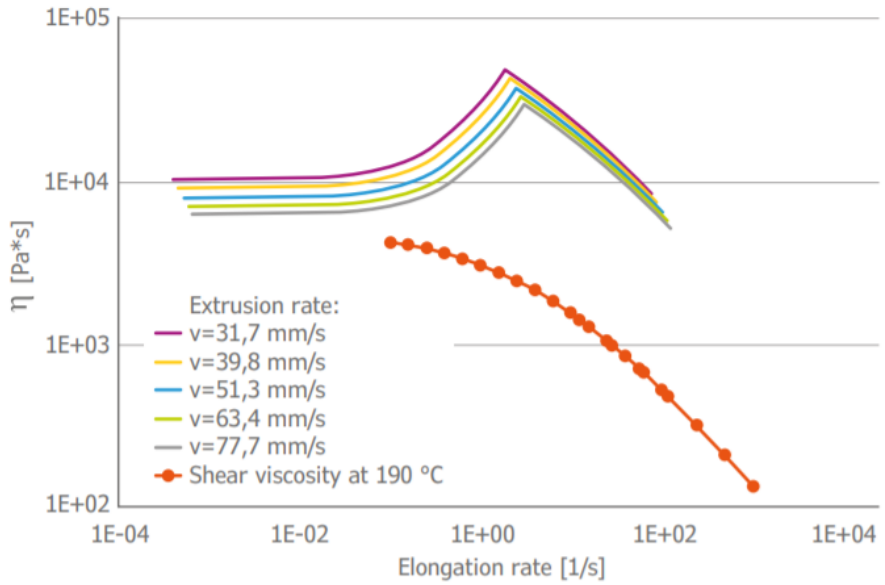

Figure 31: Elongational viscosity curves for different extrusion rate with comparison to shear viscosity [40]

In Figure 31, the initial part of the viscosity curves increases with elongational viscosity and corresponds to the viscoelastic start-up regime. The maximum is reached at the critical tension. Then at higher extensional rates, the apparent elongational viscosity decreases according to the power-law model. [39]

The Rheotens device closely resembles the HAUL-OFF machine, see Figure 32. It is also currently manufactured by Göttfert and it is intended for measurement of the melt elongation under constant pull-off speed or under linear or exponential acceleration of the pull-off strand. The HAUL-OFF has been specially designed for measurements at high pull-off

speeds. In contrast to the Rheotens, the experiment cannot be started at zero speed. The strand already needs to be pre-tensioned for the deflection at the pull-off wheel. One of the advantages is that the force resolution is 20 times better than that of the Rheotens. [40]

Figure 32: HAUL-OFF rheometer

3.2 Indirect measurement of elongational viscosity

The most popular methods of measuring elongational viscosity are the pressure drop in sudden flow contraction and the stagnation flow. To calculate the extensional viscosity from the entrance pressure-drop, Cogswell, Binding, and Gibson developed three mostly used analyses. [34]

3.2.1 Cogswell's method

To elucidate the Cogswell method, it is necessary to start with the classical capillary rheometer, which measures the fundamental quantities required for calculation. The simplified principle of capillary rheometry is presented in Figure 33. Firstly, the barrel is filled with polymer pellets. In the second phase polymer pellets are heated and simultaneously compressed by the plunger. In the third phase, the plunger pushes the melted material through a capillary die with known length *L* and diameter *D*. The computer specifies the plunger velocity through a program, and then pressure measurements are recorded. The pressure transducer is placed at the bottom of the die. [11]

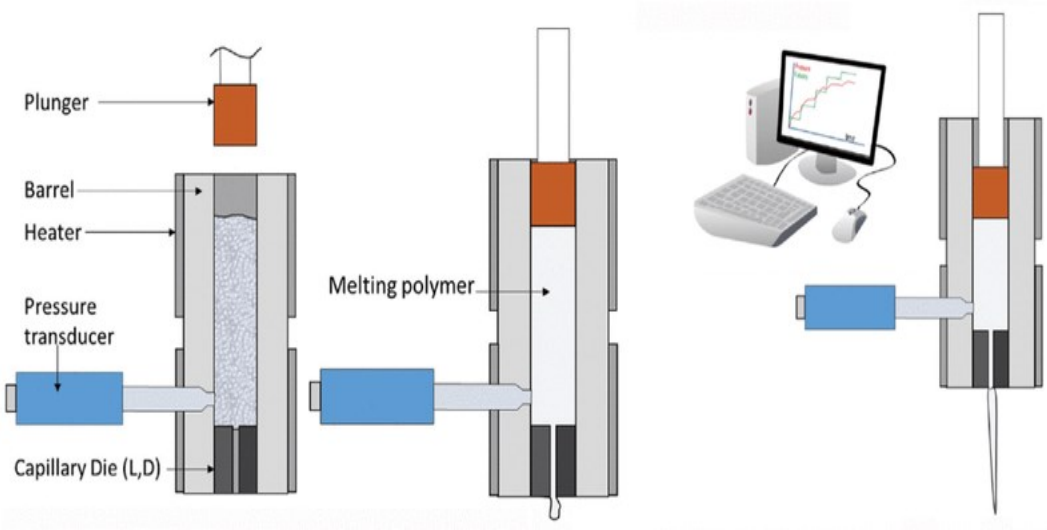

Figure 33: Principle of capillary rheometer [11]

The shear rate $\dot{\gamma}$ can be calculated by knowing the flow rate Q in the capillary die and the capillary radius R:

$$\dot{\gamma} = \frac{4 \cdot Q}{\pi \cdot R^3} \tag{41}$$

The flow rate can be calculated using Equation 42, where *S* represented barrel cross-sectional area and *v* represented the plunger's speed.

$$Q = S \cdot v \tag{42}$$

Equation 41 holds true only for Newtonian fluids. However, polymer melts are typically non-Newtonian fluids. Thus correction is necessary. Rabinowitsch proposed the correction in 1929 [41], and this correction is still widely used, see Equation 43. Rabinowitsch correction is mentioned here for the completeness of the calculations, although Cogswell has not yet considered this correction in its calculations.

$$\dot{\gamma}_c = \frac{3 \cdot n + 1}{4 \cdot n} \cdot \frac{4 \cdot Q}{\pi \cdot R^3} \tag{43}$$

To calculate the corrected shear rate at the wall $\dot{\gamma}_c$ it is necessary to evaluate the local pseudoplastic index *n*, which can be expressed as defined in Equation 44, whre τ_w is the shear stress at the wall.

$$n = \frac{\partial log(\tau_w)}{\partial \log(\dot{\gamma})} \tag{44}$$

Shear stress calculation is based on pressure measurement in the capillary die. However, the measured pressure ΔP_m is a combination of the capillary pressure drop ΔP_c and the entrance pressure ΔP_e, see Figure 34.

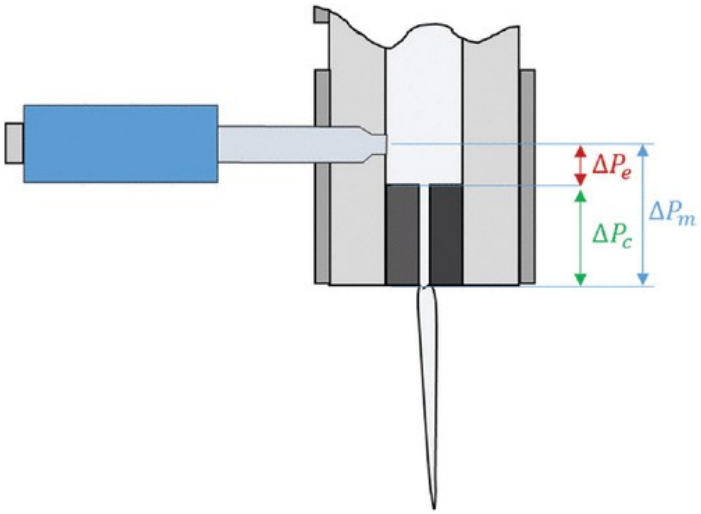

Figure 34: Schema of pressure measurement [11]

For further calculations, a correction of the measured pressure should be introduced to establish the pressure drop value in the capillary. Bagley developed this correction in the 1950s. [42] This correction use dies with several different *(L/D)* ratios. After measurements with different dies is obtained pressure chart, see Figure 35.

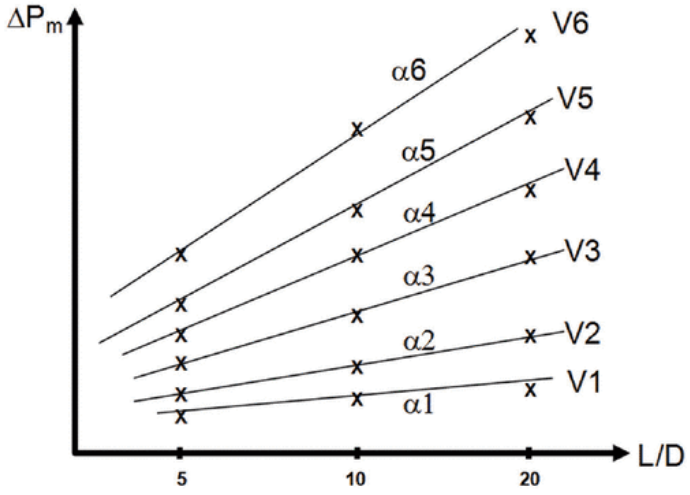

Figure 35: Pressure curves measured with three different dies [11]

The corrected shear stress at the wall can be determined by the slope of each obtained linear regression calculated based on Equation 45:

$$\tau_c = \frac{\Delta P_c \cdot R}{2 \cdot L} = \frac{(\Delta P_m - \Delta P_e) \cdot R}{2 \cdot L} \tag{45}$$

After calculation Rabinowitsch-corrected shear rates and Bagley-corrected shear stress at the wall, the corrected shear viscosity can be calculated as Equation 46. [11]

$$\eta_c = \frac{\tau_c}{\dot{\gamma}_c} \tag{46}$$

The previous text concerned the general calculation of rheological quantities using measured parameters from a capillary viscometer, now specifically Cogswell's method. Cogswell published in 1972 work describing the elongational flow in capillary [19]. The flow into a contraction has an extensional character along the centreline. For many fluids, there are recirculating vortices form in the corners, and the main flow is through a funnel-shaped section near the centre of the flow field. Contraction flow is not pure elongation flow, see Figure 36. A vortex appears in the corners. Thus Cogswell made some simplification for the calculation of flow. [2]

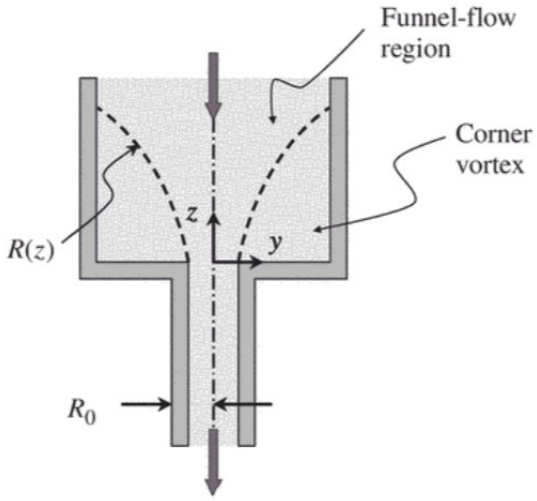

Figure 36: Flow geometry intended by Cogswell [2]

By Cogswell, the elongation voltage can be calculated according to Equation 47:

$$\sigma_E = \frac{3}{8} \cdot (n+1) \cdot P_e \tag{47}$$

The rate of deformation can be expressed by Equation 48:

$$\dot{\varepsilon} = \frac{4}{3 \cdot (n+1)} \cdot \frac{\tau_c \cdot \dot{\gamma}}{\Delta P_e} \tag{48}$$

Elongation viscosity can then be calculated by casing relationship, see Equation 49:

$$\eta_E = \frac{\sigma_E}{\dot{\varepsilon}} \tag{49}$$

[43]

3.2.2 Binding's method

Binding follows Cogswell closely in his analysis. Binding's method is only in some ways more accurate without neglecting quantities, such as Rabinowitsch correction. It has been found that the Binding model is more precise than the Cogswell model for commonly used polymers, such as low-density polyethylene (LDPE). However, for elastic fluids (for example a solution of a polyacrylamide mixed with a corn syrup) is not accurate enough. Cogswell provided a simple analytical analysis, which involved splitting entry flow into separate shear and extensional components. Cogswell was able to estimate the extensional viscosity of polymer melts from entry pressure data. Cogswell's analysis is, strictly speaking,

incorrect since he uses a shear rate based on a Newtonian fluid in conjunction with a velocity field determined for a power-law fluid.

However, to make the method solvable, Binding also resorts to some assumptions about the funnel's shape, and, like Cogswell, he neglects any influence of elasticity on the normal stresses calculated. His intended scheme of the rheometer is the same as that of Cogswell, see Figure 36. [20; 44]

3.2.3 Gibson's method

To estimate the extensional viscosity of glass fibre-filled polymer melts, commonly used in the injection moulding technology, Gibson derived another entry flow analysis [21]. Gibson used a spherical coordinate system whose origin is on the centre line at the capillary entrance to derive equations for pressure drop due to shear and extensional flow in the entrance region. A key difference from Binding and Cogswell's work is that Gibson did not attempt to predict the profile of convergence into the capillary. Gibson stated that his model is equally applicable whether the entrance flow pattern shows recirculation regions or not because he assumed that the dominant source of the entrance pressure drop is extensional flow, which does not depend strongly on the velocity profile across the die. [45]

3.3 Online rheometers

In industrial applications, there is often a demand for valid and reliable online process surveillance control. It is desired to monitor the polymer viscosity during processing. Online rheometers usually have a shear viscosity sensing capability and a bypass line integrated into the unit. Moreover, converging dies can be used in online process control by monitoring the extensional viscosity. One of the significant advantages of online rheometers over conventional laboratory testing of samples is immediate results with no time lag between production and quality problems detection.

Furthermore, the rheological behaviour of the polymer may be influenced by its processing history. Thus, when routinely preparing a sample for testing in a laboratory, the sample's material characteristics may be affected. It is, therefore, advantageous to test the material directly during production. For these reasons, there is an effort to incorporate in- and online rheometers directly into processing machines. Inline rheometers could be applied directly to the melt stream, and process data could be digitally stored and analysed. Figure 37 depicts a simplified drawing of an online rheometer and its sections. Part A indicates barrel part of

compounder with main melt stream, part B inlet of rheometer, part C melt pump, part D slit die with bores for pressure transducers and temperature sensor, part E, and part F indicates bypass valve and return to main melt stream in part G. [46]

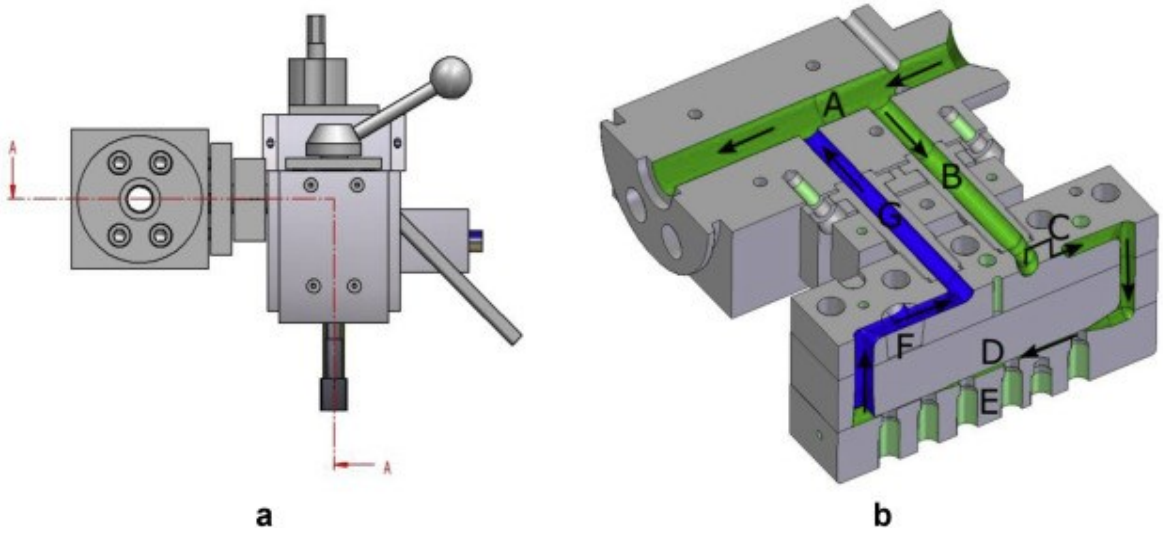

Figure 37: Schematic section of an online rheometer [46]

II. ANALYSIS

4 THE AIM OF THE WORK

This work is focused on a broadening of the rheological understanding of polymer melts processing. The characterisation of elongation viscosity of polymer materials is not yet a much-explored topic. That is why this work could help in the processes optimisation where large elongation flows are expected. The practical part examined the polypropylene material, specifically two of its types, TOTAL, an extrusion linear homopolymer type and DAPLOY branched high melt strength one (HMS), used in practice for modification of PP melt strength and elongational flow behaviour. By combining the knowledge of elongational viscosity and the ability to form a polymeric foam, coherent results were searched in order to broadening current knowledge in the field of polymer foams manufacturing.

5 MATERIALS AND SAMPLE PREPARATION

Description of employed materials and the procedure of the foam samples preparation is described in the following chapter.

5.1 Materials employed

In the experimental part of this work, the following materials have been used:

1) **Polypropylene PPH 1060 TOTAL**

Producer: Total Petrochemicals

PP TOTAL is a homopolymer of linear polypropylene. This material is intended for processes such as pipe and sheet extrusion. Typical applications are potable water pipes and profiles. The melting temperature is 165 °C and mass flow rate (MFR) at temperature 230 °C of 0.3 g/10 min. [47]

2) **Polypropylene DAPLOY WB140 HMS**

Producer: BOREALIS

DAPLOY HMS PP is used in various applications that require more performance, by using less raw material. The unique long-chain branched (LCB) structure offers superior foamability and homogenous fine cell foam structure, even at the lowest densities. HMS PP is 100 % recyclable mono-material, which can be used for a wide working temperature range from -10 °C to 125 °C, with melting point 163 °C and with MFR at 230 °C of 2.1 g/10 min. It is a re-useable service ware. The application can be the drinking cup based on HMS PP foam, which has ground-breaking potential as a possible replacement for expanded polystyrene material. [48]

5.2 Preparation of compounds of PP TOTAL and PP DAPLOY

Polymer granules of PP TOTAL and PP DAPLOY HMS materials were compounded using a twin-screw extruder Lab-Compounder Brabender KETSE 20/40 (see Figure 38). The compounds were prepared in the mass ratio PP TOTAL/PP DAPLOY_20/80 wt.% and PP TOTAL/PP DAPLOY_40/60 wt.%. Processing conditions are listed in Table 1. The extruded polymeric string was cooled in a cold-water bath, cut by a granulator, and dried by hot-air dryer.

Figure 38: Lab-Compounder Brabender KETSE 20/40 with a cooling bath and a grinding mill

Table 1: Process conditions of compounding

Zone number	**Set temperature [°C]**
1	180
2	185
2	200
4	215
5	220
Die	220
Rotations per minute	
200	

5.3 Foams manufacturing

The foams preparation and their characterization were in charge of doc. Ing. Tomáš Sedláček, Ph.D.

For the manufacturing of the foams, PP TOTAL and PP DAPLOY were utilised with the addition 3 wt.% of talc as a nucleating agent. The 40 wt.% talc concentrates made of PP TOTAL and PP DAPLOY were previously prepared under the analogue conditions as in the case of compounding described above. The production of foams was carried out using a single screw extruder at temperatures from 170 °C up to 250 °C. In two-thirds of the screw length, the physical foaming agent, CO_2, was injected under pressure into the polymer melt via high-pressure pump. Polymer melt was further transferred to a dynamic mixer (see Figure 39) in order to prepare propriate gas dispersion in the melt and accurately control temperature of polymer melt.

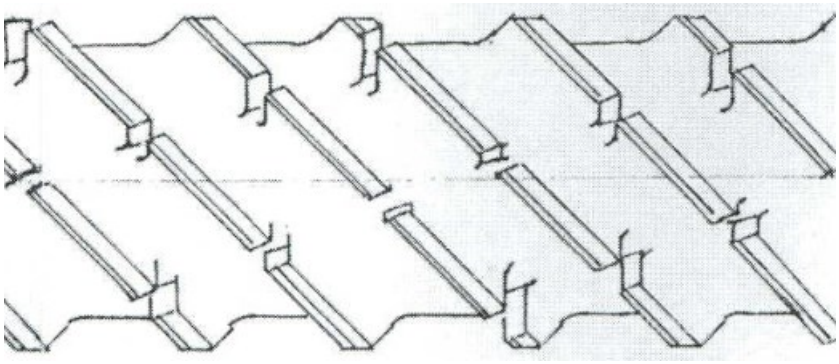

Figure 39: Schema of dynamic mixer [49]

Finally, the mixed system was extruded through a flat die of rectangular shape with dimensions (2x10 mm) at temperature between 180 °C (used for DAPLOY and compounds) and 240°C (used for TOTAL), see Figure 40. This flat die also served as an online viscosimeter for recording rheological data from the foam extrusion.

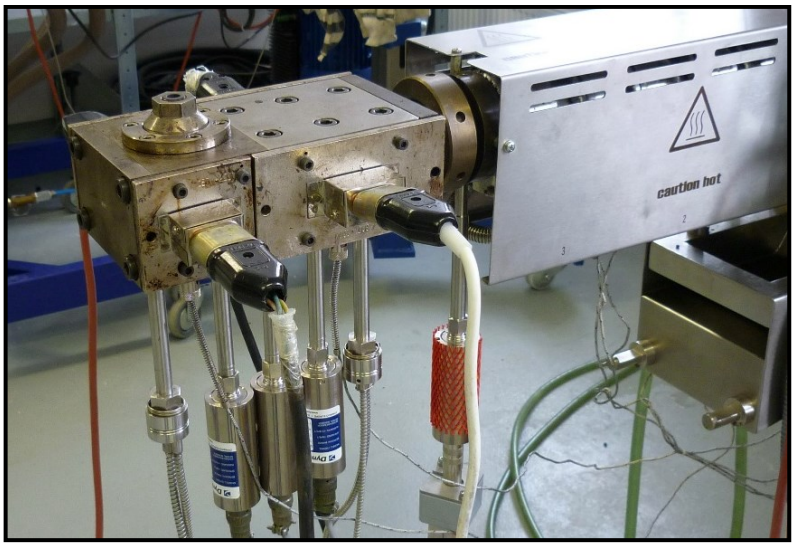

Figure 40: Flat die as an online viscosimeter

5.4 Manual pressing of testing plates

The testing specimens for rotational rheometry characterisation with dimensions of 150x150x0.5 mm were prepared at temperature of 220 °C from granules utilizing manual presses displayed in Figure 41. The specimens were consequently cooled down by cooling press tempered by the cold water of the temperature 15 °C. For each tested material (PP TOTAL, PP DAPLOY) several plates were prepared.

Figure 41: Hand presses

6 TESTING EQUIPMENTS AND METHODOLOGIES

The utilised devices and experimental methods used for characterisation of the rheological properties of foamed extrudates and employed materials are described in the following paragraphs.

6.1 Optical microscopy

Bruker Alicona G4 optical metrology system, exhibited in Figure 42, was used for description of the obtained polymeric foams pores structures. Optical microscopes have a resolution (the ability to distinguish two points) up to 0.2 μm. Results of microscopy characterization of polymer foams are presented further in Chapter 7.1. [50]

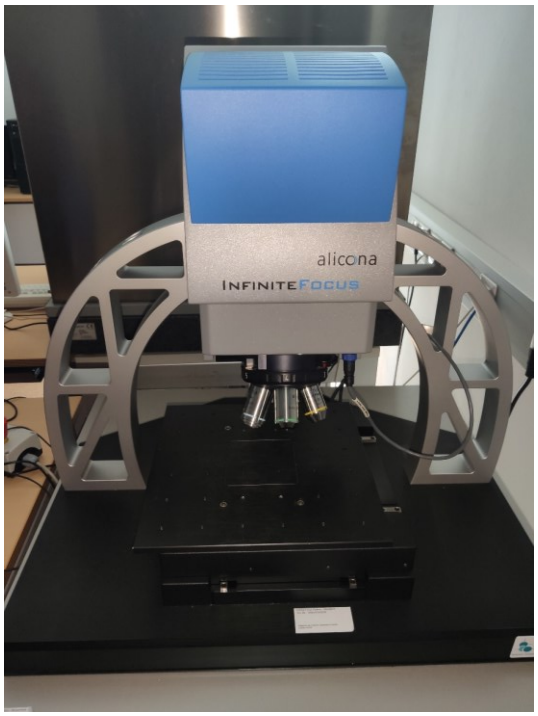

Figure 42: Bruker Alicona G4 optical metrology system

6.2 Roentgen tomography

3D Roenten microscopy scanner Bruker Skyscan 1174 based on computer tomography (CT) measuring principles was used for polymer foam structure determination, see Figure 43. This scanner uses an x-ray source with adjustable voltage. A camera has a 1.3 megapixel. Variable magnification (6-30 μm pixel size) is combined with object positioning. The full range of SkyScan software is supplied, including fast volumetric reconstruction and software for 2D/3D quantitative analysis. The attachment of the sample within the device is shown in Figure 44.

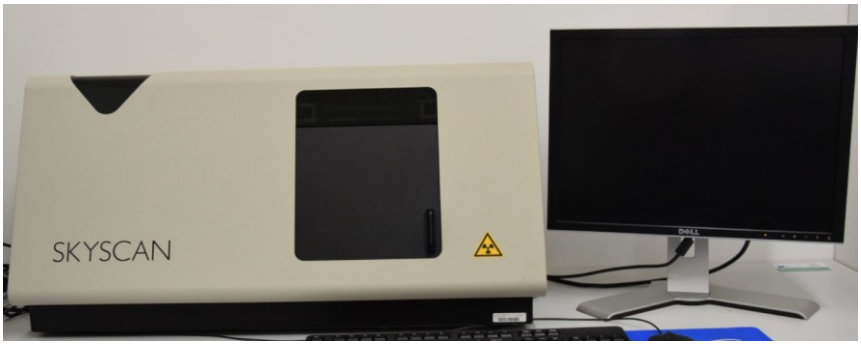

Figure 43: 3D roentgen tomograph by Bruker company

The measured sample was clamped in the tomograph manipulator between the X-ray emitter and the detector with a resolution of 1304x1024. Due to the material composition and thickness of the sample, the most suitable accelerating voltage of 33 kV, an electric current of 320 μA, and electric power of 12 W were applied. The shutter speed, the length of time one frame is taken, has been set to 9000 ms. The measured sample was scanned in a 0.5 ° step in the range of 0 ° to 360 °. At each step, the sample was scanned 3 times. The scanning time of one sample under the mentioned conditions was about 400 minutes. Once the sample scan was completed, the acquired images were evaluated using software analysis, which consists of removing circular artefacts and smoothing individual images, followed by assembling a 3D model of the measured samples and creating images and videos in individual sections of the sample. Results of tomography characterization of polymer foams are presented further in Chapter 7.2. [51]

Figure 44: Attachment of the sample in Skyscan device

6.3 Online viscometry

A Leistritz Elongational Rheometer, the same one as used in [46], was utilised for description of employed materials rheological behaviour, see Figure 45.

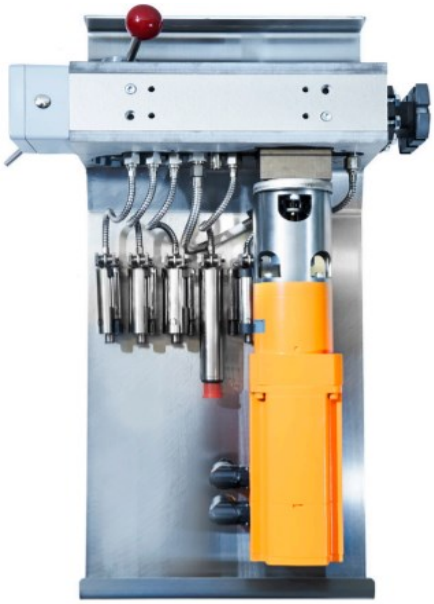

Figure 45: Leistritz online rheometer [52]

The rheometer has a patented die geometry with a hyperbolic narrowing that generates a constant elongational flow. During the extrusion process, a small amount of the melt flow is channelled off via a bypass system and pushed through the rheometer's slot die. After the viscosity evaluation, the material is transferred back into the main processing line without losing any material. The online rheometer is described in more detail in Chapter 3.3. [52]

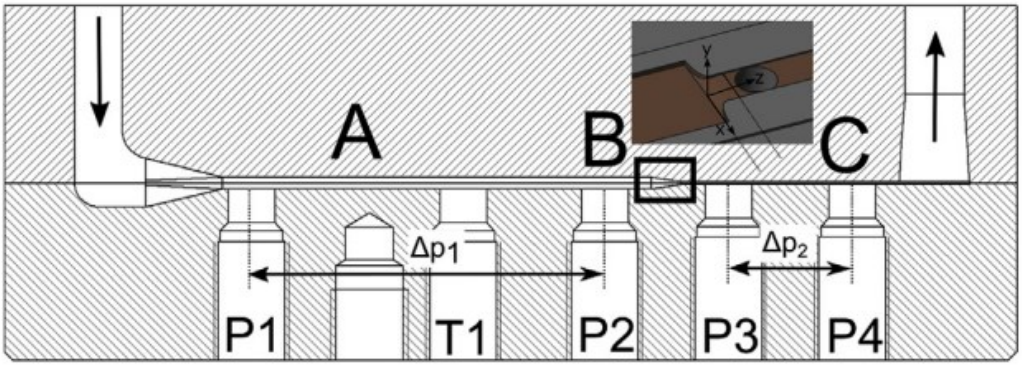

Figure 46: Schema of the slit die for online extensional and shear viscosity measurement [46]

There are several parts of the online rheometer, see Figure 46, A is the first slit section with pressure drop Δp_1, B represents contraction part with pressure drops $\Delta p_{shear} + \Delta p_E$, C is the second slit section with pressure drop Δp_2 and T_1 represents temperature sensor.

6.4 High-pressure capillary viscometer

The capillary rheometer Göttfert RG 50, presented in Figure 47, was used for evaluation of the shear/elongation viscosity at high shear/elongation strain rates of the tested polymer melts.

6.4.1 Shear viscosity measurements

In the capillary rheometer, the piston exerts the pressure required for the generation of shear stress. The measured values are the pressure drop along the capillary length, the temperature and the material volume flow. The calculated shear stress and shear rate are usually corrected with Bagley (correction of the entrance pressure drop) and Rabinowitsch (correction of non-Newtonian behaviour) correction. The method is described in more details in Chapter 3.2.1, where the necessary corrections are also defined mathematically.

6.4.2 Elongation viscosity determination

The capillary rheometer is beside evaluation of the shear viscosity able also to determine the elongation viscosity. In a such case, the Cogswell model based on the principle of transferring the measured material from a wide cylinder to a narrow capillary and evaluating the pressure at the inlet to the capillary is employed. The Cogswell model is in more details described in Chapter 3.2.1 together with fundamental mathematical description.

Figure 47: Göttfert RG 50 device

6.5 Rotational rheometer with SER geometry

Rotational rheometer Advanced Rheometric Expansion System (ARES 2000) was employed as another experimental device, see Figure 48. This type of rheometer is used for characterization of polymer melt flow and viscoelastic properties at low and medium strain rates. A sample utilised for extensional viscosity measurements in the form of a thin film inserted between the rotating cylinders of the measuring geometry. The torque sensor records the resistance of tested specimen to extension. Measurements with ARES 2000 are based on the rotation of lower geometry and sensing of the torque, and measurement of normal force on top geometry. A more detailed explanation of this measurement method, together with sketches of geometry, is given in Chapter 3.1.1. This chapter also presents the formulae by which elongation viscosity is defined.

To verify the data's accuracy, the selected measurements were repeated on the Anton Paar MCR 501 device, see Figure 49, which measures on the same principle as ARES 2000, however with different geometry design without bottom mount. [37]

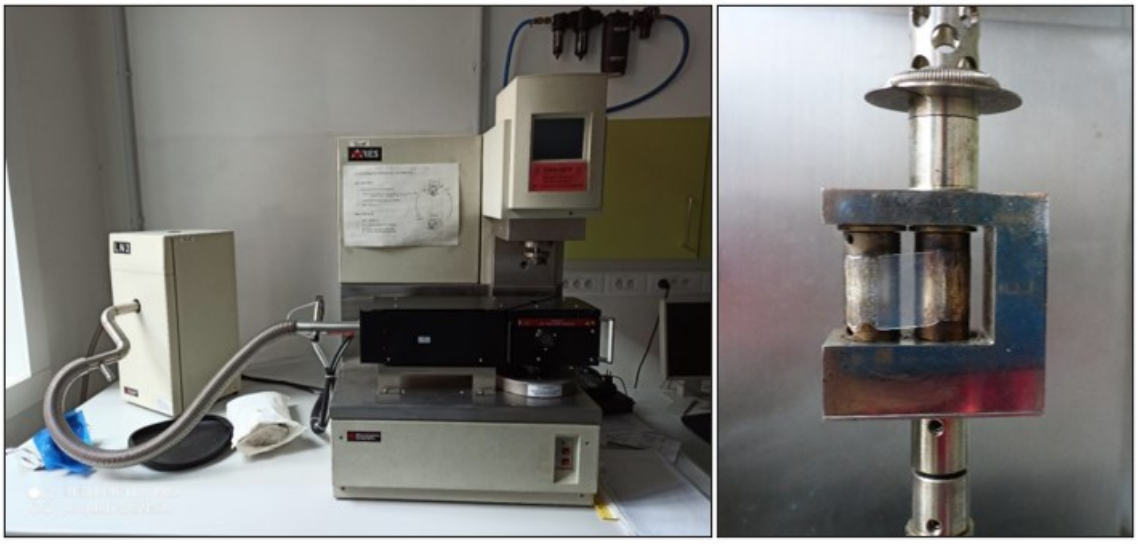

Figure 48: ARES 2000 device and measuring geometry with the attached sample

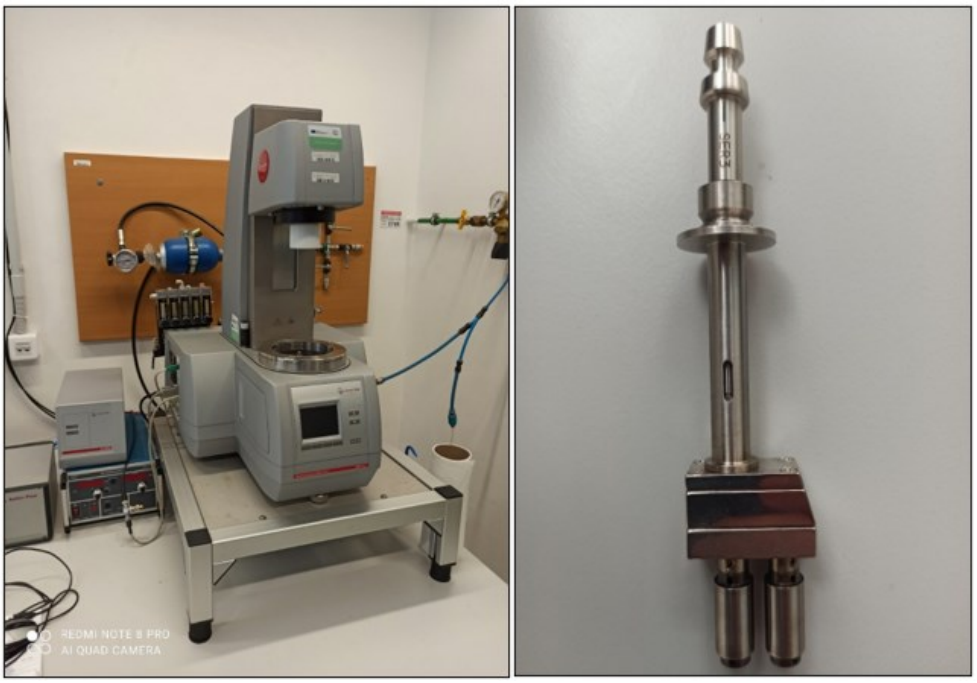

Figure 49: Anton Paar MCR 501 device and measuring geometry

6.6 High pressure capillary viscometry equipped with Rheotens device

By attaching the Rheotens device to the Göttfert RG 50 capillary rheometer, see Figure 50, an elongation viscosity measuring device can be obtained. A capillary rheometer plunger pushes the polymer melt through the capillary. The piston speed of 1.2 $mm.s^{-1}$ was chosen for material movement through the capillary of diameter 2 mm with the ratio L/D=20/2. Extruded string is then pulled with the power of four wheels of the Rheotens device. The wheels gradually increase their rotation speed until the pulled string is ruptured while the drawdown force is recorded. The gap between wheels was 1.2 mm, and the initial towing speed was 20 $mm.s^{-1}$. Detail device description together with the corresponding mathematical formulations used in Göttfert software are presented in Chapter 3.1.4.

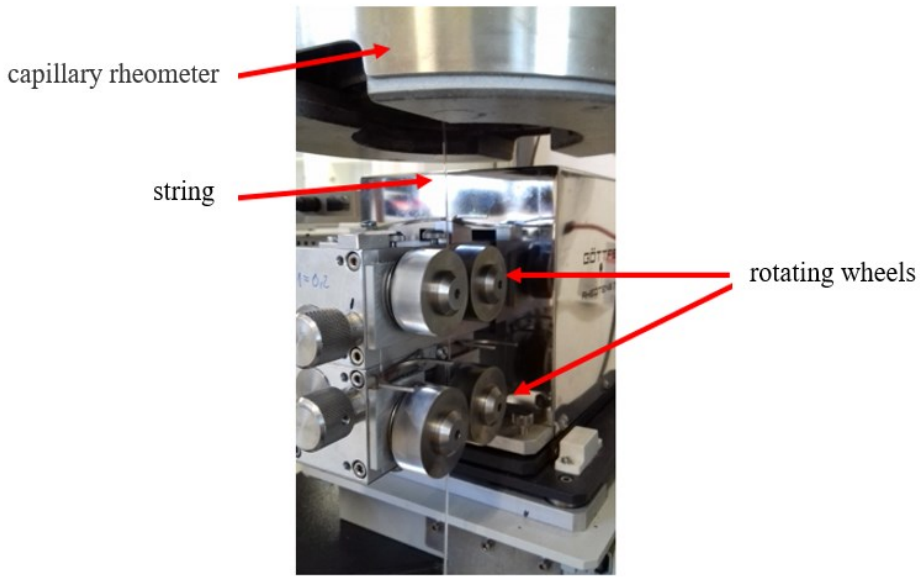

Figure 50: Rheotens device

7 EXPERIMENTAL DATA AND DISCUSSION OF RESULTS

The data results obtained using described experimental methods are presented and discussed further in this chapter.

7.1 Optical microscopy

Polymer foam samples of pure PP TOTAL, PP DAPLOY, and their compound consisting of PP TOTAL/PP DAPLOY_20/80 wt.% and PP TOTAL/PP DAPLOY_40/60 wt.% were characterized via optical microscope Bruker Alicona G4. The size distribution of the pores was visually evaluated using original supplied software on a connected computer.

Together with the optical characterization, the foam's density was determined by definition of the samples dimensions and their weight. This procedure was applied to ten samples of each type of specimens. The average density values are presented in Table 2 together with results of microscopy analysis.

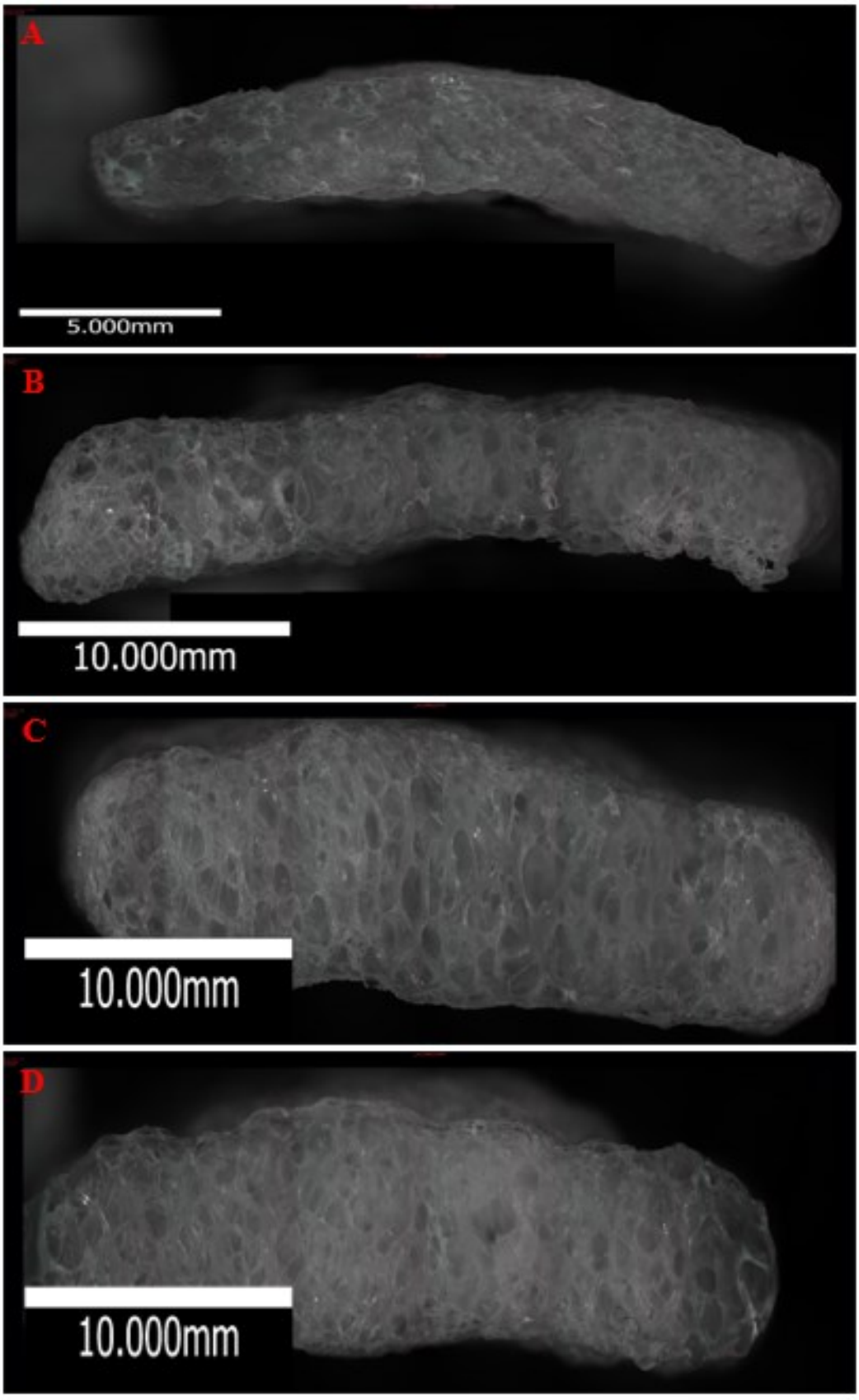

Figure 51: Optical microscopy of polymer foam made of A) PP TOTAL B) PP DAPLOY C) PP TOTAL/PP DAPLOY_20/80 wt.% compound D) PP TOTAL/PP DAPLOY_40/60 wt.% compound

Table 2: The average pore size and density of polymer foams

	Average pore size [µm]	**Average density [g.cm^{-3}]**
PP TOTAL	400	0.44
PP DAPLOY	800	0.15
TOTAL/PP DAPLOY _20/80	900	0.15
TOTAL/PP DAPLOY _40/60	950	0.22

7.1.1 Discussion of microscopy results

Microscopic images of the prepared foams are presented in Figure 51. As it is clear from the picture, the foam made of pure PP TOTAL has the smallest pores with average pores diameter of 400 µm. Obviously, the overall dimensions of the sample were defined as the smallest (approximately 20x3 mm) in comparison with the other foams, thus also having the highest density (see detail in Table 2). This is probably due to the higher viscosity of the PP TOTAL, as it was indicated within viscosity experiments, so the melt was not able to be expanded by the gas too much. Another reason is probably connected to a lower melt strength causing leakage of gas out of the extruded profile during its expansion. Even the pure PP DAPLOY HMS foams have twice the average pore size, 800 µm, they have noticeably larger dimensions (approximately 35x8 mm) thus lower density. This could be connected to the lower viscosity of the PP DAPLOY melt during foam extrusion enabling easier bubble expansion. Compound foams reached the largest dimensions of the pores. The foam with the composition PP TOTAL/PP DAPLOY_40/60 wt.% had a slightly larger average pore size of 950 µm compared to the foam with the composition PP TOTAL/PP DAPLOY_20/80 wt.% with an average pore size of 900 µm. The total sample sizes were similar (approximately 35x10 mm). Thus, all materials were able to form an acceptable foam structure, except PP TOTAL, due to the small expansion of the gas bubbles.

In addition, average densities of prepared polymeric foams are listed in Table 2. PP DAPLOY foam has a lower density of 0.15 g.cm^{-3} than PP TOTAL foam of 0.44 g.cm^{-3}. Low density of foamed extrudate was also observable for compounded materials. The results of the density measurements only confirm that the foam containing PP DAPLOY material could be expanded to significantly higher level.

7.2 Roentgen tomography

3D Roentgen microscopy scanner was used for characterization of the internal polymer foam structures. All tested samples of foamed extrudates were characterized using the same experimental setting.

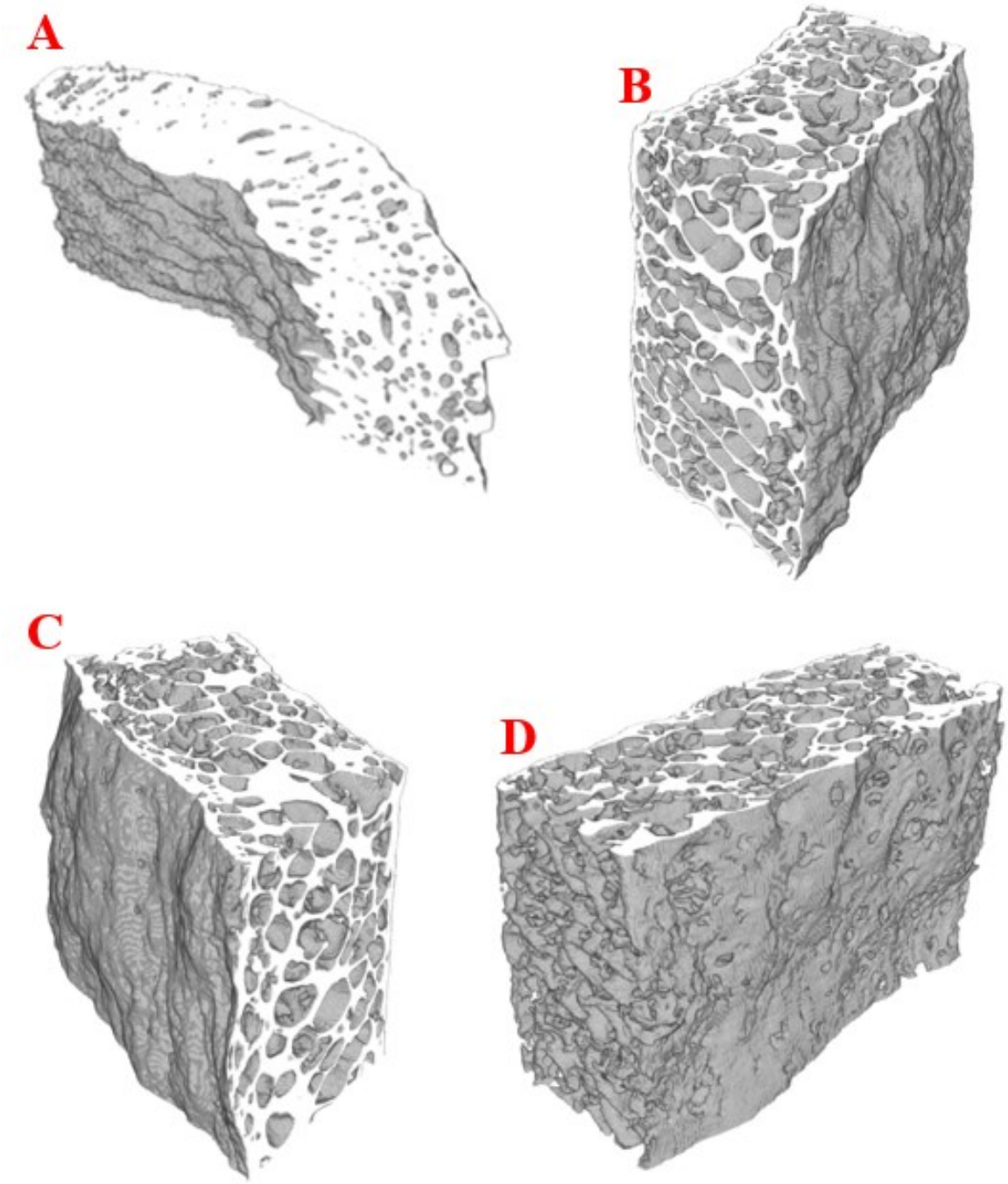

Figure 52: Scanned models of polymer foams consisting of: A) PP TOTAL B) PP DAPLOY C) PP TOTAL/PP DAPLOY_20/80 wt.% D) PP TOTAL/PP DAPLOY_40/60 wt.%

Table 3: Foam characteristics evaluated via a roentgen tomography

	Number of closed pores [1]	Volume of closed pores [mm^3]	Closed porosity [%]	Total porosity [%]	Object volume [mm^3]
PP TOTAL	2389	19.33	6.94	87.86	258.96
PP DAPLOY	164	0.52	0.33	92.74	156.66
TOTAL/PP DAPLOY _20/80	175	0.73	0.43	92.27	166.97
TOTAL/PP DAPLOY _40/60	123	0.25	0.16	92.65	158.75

7.2.1 Discussion of computer tomography results

Scanned CT models of polymeric foams are displayed in Figure 52. Minimal expansion of the gas bubbles and the smallest pores dimensions are indicated for the PP TOTAL material. The remaining three samples containing PP DAPLOY reveal significantly larger pores and a higher level of lightening, in other words, lower density level. The measured values of average pores size of tested polymer foams and their subsequent analysis are given in Table 3.

A large number of closed pores (2389) was detected for PP TOTAL specimen. On the other hand, the detected amount of closed pores for other specimens with DAPLOY PP was below 0.75 mm^3. This finding is moreover connected with the highest volume of polymer material within this specimen (259 mm^3) in comparison to the others (156–166 mm^3) and the smallest closed porosity (7 %), contrary to a maximum of 0.4 % for the rest of tested specimens, indicating thus the highest density and the lowest expansion of TOTAL PP foam sample.

Furthermore, the selected materials' rheological behaviour was characterised to define a connection between processing conditions and foams characteristics. The online rheometer Leistritz was chosen as the first method for flow behaviour evaluation since it has the highest practical applicability.

7.3 Online rheology measurements

Rheological measurement on the Leistritz rheometer was chosen due to the best practical applicability of online rheometers in industrial practice. The measurements were performed at a temperature of 250 °C due to a low power of online viscometer melt pumps. At lower temperatures, there was an enormous increase of pressure in the measuring device, which then caused aborting of experiments. The melt pump, which was delivering the polymeric melts, was set to 10–40 rotations per minute, which guarantee evaluation of the shear and elongational viscosity as a function of strain rates in the range of shear rate 10–10 000 s^{-1} and the elongation rate 5–75 s^{-1} (see obtained results in Chart 1)

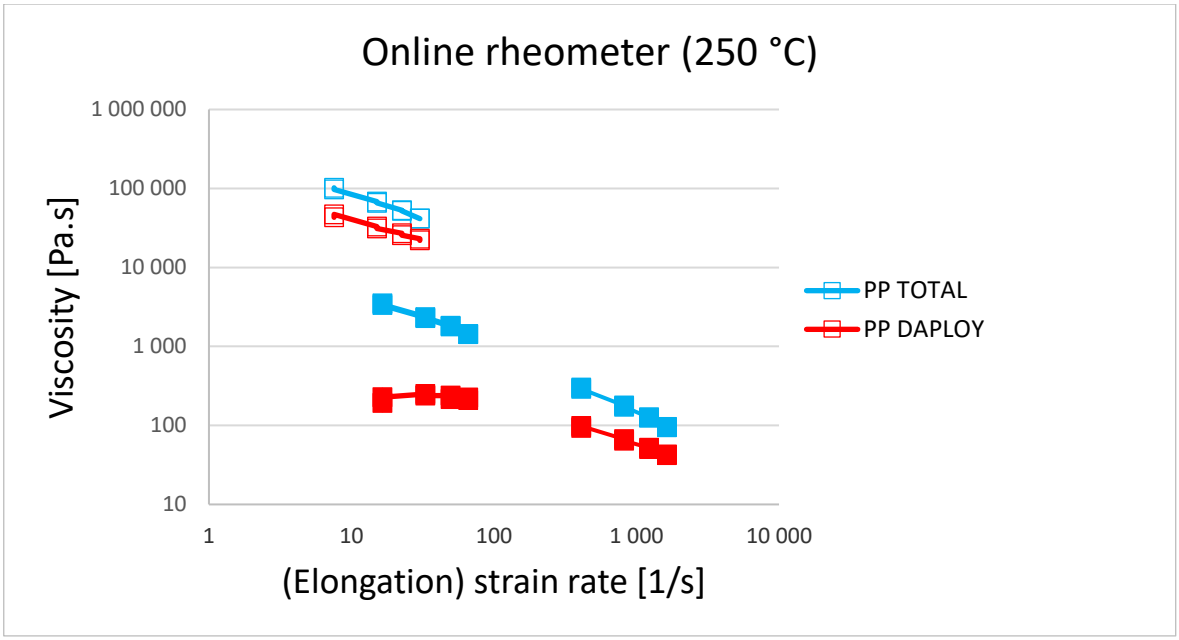

Chart 1: Viscosity dependence on (Elongation) strain rate for material PP TOTAL and PP DAPLOY at temperature 250 °C, filled squares belong to shear viscosity, and empty squares belong to elongation viscosity, blue corresponds to PP TOTAL and red corresponds to PP DAPLOY

7.3.1 Discussion of online viscosity measurements

In Chart 1 it can be seen that PP TOTAL has higher values of both shear and elongation viscosity in comparison to PP DAPLOY. The Trouton ratio at a deformation rate of 15 s^{-1} was defined 20 for the PP TOTAL material, while it was defined 135 for the PP DAPLOY. Even the results indicate that higher level of elongational viscosity and simultaneous lower level of shear viscosity defined for PP DAPLOY could probably ensure higher processing stability and higher efficiency for foaming process, since it was not possible utilizing

Leistritz online rheometer to evaluate viscosity behaviour at lower temperature then 240 °C (corresponding to foam extrusion condition) this experimental setup was applied only to evaluation of rheological behaviour of pure PP materials.

7.4 High-pressure capillary rheometer data evaluation

Rheometer Göttfert RG 50 was chosen as the laboratory device for evaluation of PP TOTAL and PP DAPLOY materials' shear and elongational viscosity behaviour. The measurements of viscosity data were taken for each material in a series of defined apparent shear rates, see Table 4. A ratio L/D=20/1 and L/D=0/1 were chosen for employed capillaries. Pressure transducers were chosen a 1000 bar one for a barrel with a capillary length of 20 mm and a 200 bar one for a zero-length capillary.

The defined apparent viscosity data were corrected by Bagley and Rabinowitsch corrections. Corrected shear viscosity as a function of corrected shear rate is shown in charts below, together with elongation viscosity data calculated via Cogswell analysis as a function of extensional strain rate.

Table 4: Setup of piston speed

Göttfert RG 50 rheometer					
Number	**Piston speed [mm/s]**	**Shear rate [1/s]**	**Number**	**Piston speed [mm/s]**	**Shear rate [1/s]**
1	0.00556	10	8	0.28833	519
2	0.01944	35	9	0.45222	814
3	0.03056	55	10	0.70889	1276
4	0.04778	86	11	1.11111	2000
5	0.07500	135	12	1.38889	2500
6	0.11722	211	13	1.66667	3000
7	0.18389	331	14	5.00001	9000

7.4.1 Discussion of capillary viscosity experiments results

The viscosity curves at various temperature for PP TOTAL and PP DAPLOY could be seen in Chart 2 and Chart 3, respectively. Even there is an evident trend of decreasing of flow curves with increasing temperature, the most significant decrease could be found for elongational flow curves at temperature of 250 °C.

Based on the results, it could be noted that the Trouton ratio at 100 s^{-1} was defined for temperature of 180 °C of 4.7 and 2.5 for 250 °C at 1000 s^{-1} for PP TOTAL, while it was found to be 20 for temperature of 180 °C at 100 s^{-1} and 4.4 for 250 °C for PP DAPLOY at 100 s^{-1}. PP TOTAL, therefore, has a lower Trouton ratio than PP HMS. Due to the foaming process, it appears that a material with a higher value of the Trouton ratio is more suitable for foaming.

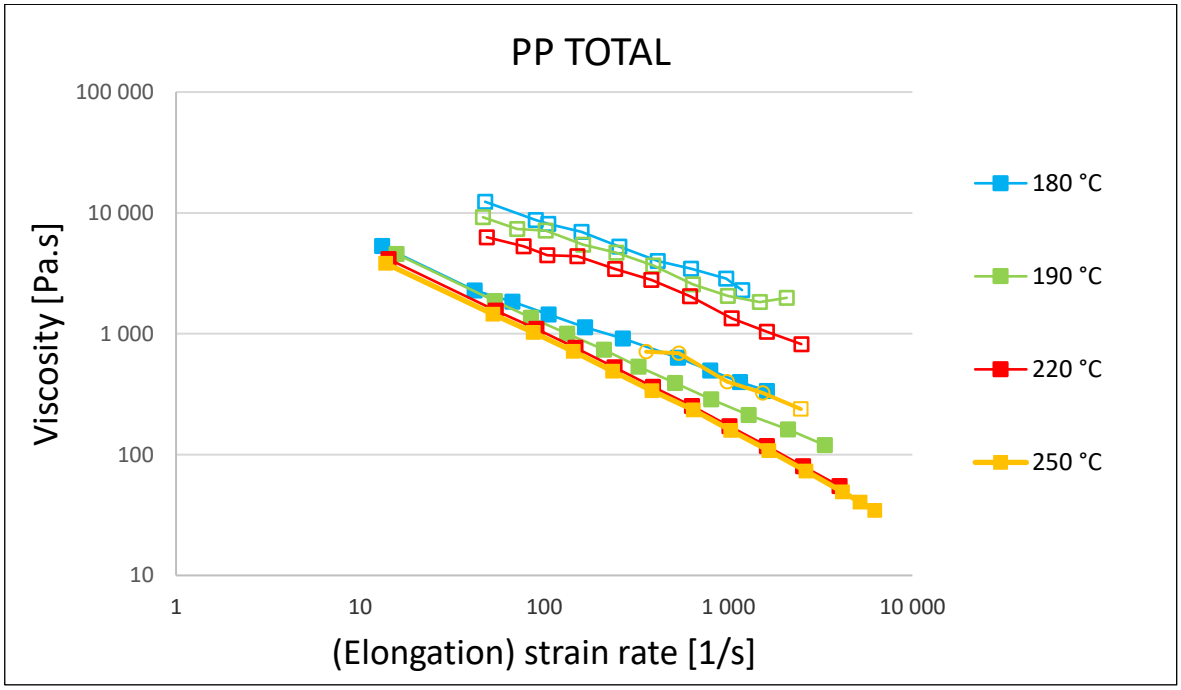

Chart 2: Viscosity dependence on (Elongation) strain rate for material PP TOTAL at different temperatures, filled squares belong to shear viscosity, and empty squares belong to elongation viscosity, blue corresponds to 180 ° C, green corresponds to 190 ° C, red corresponds to 220 ° C, orange corresponds to 250 ° C

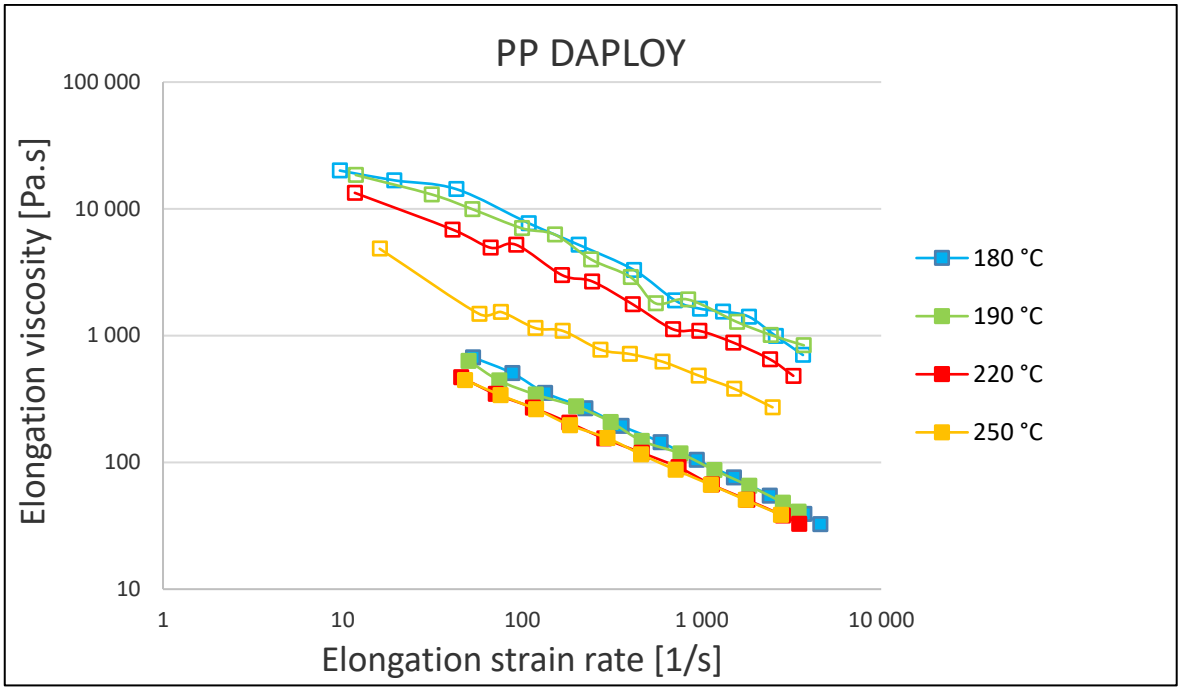

Chart 3: Viscosity dependence on (Elongation) strain rate for material PP TOTAL at different temperatures, filled squares belong to shear viscosity, and empty squares belong to elongation viscosity, blue corresponds to 180 ° C, green corresponds to 190 ° C, red corresponds to 220 ° C, orange corresponds to 250 ° C

Comparing the viscosity curves of both materials, it is clear, that even PP TOTAL have significantly higher level of shear viscosity flow curves, the elongational viscosity of both materials is rather similar. It could be highlighted that these findings are in good agreement with the results from the online rheometer. Accordingly, it could be concluded that high-pressure capillary viscosity measurements are useful tool for evaluation of viscosity behaviour of PP melts at various temperature at moderate and higher strain rates (elongational viscosity above 100 s^{-1} and 20 s^{-1} was described for PP TOTAL and PP DAPLOY, respectively). Unfortunately, since extrusion of polymer foams and more specifically their foaming itself is done under low strain rates, evaluation via this type of rheometer was again limited only to pure PP materials and additional method of rheological behaviour characterization was chosen - namely a rheological behaviour evaluation via rotational rheometer equipped with SER geometry.

7.5 Measurement of elongation viscosity using a rotational rheometer with SER geometry

The elongation viscosity was firstly evaluated using ARES 2000 instrument. Small samples of dimensions (20x12.5x0.5) mm were cut out from the prepared plates. The measurements of PP TOTAL and PP DAPLOY at elongation strain rates of 10, 1, 0.1, 0.01 s^{-1} were carried out at temperatures of 180, 190, 220, and 250 °C under a protective nitrogen atmosphere.

7.5.1 Obtained data for PP TOTAL

The measurement of elongation viscosity on the ARES 2000 instrument for tested materials are displayed in Chart 4 - Chart 7, while defined viscosity data are listed in Table 5.

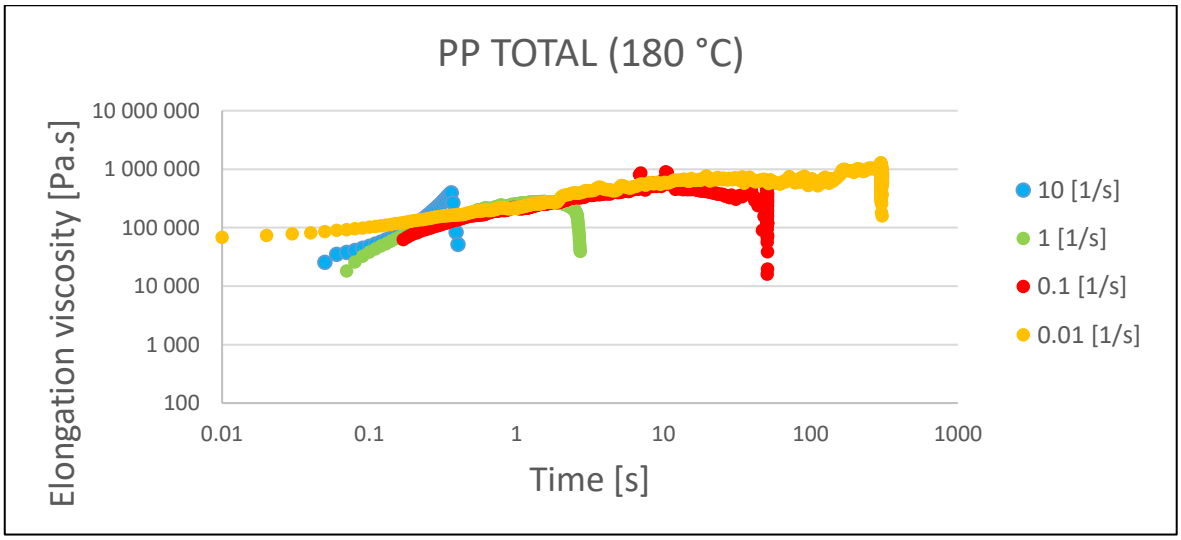

Chart 4: Elongation viscosity dependence on time for temperature 180 °C measured on ARES 2000 device, blue colour corresponds to strain rate of 10 s^{-1}, green colour corresponds to strain rate of 1 s^{-1}, red colour corresponds to strain rate of 0.1 $s^{-1}$and orange colour corresponds to strain rate of 0.01 s^{-1}

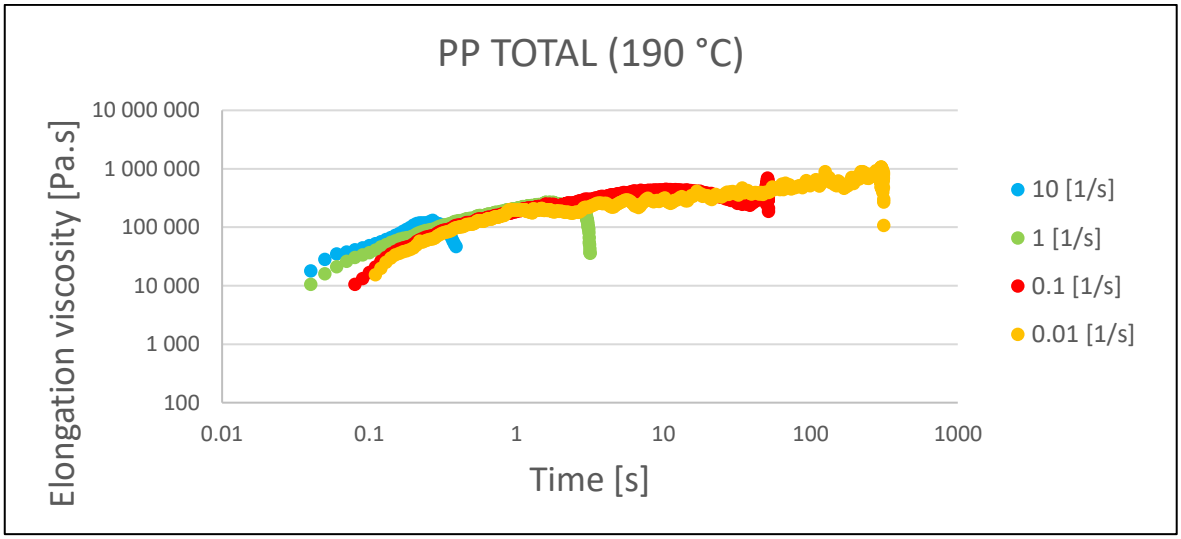

Chart 5: Elongation viscosity dependence on time for temperature 190 °C measured on ARES 2000 device, blue colour corresponds to strain rate of 10 s^{-1}, green colour corresponds to strain rate of 1 s^{-1}, red colour corresponds to strain rate of 0.1 $s^{-1}$and orange colour corresponds to strain rate of 0.01 s^{-1}

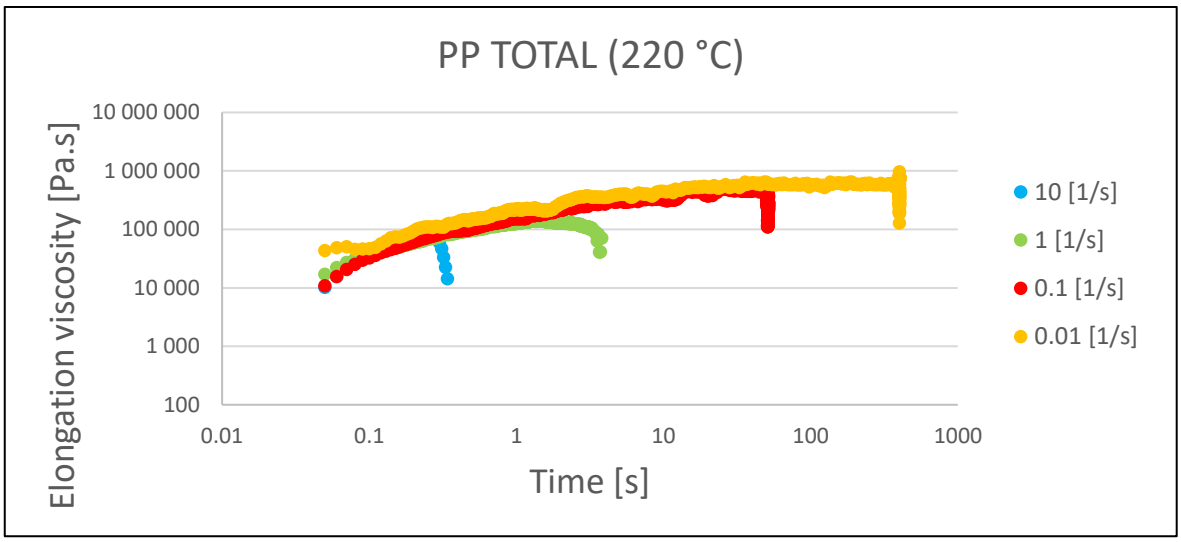

Chart 6: Elongation viscosity dependence on time for temperature 220 °C measured on ARES 2000 device, blue colour corresponds to strain rate of 10 s^{-1}, green colour corresponds to strain rate of 1 s^{-1}, red colour corresponds to strain rate of 0.1 $s^{-1}$and orange colour corresponds to strain rate of 0.01 s^{-1}

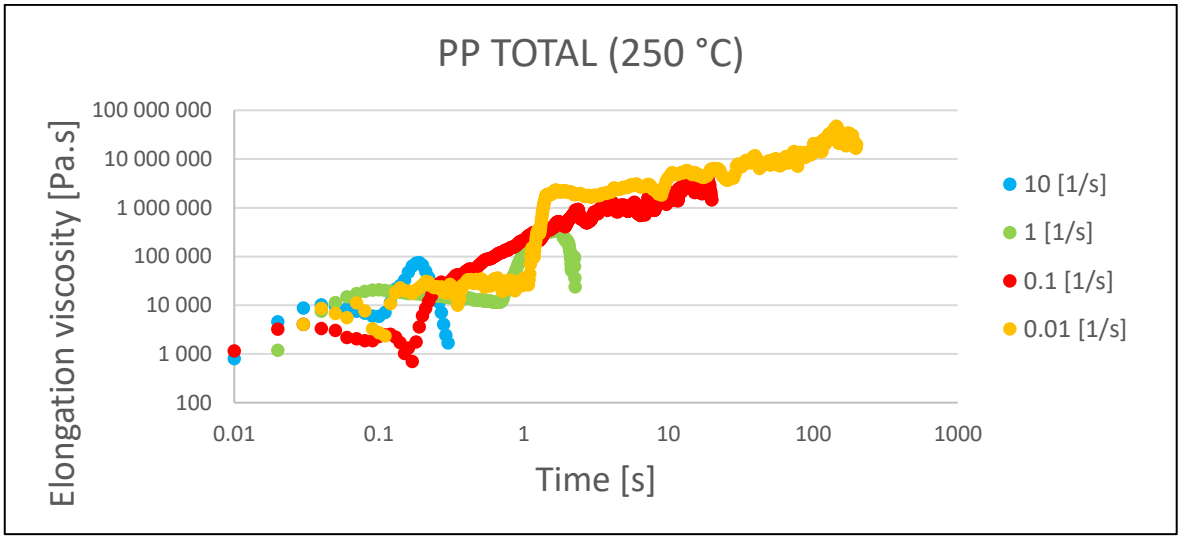

Chart 7: Elongation viscosity dependence on time for temperature 250 °C measured on ARES 2000 device, blue colour corresponds to strain rate of 10 s^{-1}, green colour corresponds to strain rate of 1 s^{-1}, red colour corresponds to strain rate of 0.1 $s^{-1}$and orange colour corresponds to strain rate of 0.01 s^{-1}

Table 5: Results of measurement of elongation viscosity from the ARES 2000 rotary rheometer for PP TOTAL material

Elongation strain rate [1/s]	Temperature [°C]	Maximum of elongation viscosity [Pa.s]	Sample drag time [s]
10	180	393 820	0.36
	190	130 481	0.24
	220	108 812	0.32
	250	66 208	0.20
1	180	274 514	1.74
	190	197 023	1.70
	220	174 963	1.78
	250	503 135	1.77
0.1	180	631 001	51.75
	190	692 511	50.90
	220	581 310	54.76
	250	2 103 247	17.02
0.01	180	1 071 015	305.65
	190	1 043 460	301.03
	220	815 562	400.04
	250	39 276 795	190.21

7.5.2 Discussion of SER analysis results of PP TOTAL melt

Samples broke roughly at the same time for given speeds of elongation strain rate, except at slow rates at high temperatures when the measurements were necessary to stop manually. The specimens in these cases were found to be wounded on the cylinder, and the material contact between the cylinders occurred. This error can also be seen in the absurdly high elongation viscosity values of these measurements. For measurements where no contact has been detected, elongation viscosity evidently decreased with increasing temperature. With the elongation strain rate decreasing, the elongation viscosity should shift to higher values, but this behaviour was not proved for this material. There is also no evidence of strain hardening, an increase in elongation viscosity before the end of the measurement. This will be probably connected to a lack of molecules branching. In Chart 7, a steep increase in elongation viscosity to large nonsensical values can always be observed. This indicates a measurement error. Since the measuring cell is closed, it is not possible to judge exactly what error is occurring. However, this suggests that this method will not be completely reliable.

Illustrative temperature comparison for chosen elongation strain rate (10 s^{-1}) could be found in Chart 8. Elongation viscosity decreases with increasing temperature, and a shorter time to break the sample is also needed at a higher temperature.

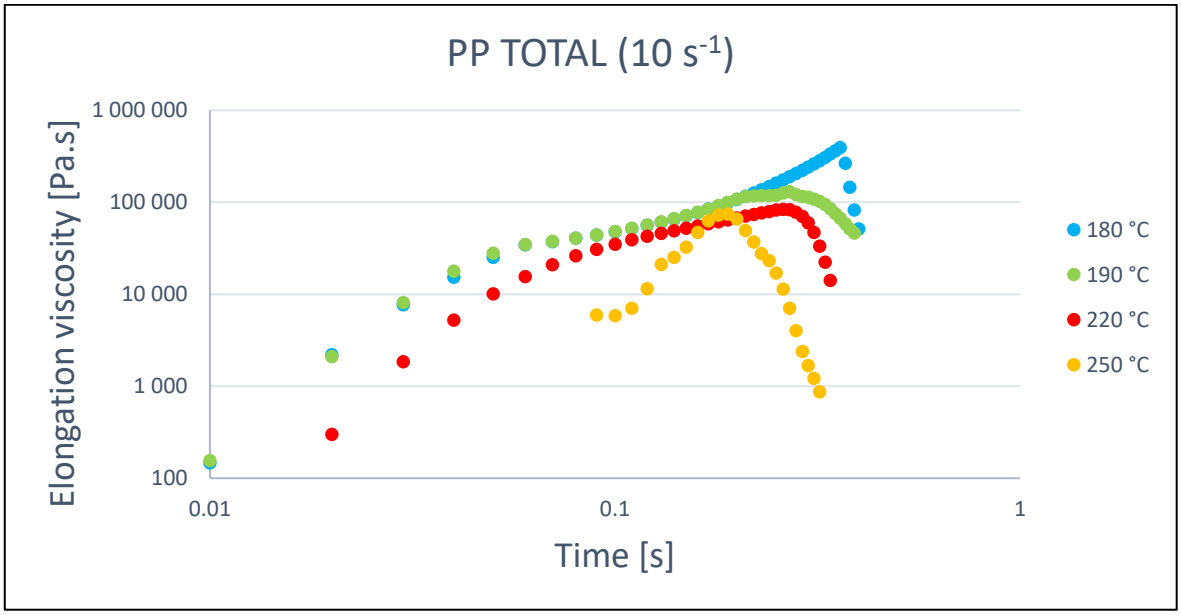

Chart 8: Elongation viscosity dependence on time for different temperatures measured on ARES 2000 device at strain rate of 10 s^{-1}

7.5.3 Obtained data for PP DAPLOY

The measurement of elongation viscosity using the ARES 2000 instrument of PP DAPLOY is presented in Chart 9 - Chart 12, while selected numerical results are listed in Table 6.

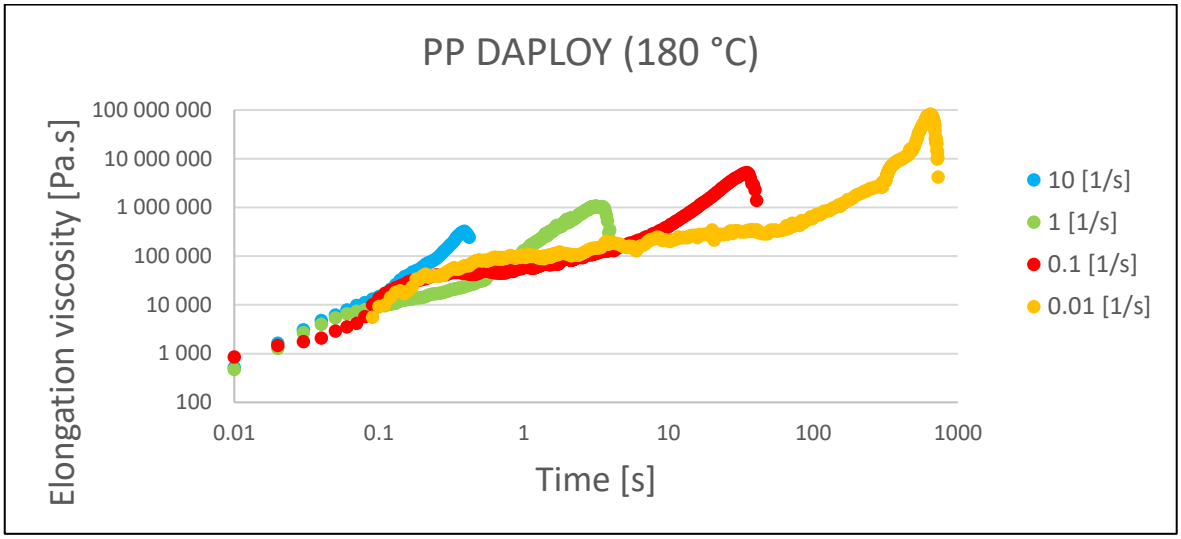

Chart 9: Elongation viscosity dependence on time for temperature 180 °C measured on ARES 2000 device, blue colour corresponds to strain rate of 10 s^{-1}, green colour corresponds to strain rate of 1 s^{-1}, red colour corresponds to strain rate of 0.1 $s^{-1}$and orange colour corresponds to strain rate of 0.01 s^{-1}

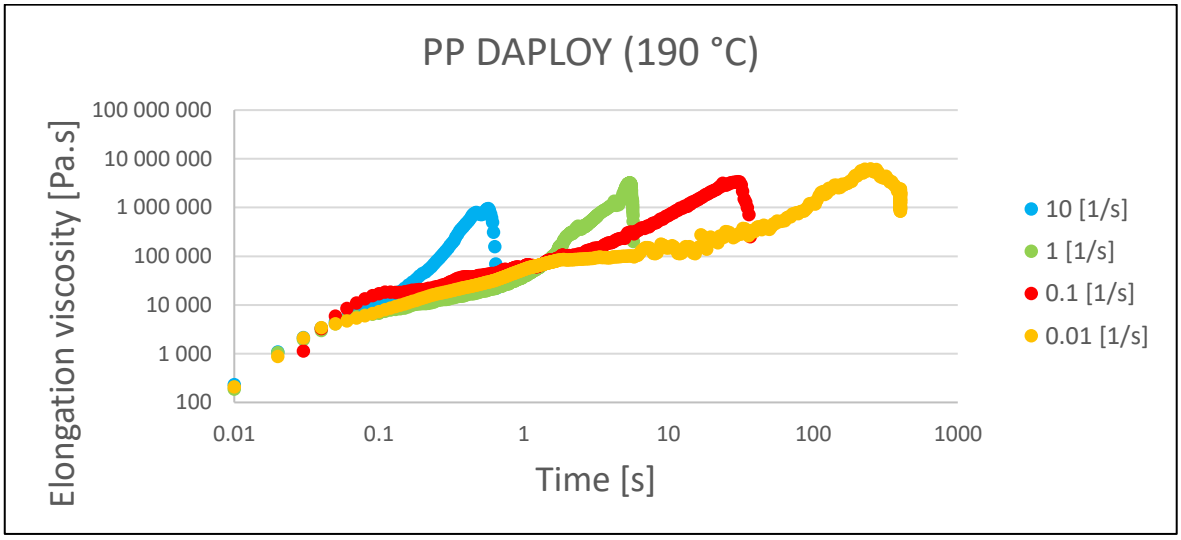

Chart 10: Elongation viscosity dependence on time for temperature 190 °C measured on ARES 2000 device, blue colour corresponds to strain rate of 10 s^{-1}, green colour corresponds to strain rate of 1 s^{-1}, red colour corresponds to strain rate of 0.1 $s^{-1}$and orange colour corresponds to strain rate of 0.01 s^{-1}

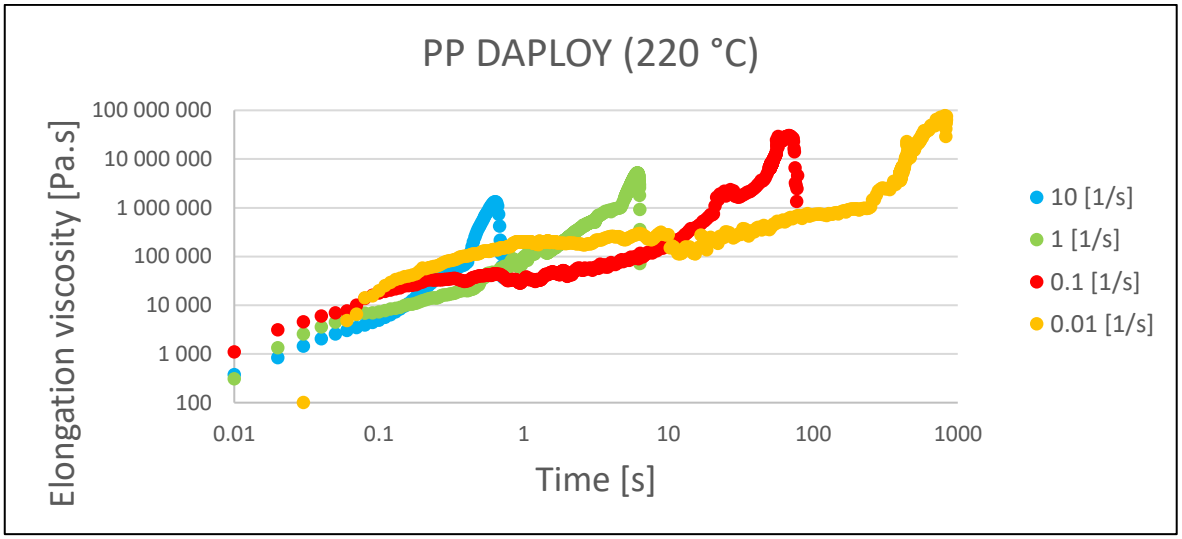

Chart 11: Elongation viscosity dependence on time for temperature 220 °C measured on ARES 2000 device, blue colour corresponds to strain rate of 10 s^{-1}, green colour corresponds to strain rate of 1 s^{-1}, red colour corresponds to strain rate of 0.1 $s^{-1}$and orange colour corresponds to strain rate of 0.01 s^{-1}

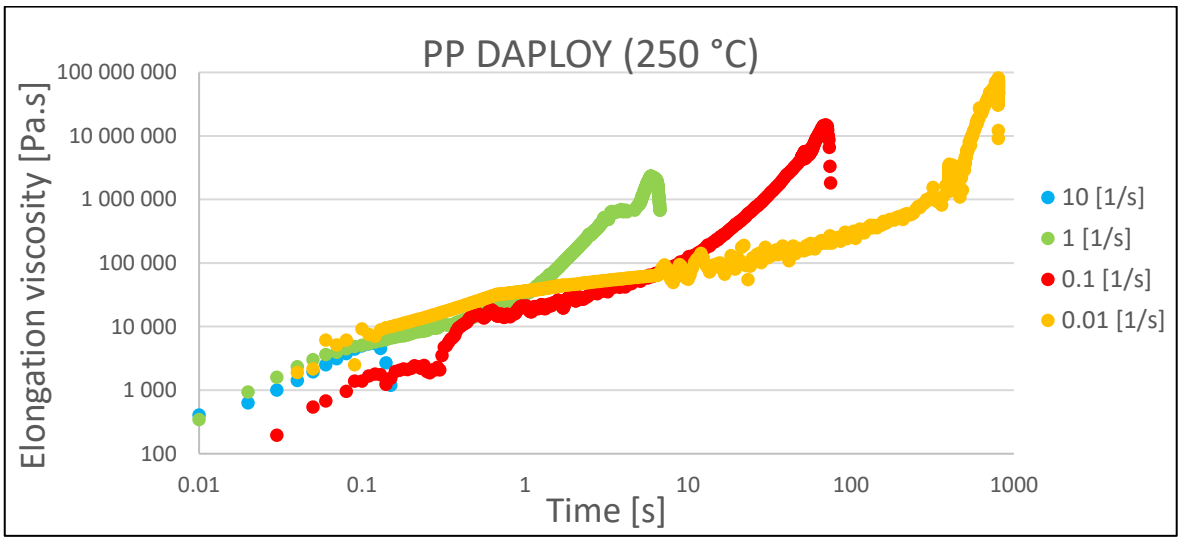

Chart 12: Elongation viscosity dependence on time for temperature 250 °C measured on ARES 2000 device, blue colour corresponds to strain rate of 10 s^{-1}, green colour corresponds to strain rate of 1 s^{-1}, red colour corresponds to strain rate of 0.1 $s^{-1}$and orange colour corresponds to strain rate of 0.01 s^{-1}

Table 6: Results of measurement of elongation viscosity from the ARES 2000 rotary rheometer for PP DAPLOY material

Elongation strain rate [1/s]	Temperature [°C]	Maximum of elongation viscosity [Pa.s]	Sample drag time [s]
10	180	275 310	0.41
	190	873 376	0.52
	220	1 092 253	0.66
	250	7 020	0.12
1	180	1 023 595	3.54
	190	3 169 308	5.41
	220	5 141 645	6.15
	250	2 119 746	6.31
0.1	180	4 855 241	35.98
	190	2 918 164	31.85
	220	27 927 692	71.03
	250	12 326 279	72.09
0.01	180	73 801 119	669.53
	190	5 306 376	400.42
	220	75 643 330	834.73
	250	78 602 320	802.72

7.5.4 Discussion of SER analysis results of PP DAPLOY melt

Samples broke roughly at the same time for given speeds of elongation strain rate, except at high temperatures. It turns out that temperatures 220 °C and 250 °C were probably too high for this measurement, and the measured data at these low temperatures are not very correct. Strain hardening is significant for this material, expressed as a large increase in elongation viscosity close to the end of the measurements. It could be expected that this increase is connected to molecules branching presence. PP DAPLOY belongs to the group of long-chain branched polypropylenes. An illustrative temperature comparison for one elongation strain rate (10 s^{-1}) is displayed in Chart 13. Obviously, elongation viscosity decreases with increasing temperature. Moreover, it could be noted that a shorter time is needed to break the sample as the temperature is higher.

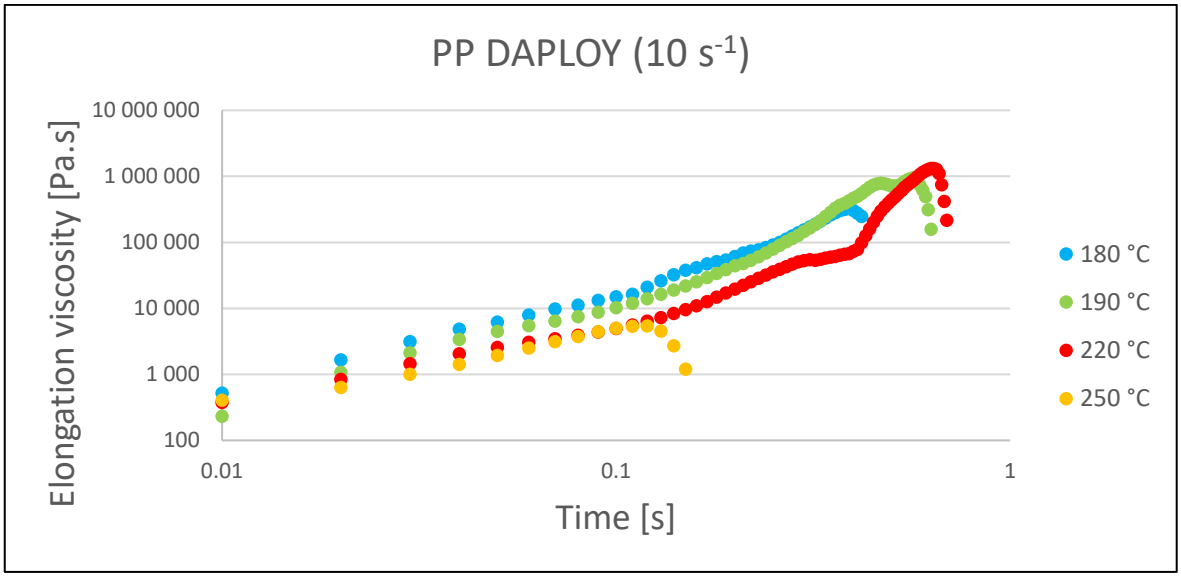

Chart 13: Elongation viscosity dependence on time for different temperatures measured on ARES 2000 device at strain rate of 10 s^{-1}

7.5.5 Discussion of comparison of ARES and Anton Paar SER analysis results

Because of the high level of obtained SER analysis data inaccuracy defined by ARES instrument the same evaluation was carried out using the second geometry connected to Anton Paar device. The error rate of the data is mainly visible in the increase of the elongation viscosity to huge meaningless values.

The evaluation of elongational viscosity was performed utilizing Anton Paar MCR 501 device at the Institute for Hydrodynamics of the Academy of Sciences of the Czech Republic in Prague. The applied experimental conditions were the same as those used for ARES 2000 analysis. The measurement was repeated several times due to observed method's error rate and average result values were consequently employed for the comparison. It was found that experimental results defined by both apparatuses are very similar. Selected graphs comparing the results of measurements performed on ARES 2000 and Anton Paar are attached below. The points shown in the attached graphs correspond to the maximum from the measured elongation viscosity curve using the given instrument.

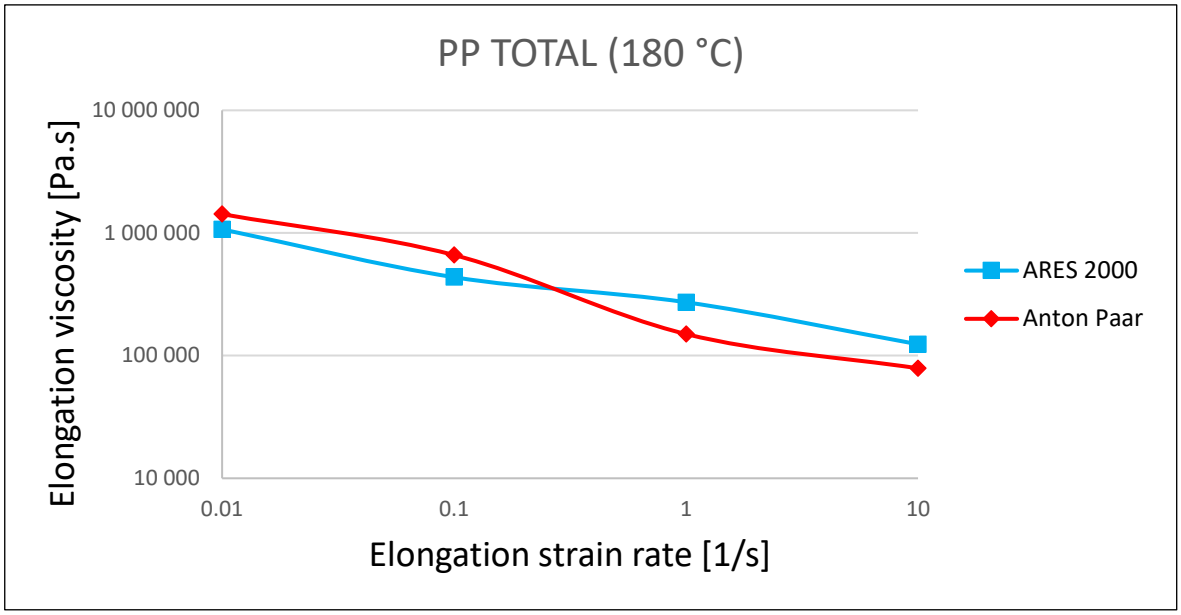

Chart 14: Comparison of elongation viscosity dependence on elongation strain rate, measured on ARES 2000 and Anton Paar device

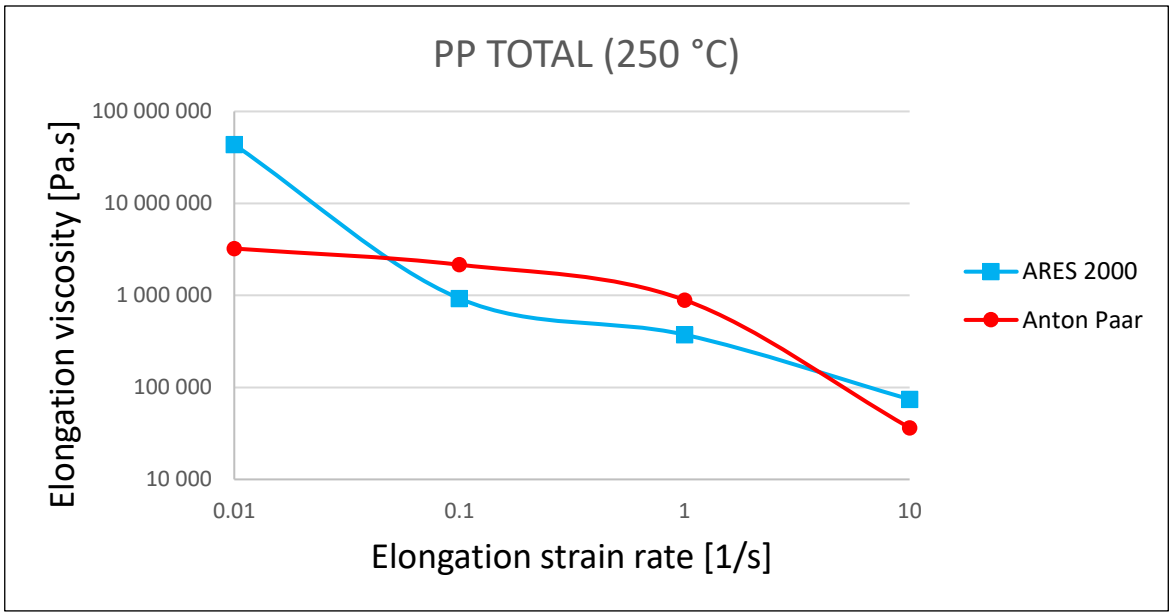

Chart 15: Comparison of elongation viscosity dependence on elongation strain rate, measured on ARES 2000 and Anton Paar device

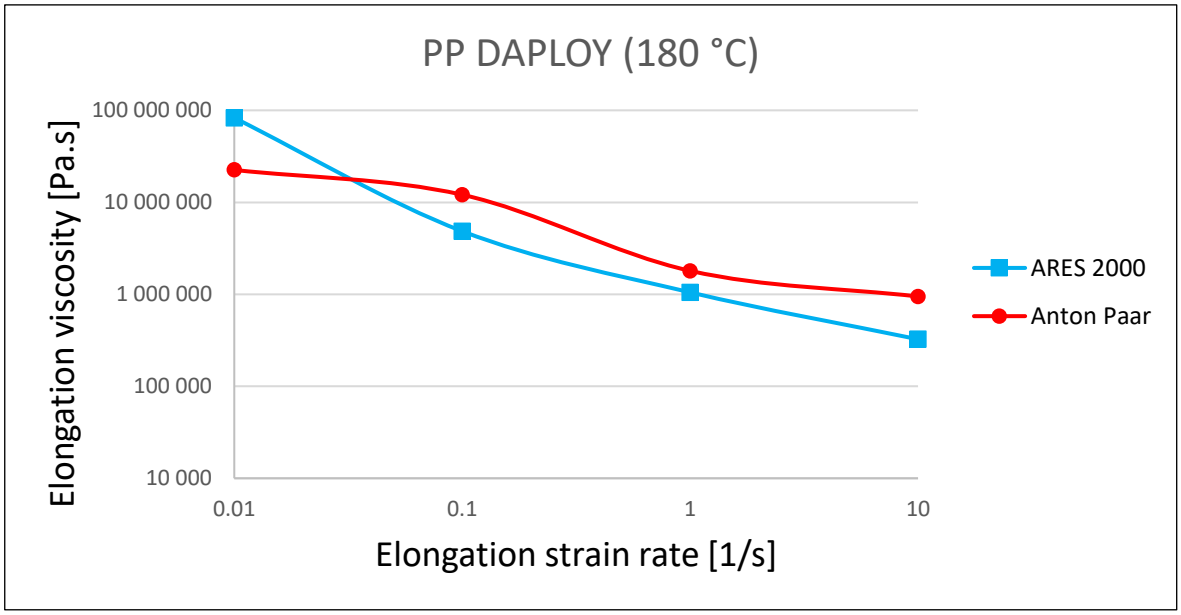

Chart 16: Comparison of elongation viscosity dependence on elongation strain rate, measured on ARES 2000 and Anton Paar device

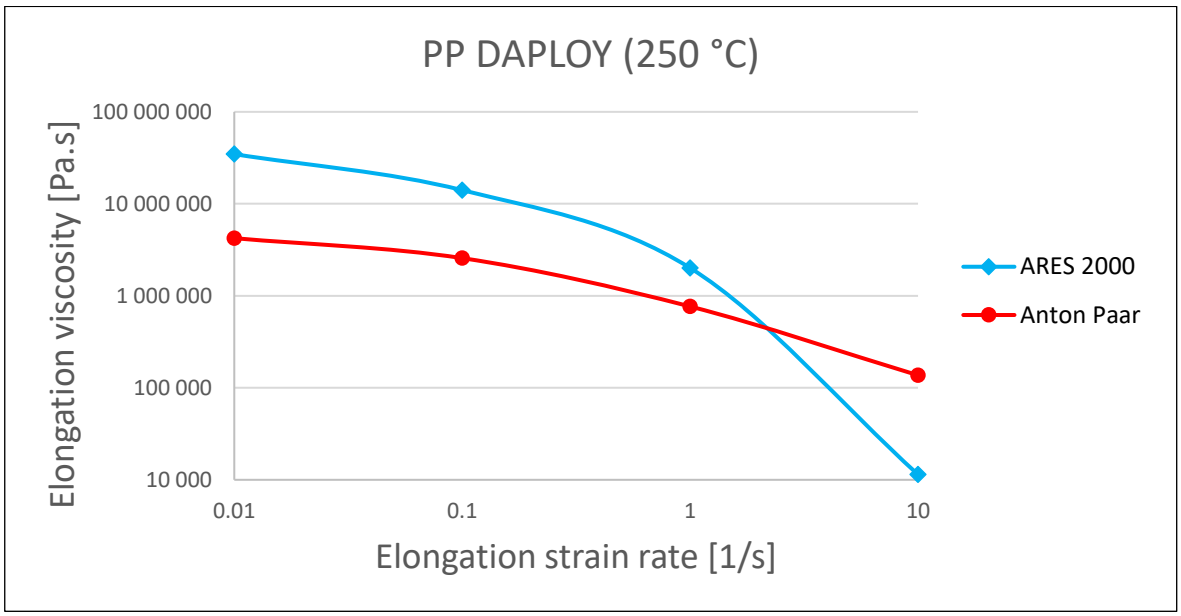

Chart 17: Comparison of elongation viscosity dependence on elongation strain rate, measured on ARES 2000 and Anton Paar device

A comparison between elongational flow behaviour defined by the devices ARES 2000 and Anton Paar are presented in Chart 14 - Chart 17. It was employed for examination whether the unstable data measured on the ARES 2000 were reliable. For a temperature of 180 °C, there is no significant difference between the data, so this measurement is probably reliable at low temperatures. At temperature of 250 °C, considerable differences were apparent at

some points. For example, the difference in PP DAPLOY material at 250 °C for the elongation strain rate of 10 s^{-1} is up to one order of magnitude.

Due to the above-mentioned disadvantages, compounds have not been characterized by this method and another method of characterizing the elongation viscosity had to be chosen.

7.6 Measurement of elongation viscosity using a Rheotens device

Measured viscosity data of PP TOTAL and DAPLOY melts defined using Rheotens tester is presented in ChartsChart 18–Chart 20.

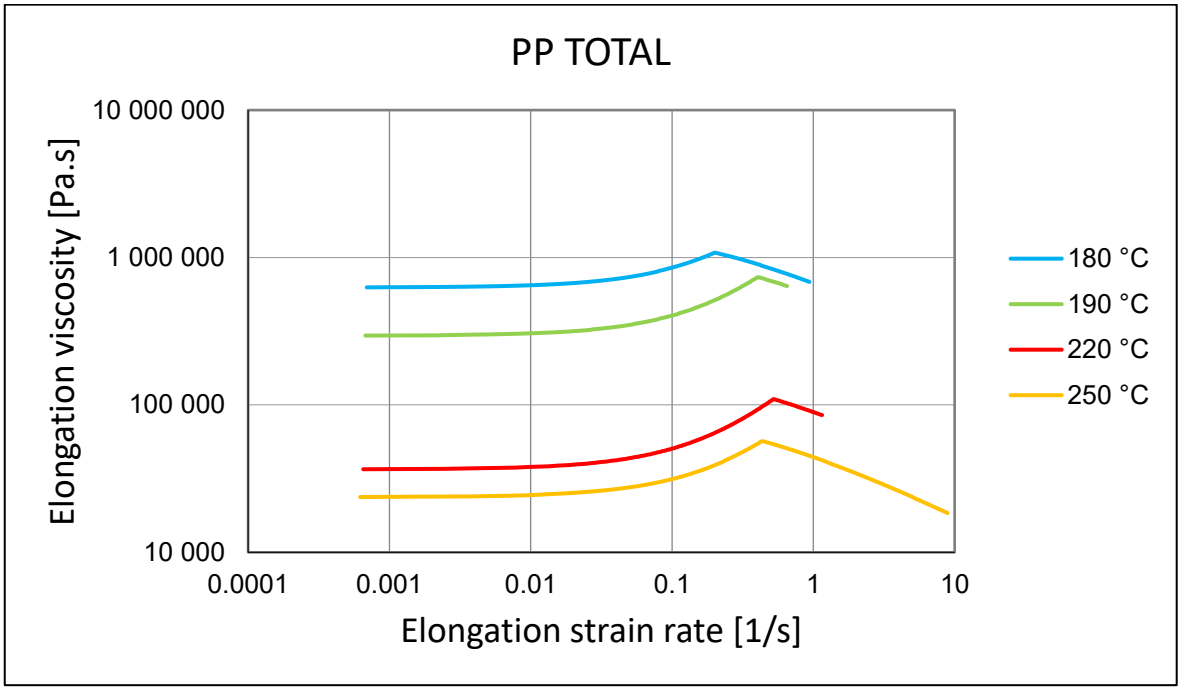

Chart 18: Elongation viscosity dependence on elongation strain rate for different temperatures

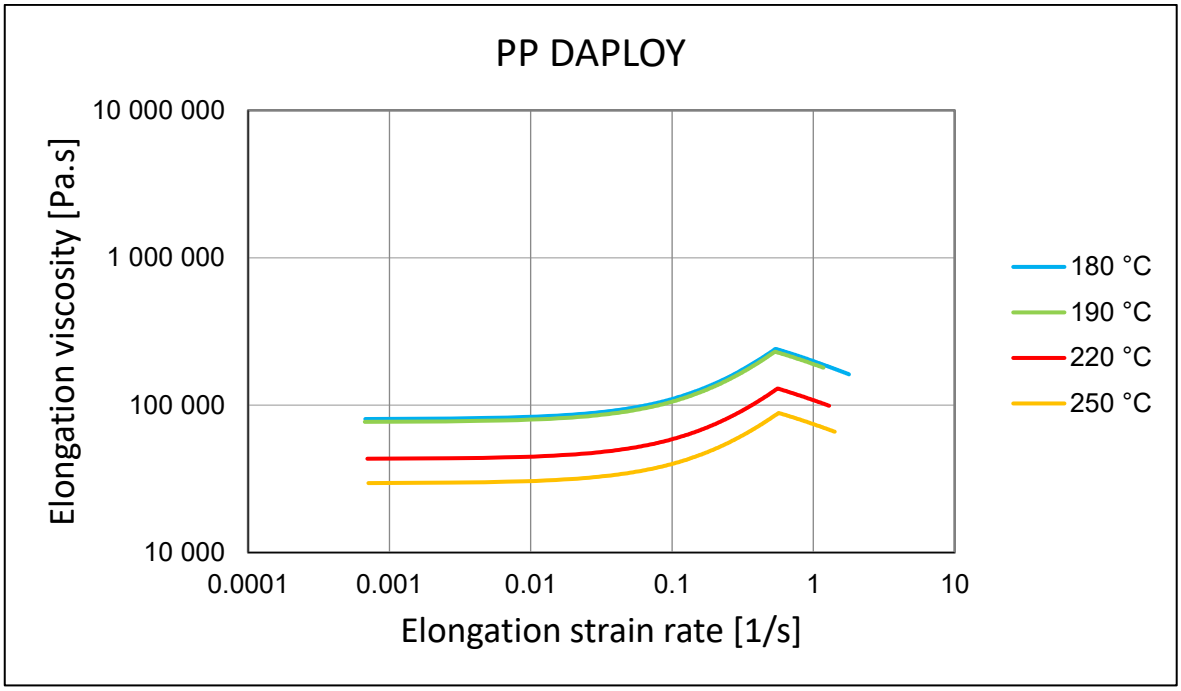

Chart 19: Elongation viscosity dependence on elongation strain rate for different temperatures

7.6.1 Discussion of Rheotens analysis results of pure materials

The viscosity curves of PP TOTAL at different temperatures are compared in Chart 18 for material. As it was already defined using other experimental methods, there is a noticeable trend proving that elongation viscosity is significantly affected by change of temperature. This finding negatively affects foam manufacturing stability and the width of a processing window. Moreover, as it is clear, elongational viscosity level of PP TOTAL at lower temperatures (180 °C and 190 °C) reaches values of 1 000 000 Pa.s. Based on foaming experiments this level is obviously unacceptable for foaming expansion. Evidently, acceptable level of elongational viscosity plateau (melt strength) is achieved at higher temperatures (above 220 °C) around 100 000 Pa.s, Nevertheless, as it could highlighted based on standard high-pressure viscosity measurements, there is significantly higher level of shear viscosity of PP TOTAL melt defined for temperature of 220 °C in comparison with PP DAPLOY. Furthermore, there is lack of strain hardening of this material probably causing the lack of bubble wall strength. Elongational flowing behaviour of PP DAPLOY is presented in Chart 19. Obviously, it has the significantly lower sensitivity of flow curves to temperature change. While there is no noticeable drop between 180 °C and 190 °C (keeping level of 75 000 Pa.s), the level of viscosity plateau slightly decreased to approximately 40 000 with temperature increase to 220 °C and to level of 30 000 Pa.s at 250 °C indicating thus acceptable stability of processing window.

Since the data obtained using the Rheotens device seemed to be accurate and were measured at the required strain rates. Rheological quantities were also measured for polymer compounds.

In addition to the pure materials PP TOTAL and PP DAPLOY, also their mixtures were measured by this method. The mass percentage was TOTAL/DAPLOY_20/80 wt.% and TOTAL/DAPLOY_40/60 wt.%. These measurements were carried out at temperatures of 180 °C, in order to follow temperature conditions of foaming process. Further are thus compared curves defined at 180°C for materials containing PP DAPLOY and 250 °C for pure PP TOTAL.

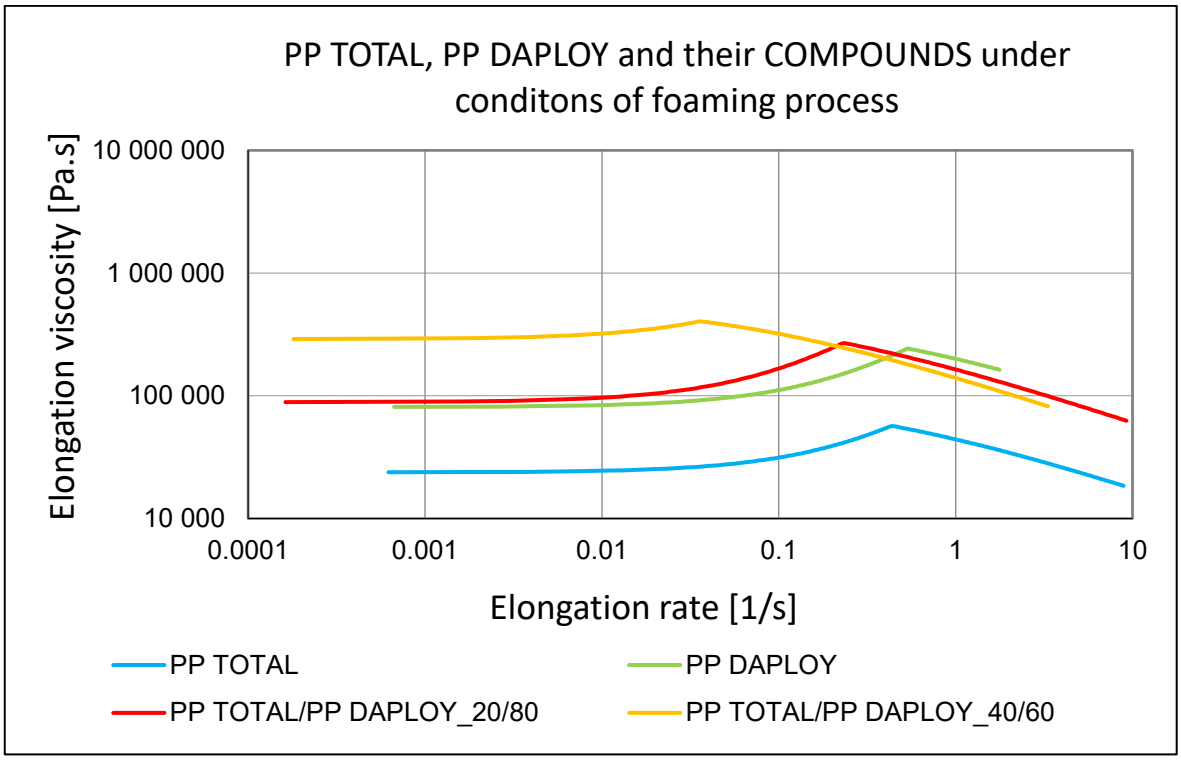

Chart 20: Elongation viscosity dependence on elongation strain rate, comparison of materials, materials containing DAPLOY PP measured at 180 °C, PP TOTAL measured at 250 °C

7.6.2 Discussion of Rheotens analysis results of pure materials and compounds

Table 7 displays the maximum of elongation viscosity values defined for the measurements carried out utilizing Rheotens.

Table 7: Results of elongation viscosity maximum measured on Rheotens tester, at different temperatures

	PP TOTAL	**PP DAPLOY**	**PP TOTAL/PP DAPLOY_20/80**	**PP TOTAL/PP DAPLOY_40/60**
Temperature [°C]	**Maximum of elongation viscosity [Pa.s]**			
180	1 076 000	229 300	244 700	396 100
190	732 000	226 200	-	-
220	108 000	127 900	-	-
250	56 090	87 370	-	-

For curves measured using a Rheotens device, the ratio between the peak of elongation viscosity and the melt strength value, plateau at the beginning of the curve, can also be considered. This ratio is given in Table 8.

Table 8: The ratio between the peak of elongation viscosity and plateau at the beginning of the curve

	PP TOTAL	**PP DAPLOY**	**PP TOTAL/PP DAPLOY_20/80**	**PP TOTAL/PP DAPLOY_40/60**
Temperature [°C]	**Ratio [-]**			
180	1.7	2.8	2.7	1.4
190	2.5	2.9	-	-
220	2.4	3.0	-	-
250	2.0	3.0	-	-

The PP DAPLOY material has the highest ratio values. This material, therefore, has a large fibre strength hardening at the same time with low melt strength. The low melt strength indicates easier processing in the extruder, and the high strength hardening indicates high fibre strength and greater bubble stability in polymer foams. However, by comparing the data from the foaming process (comparing PP TOTAL at 250°C and TOTAL/

DAPLOY_40/60 at 180°C), this ratio does not seem to be fully indicative of how well the material will foam.

Finally, the obtained curves can also be compared at what value of elongation deformation rate the string was broken. The values are presented in Table 9. The maximum values range from 1.75 to 9.24 for the individual materials. Since both the material with these values have been foamed, this value do not seems to be suitable to indicate a course of the foaming process. However, based on our existing experiences knowledge of this value is profitable for evaluation of material spinnability.

Table 9: The maximum extension rate

	PP TOTAL	**PP DAPLOY**	**PP TOTAL/PP DAPLOY_20/80**	**PP TOTAL/PP DAPLOY_40/60**
Temperature [°C]	**Maximum elongation rate [s-1]**			
180	0.94	1.75	9.24	3.33
190	0.64	1.17	-	-
220	1.16	1.30	-	-
250	8.90	1.42	-	-

Based on the results discussed above, it could be concluded that the maximum of elongational viscosity curve defined via Rheotens in the area, together with the Trouton ratio in the area between 0.1 s^{-1} and 1 s^{-1} (defined from combination with high-pressure capillary shear viscosity data), seems to be valuable parameter for foamability definition.

CONCLUSION

At the beginning of this work, polymer foams were prepared. The melt temperature had to be maintained at 250 °C for PP TOTAL and 180 °C for PP DAPLOY and TOTAL/DAPLOY compounds. At a lower temperature, the gas bubble could not expand due to the high viscosity. At higher temperatures, the viscosity of the melt was already so low that the blowing gas escaped.

An optical microscopy was used for the characterisation of foamed structure. Based on microscopy analysis, it could be concluded that PP melts containing PP DAPLOY could be prepared into comparable foams. The pure PP TOTAL foam contained too small gas bubbles and a low level of expansion.

The results from the roentgen tomography also confirm the findings of optical microscopy. Comparing the scanned foam models, it is evident that the polymer foam PP TOTAL did not expand as other foams. The combination of PP TOTAL and PP DAPLOY affected the ratio of closed and open cells within extruded foams. Thus, the addition of linear PP to branched one could influence the final properties of prepared foams, depending on the application requirements.

The elongation viscosity obviously play an important role in the foaming process. Therefore, it was decided to evaluate it via accessible experimental methods and compare defined results respectively. The first choice was an online rheometer, which can be used directly in the manufacturing process in practice. Unfortunately, the online rheometer did not provide elongation viscosity values in the required temperature range. At lower temperatures, around 200 °C, there was a huge increase in pressure in the device, and the temperature had to be raised up to 250 °C.

The capillary rheometer has proven to be suitable for determining the elongation viscosity of the used materials. However, viscosity data at low strain rates were not obtained with a capillary rheometer, so additional characterization methods were chosen.

The rotary rheometer was already a more suitable method. There was also a visible phenomenon of strength hardening of PP DAPLOY material. Nevertheless, due to the significant experimental error defined by this method, it was pursuit with characterization of the elongation viscosity by further method.

Since results of elongation viscosity characterisation carried out by the Rheotens device offer stabile and reproducible results in the low strain rates region supposed to represent foaming conditions, this device was used for final comparison of all materials used for foams production. Significant differences in elongation viscosities of tested materials can be found, namely lower level was defined for PP TOTAL melt. Moreover, based on the obtained results it could be concluded that other requirement significantly influencing foamability of polymer melts is its low shear viscosity directly mastering the grow of air bubbles. It means that a lower shear melt viscosity itself offer easier expansion, while high elongational viscosity guarantee through the high melt strength foam stability. Thus materials with the optimum value of Trouton ratio have been shown to have required polymeric foam structures. With a small ratio value, it was practically impossible to produce foam. At a high ratio value, the polymer foam had large pores. The last part of the Rheotens elongational curve also carries useful information. In this final descending part, achievement of higher strain rates is advantageous for increase resistance of fibres to be rupture during their elongation. For example, pure PP TOTAL expel significantly improved elongation at 250 °C, which would suggest that the production of fibres from this material would be more effective at enough high temperatures (leaving faster polymer melt degradation out of consideration). Flow behaviour of prepared polymer blends also indicate this great endurance, noting the synergistic effect of the two materials which could be seen on the resulting extensibility of the blend.

The individual used measurement methods are compared in Chart 21 and Chart 22. Rheological data defined via employed techniques is displayed here together with the shear viscosity data from the rotational rheometer. The flow curves in these graphs are for easier visualisation presented at temperatures used for polymeric foams production (250 °C for PP TOTAL and 180 °C for PP DAPLOY).

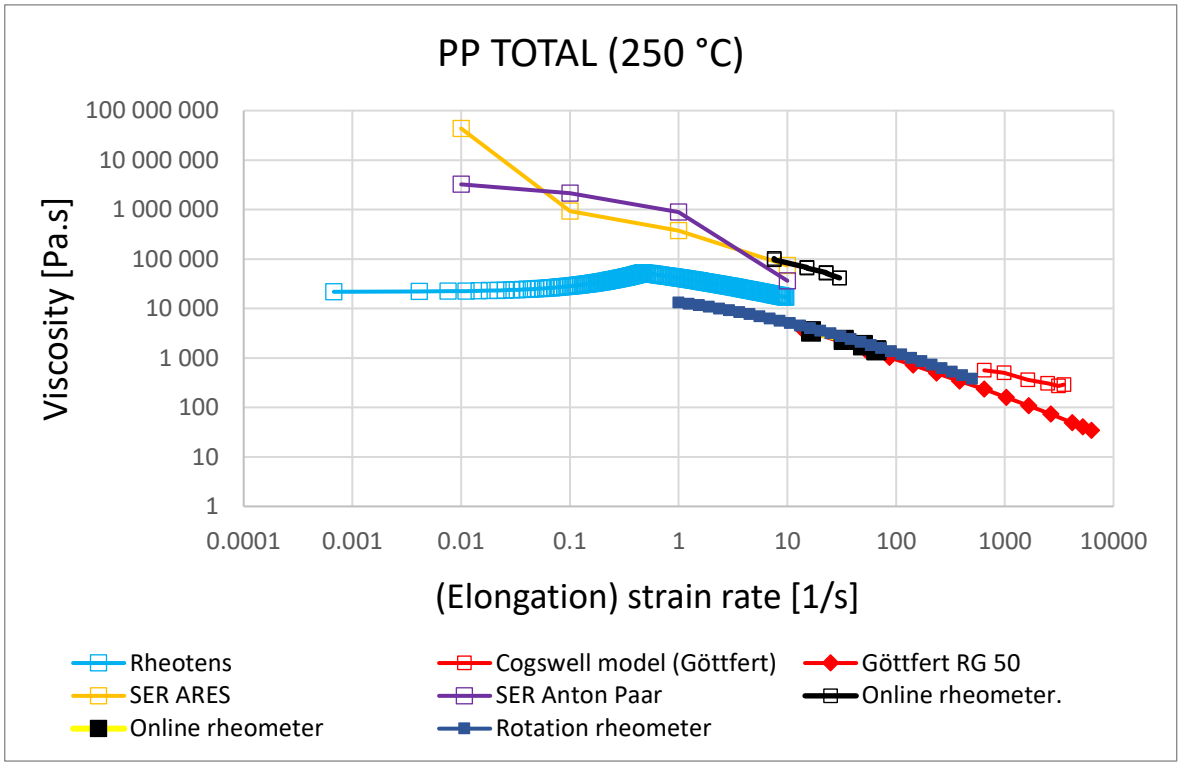

Chart 21: Comparison of data obtained from measurement methods for material PP TOTAL, filled squares belong to shear viscosity, and empty squares belong to elongation viscosity

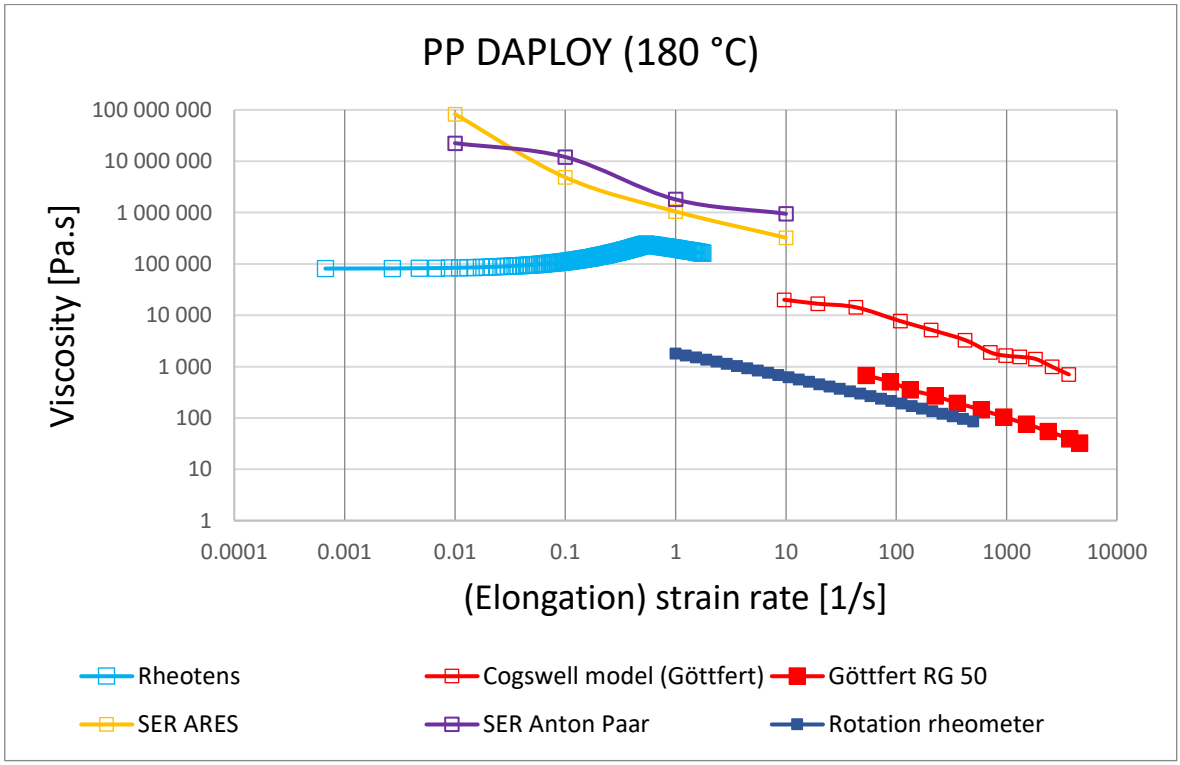

Chart 22: Comparison of data obtained from measurement methods for material PP DAPLOY, filled squares belong to shear viscosity, and empty squares belong to elongation viscosity

As mentioned earlier, low strain rate region is crucial for the foaming process. In this area, the value of shear viscosity and ration between shear and elongational viscosity (Trouton ratio) will define whether the gas bubbles do not escape from the polymer melt, whether bubble wall will have enough strength to sustain its elongation, thus whether created foam could be expanded optimally. Based on the results of our experiments and results, it could be concluded, that a material with a larger Trouton ratio value in the low strain rate region (between 0.1 and 1 s^{-1}) appears to be more suitable for foaming. On the other hand, up to now we also found that the position of strain rate defining rupture of elongated fibre taking out from the end of capillary describing ability of used material to withstand its spinning. In this way, the knowledge of the elongational viscosity curve evaluated by the Rheotens device and the knowledge of the shear viscosity represent useful tools for optimizing of both processes.

REFERENCES

[1] BUSCHOW, K. H. J., CAHN, R. W., FLEMINGS, M. C., ILSCHNER, B., KRAMER, E. J., MAHAJAN, S., 2001. Encyclopedia of Materials - Science and Technology: Volumes 1–11 - Viscoelasticity/Anelasticity. Elsevier. ISBN 978-0-08-052358-3. Retrieved from: https://app.knovel.com/hotlink/pdf/id:kt00B7AWE1/encyclopedia-materials/viscoelasticity-anelasticity

[2] MORRISON, F. A., 2001. Understanding Rheology. Oxford University Press, 2001. ISBN 978-1-62870-855-4. Retrieved from: https://app.knovel.com/hotlink/toc/id:kpUR00000I/understanding-rheology/understanding-rheology

[3] TROUTON, F.T., 1906. On the coefficient of viscous traction and its relation to that of viscosity. Royal Society. Vol. 77, iss. 519, pp. 426–440.

[4] Journal of Non-Newtonian Fluid Mechanics. ISSN 0377-0257.

[5] KEMPNER, D., SENDIJAREVIC, V., Handbook of Polymeric Foams and Foam Technology. 2 nd ed. Hanser, 2012. ISBN 978-1569903360.

[6] SALENCON, J., 2019. Viscoelastic Modelling for Structural Analysis. John Wiley. ISBN 978-1-5231-2858-7. Retrieved from: https://app.knovel.com/hotlink/toc/id:kpVMSA0005/viscoelastic-modeling/viscoelastic-modeling

[7] DAE, H. CH., 2007. Rheology and Processing of Polymeric Materials, Volume 1 - Polymer Rheology. Oxford University Press. ISBN 978-1-61344-542-6. Retrieved from: https://app.knovel.com/hotlink/toc/id:kpRPPMVPR4/rheology-processing-polymeric/rheology-processing-polymeric

[8] BERGSTRÖM, J., 2015. Mechanics of Solid Polymers - Theory and Computational Modelling. Elsevier. ISBN 978-0-32332-296-6. Retrieved from: https://app.knovel.com/hotlink/toc/id:kpMSPTCM06/mechanics-solid-polymers/mechanics-solid-polymers

[9] ZATLOUKAL, M., Applied rheology [lectures]. Tomas Bata University in Zlín, Faculty of Technology, Zlín, 2019

[10] KULKARNI, S., 2017. Robust Process Development and Scientific Molding - Theory and Practice. 2 nd ed. Hanser Publishers. ISBN 978-1-5231-1186-2. Retrieved from: https://app.knovel.com/hotlink/toc/id:kpRPDSMT03/robust-process-development/robust-process-development

[11] DURLING, W., 2017. Extrusion Coating Manual. 5 th. TAPPI. ISBN 978-1-5231-3075-7. Retrieved from: https://app.knovel.com/hotlink/toc/id:kpECME0016/extrusion-coating-manual/extrusion-coating-manual

[12] OSSWALD, T., RUDOLPH, N., 2015. Polymer Rheology - Fundamentals and Applications. Hanser Publishers. ISBN 978-1-5231-0129-0. Retrieved from: https://app.knovel.com/hotlink/toc/id:kpPRFA0005/polymer-rheology-fundamentals/polymer-rheology-fundamentals

[13] MACNAMARA, J. F., 2020. Film Extrusion Manual - Process, Materials, Properties. 3 rd. TAPPI. ISBN 978-1-5231-3078-8. Retrieved from: https://app.knovel.com/hotlink/toc/id:kpFEMPMPE3/film-extrusion-manual/film-extrusion-manual

[14] AHO, J. et al., 2015. Rheology as a tool for evaluation of melt processability of innovative dosage forms. International Journal of Pharmaceutics. Vol. 494, iss. 2, pp. 623–642. Retrieved from: https://doi.org/10.1016/j.ijpharm.2015.02.009

[15] OSSWALD, T. A., MENGES, G., 2012. Material Science of Polymers for Engineers. 3 rd. Hanser Publishers. ISBN 978-1-62870-199-9. Retrieved from: https://app.knovel.com/hotlink/toc/id:kpMSPEE002/material-science-polymers/material-science-polymers

[16] HALLEY, P. J., GEORGE, G. A., 2009. Chemorheology of Polymers - From Fundamental Principles to Reactive Processing. Cambridge University Press. ISBN 978-0-511-53754-7. Retrieved from: https://app.knovel.com/hotlink/toc/id:kpCPFFPRP4/chemorheology-polymers/chemorheology-polymers

[17] MEIßNER, J., Rheometer zur Untersuchung der deformationsmechanischen Eigenschaften von Kunststoff-Schmelzen unter definierter Zugbeanspruchung. Rheologica Acta. Vol. 8, pp. 78–88. Retrieved from: https://doi.org/10.1007/BF02321358

[18] MÜNSTEDT, H., LAUN, H. M., Elongational behaviour of a low density polyethylene melt. Rheologica Acta. 1979, Vol. 18, pp. 492–504. Retrieved from: https://doi-org.proxy.k.utb.cz/10.1007/BF01736955

[19] COGSWELL, F. N., 1972. Converging flow of polymer melts in extrusion dies. Polymer engineering and science. Vol. 12, iss. 1, pp. 64–73. Retrieved from: https://doi.org/10.1002/pen.760120111

[20] BINDING, D. M., 1988. An approximate analysis for contraction and converging flows. Journal of Non-Newtonian Fluid Mechanics. Vol. 27, iss. 2, pp. 173–189. Retrieved from: https://doi.org/10.1016/0377-0257(88)85012-2

[21] GIBSON, A. G., 1989. Die entry flow of reinforced polymers. Composites. Vol. 20, iss. 1, pp. 57–64. Retrieved from: https://doi.org/10.1016/0010-4361(89)90683-6

[22] SENTMANAT, M., Novel device for characterizing polymer flows in uniaxial extension. ANTEC 03. New York: Soc Plastics Eng Tech Papers 49, 2003.

[23] PETRIE, Ch. J. S., 2006. Extensional viscosity: A critical discussion. Journal of Non-Newtonian Fluid Mechanics. Vol. 137, iss. 1–3, pp. 15–23. Retrieved from: https://doi.org/10.1016/j.jnnfm.2006.01.011

[24] MORRIS, B. A., 2017. Science and Technology of Flexible Packaging: Multilayer Films from Resin and Process to End Use. Elsevier. ISBN 978-0-323-24325-4. Retrieved from: https://app.knovel.com/hotlink/toc/id:kpSTFPMFR2/science-technology-flexible/science-technology-flexible

[25] DAE, H. CH., 2007. Rheology and Processing of Polymeric Materials, Volume 2 - Polymer Processing. Oxford University Press. ISBN 978-1-61344-543-3. Retrieved from: https://app.knovel.com/hotlink/toc/id:kpRPPMVPP3/rheology-processing-polymeric/rheology-processing-polymeric

[26] STOKES, V. K., 2020. Introduction to Plastics Engineering. John Wiley. ISBN 978-1-5231-3304-8. Retrieved from: https://app.knovel.com/hotlink/toc/id:kpIPE0003L/introduction-plastics/introduction-plastics

[27] VIKAS, M., 2015. Manufacturing of Nanocomposites with Engineering Plastics. Elsevier. ISBN 978-1-78242-321-8. Retrieved from: https://app.knovel.com/hotlink/toc/id:kpMNEP0006/manufacturing-nanocomposites/manufacturing-nanocomposites

[28] MENNIG, G., STOECKHERT, K., 2013. Mold-Making Handbook. 3 rd. Hanser Publisher. ISBN 978-1-68015-483-2. Retrieved from: https://app.knovel.com/hotlink/toc/id:kpMMHE001C/mold-making-handbook/mold-making-handbook

[29] RAUWENDAAL, CH., 2014. Polymer Extrusion. 5 th. Hanser Publishers. ISBN 978-1-5231-0127-6. Retrieved from: https://app.knovel.com/hotlink/toc/id:kpPEE00022/polymer-extrusion-5th/polymer-extrusion-5th

[30] SCHWARTZ, H., WEBBER, M., 2019. Effect of Processing Aid Additives on Flow Instabilities and Die Build Up. Kafrit. Retrieved from: https://kafrit.com/effect-of-processing-aid-additives-on-flow-instabilities-and-die-build-up/

[31] MARTYN, M. T., SPARES, R., COATES, P. D., ZATLOUKAL, M., Imaging and analysis of wave type interfacial instability in the coextrusion of low-density polyethylene melts. Journal of Non-Newtonian Fluid Mechanics. 2009, Vol. 156, iss. 3, pp. 150-164. Retrieved from: https://doi.org/10.1016/j.jnnfm.2008.08.001

[32] LANGHE, D., PONTING, M., 2016. Manufacturing and Novel Applications of Multilayer Polymer Films. Elsevier. ISBN 978-0-323-37466-8. Retrieved from: https://app.knovel.com/hotlink/toc/id:kpMNAMPF08/manufacturing-novel-applications/manufacturing-novel-applications

[33] ZATLOUKAL, M., 2014. Applied rheology for polymers: From characterisation to modeling and flow instabilities. Zlín. Theses of Dissertation. Tomas Bata University in Zlín.

[34] NARANJO, A. et al., 2008. Plastics Testing and Characterization - Industrial Applications. Hanser Publishers. ISBN 978-1-61344-299-9. Retrieved from: https://app.knovel.com/hotlink/toc/id:kpPTCIA008/plastics-testing-characterization/plastics-testing-characterization

[35] KÖPPLMAYR, T. et al., 2016. A novel online rheometer for elongational viscosity measurement of polymer melts. Polymer Testing. Vol. 50, pp. 208–215. ISSN 0142-9418. Retrieved from: https://doi.org/10.1016/j.polymertesting.2016.01.012.

[36] GRELLMANN, W., SEIDLER, S., 2013. Polymer Testing. 2 nd. Hanser Publishers. ISBN 978-1-68015-484-9. Retrieved from: https://app.knovel.com/hotlink/toc/id:kpPTE00012/polymer-testing-2nd-edition/polymer-testing-2nd-edition

[37] SENTMANAT, M. L., 2004. Miniature universal testing platform: from extensional melt rheology to solid-state deformation behaviour. Rheologica Acta. Vol. 43, iss. 6, pp. 657–669. Retrieved from: https://doi-org.proxy.k.utb.cz/10.1007/s00397-004-0405-4

[38] MACOSKO, Ch. W., 1994. Rheology - Principles, Measurements and Applications. John Wiley & Sons. ISBN 978-1-60119-575-3. Retrieved from: https://app.knovel.com/hotlink/toc/id:kpRPMA0004/rheology-principles-measurements/rheology-principles-measurements

[39] BUSCHOW, K. H. J., CAHN, R. W., FLEMINGS, M. C., ILSCHNER, B., KRAMER, E. J., MAHAJAN, S., 2001. Encyclopedia of Materials - Science and Technology: Volumes 1–11 - Polymer Fiber Processing: Modeling. Elsevier. ISBN 978-0-08-052358-3. Retrieved from: https://app.knovel.com/hotlink/pdf/id:kt00B7AKA5/encyclopedia-materials/packaging--polymer-fiber

[40] ELONGATION. Göttfert [online]. [cit. 2021-04-15]. Retrieved from: https://www.goettfert.com/fileadmin/assets/Downloads/EN/PDF/Produkte/Dehnungstester/EN_BRO_Elongation_Rev.C.pdf

[41] RABINOWITSCH, B., 1929. Über die Viskosität und Elastizität von Solen. Zeitschrift für Physikalische Chemie. Vol. 145, iss. 1, pp. 1–26. Retrieved from: https://doi.org/10.1515/zpch-1929-14502

[42] BAGLEY, E. B., 1957. End Corrections in the Capillary Flow of Polyethylene. Journal of Applied Physics. Vol. 28, iss. 5, pp. 624–627. Retrieved from: https://doi.org/10.1063/1.1722814

[43] RAO, N. S., SCHUMACHER, G., 2004. Design Formulas for Plastics Engineers. 2 nd. Hanser Publishers. ISBN 978-1-59124-864-4. Retrieved from: https://app.knovel.com/hotlink/toc/id:kpDFPEE007/design-formulas-plastics/design-formulas-plastics

[44] BINDING, D. M., COUCH, M. A., WALTERS, K., 1998. The pressure dependence of the shear and elongational properties of polymer melts. Journal of Non-Newtonian Fluid Mechanics. Vol. 79, iss. 2–3, pp. 137–155. Retrieved from: https://doi.org/10.1016/S0377-0257(98)00102-5

[45] RAJAGOPALAN, D., 2000. Computational analysis of techniques to determine extensional viscosity from entrance flows. Rheologica Acta. Vol. 39, pp. 138–151. Retrieved from: https://doi-org.proxy.k.utb.cz/10.1007/s003970050014

[46] LUGER, H. J., MIETHLINGER, J., 2019. Development of an online rheometer for simultaneous measurement of shear and extensional viscosity during the polymer extrusion process. Polymer Testing. Vol. **77**, 105914. Retrieved from: https://doi.org/10.1016/j.polymertesting.2019.105914

[47] PPH 1060. TOTAL Polymers [online]. [cit. 2021-03-22]. Retrieved from: https://www.polymers.total.com/pph-1060

[48] Borealis strengthens cooperation with Taiwanese firm for development of lightweight, recyclable foam use concepts. BOREALIS [online]. [cit. 2021-03-21]. Retrieved from: https://www.borealisgroup.com/news/borealis-strengthens-cooperation-with-taiwanese-firm-for-development-of-lightweight-recyclable-foam-use-concepts

[49] COSSE, R.L., et al., 2019. Effects of the type of processing on thermal, morphological and acoustic properties of syntactic foams. Composites Part B: Engineering. Vol. 173, 106933. Retrieved from: https://doi.org/10.1016/j.compositesb.2019.106933

[50] ALMAADEED, M. A., PONNAMMA, D., CARIGNANO, M. A., Morphology analys. Polymer Science and Innovative Applications - Materials, Techniques, and Future Developments. Elsevier, 2020. ISBN 978-0-12-817303-9. Retrieved from: https://app.knovel.com/hotlink/pdf/id:kt012H3WD7/polymer-science-innovative/polymer-morphology

[51] BRUKER [online]. [cit. 2021-04-30]. Retrieved from: https://www.bruker.com/en.html

[52] Elongational rheometer. Leistritz [online]. [cit. 2021-04-25]. Retrieved from: https://extruders.leistritz.com/de-de/extrusion/brochures/leistritz-elongational-rheometer-datasheet.pdf

LIST OF SYMBOLS

Roman symbols

A	Surface	m^2
b	Shifting factor	1
d	Diameter	m
D_{ij}	Strain rate tensor	s^{-1}
e	Euler number	1
F	Force	N
G	Modulus	Pa
h	Height	m
L	Length	m
n	Power-law index	1
O	Axis of rotation	1
p	Pressure	Pa
P	Factor	1
Q	Volume flow rate	m^3s^{-1}
R	Radius	m
S	Barrel cross-sectional area	m^2
T	Temperature	°C
T	Torque	N.m
t	Time	s
v	Velocity	$m.s^{-1}$
V	Draw ratio	1
wt.%	Weight percentage	%

Greek symbols

α	Constant	1
β	Constant	1
$\dot{\gamma}$	Rate of shear deformation	s^{-1}
Δ	Delta	1
$\dot{\varepsilon}$	Rate of elongation deformation	s^{-1}
∂	Derivation	1
η	Viscosity	Pa.s
η_E	Elongation viscosity	Pa.s
$\eta_E^+(t)$	Stress growth function	1
λ	Relaxation time	s
π	Pi	1
σ_N	Normal stress	Pa
σ_p	Critical tension	Pa
τ	Shear stress	Pa
τ_{ij}	Stress tensor	Pa
Ω	Rotation rate	s^{-1}

LIST OF ABBREVIATIONS

CO_2	Carbon dioxide
CT	Computer tomography
HMS	High melt strength
LCB	Long-chain branched
LDPE	Low density polyethylene
MFR	Mass flow rate
MWD	Molecular weight distribution
NR-RSS2	Rib smoked sheet grade natural rubber
PP	Polypropylene
SER	Sentmanat extensional rheometer

LIST OF FIGURES

LIST OF TABLES

LIST OF CHARTS

APPENDICES